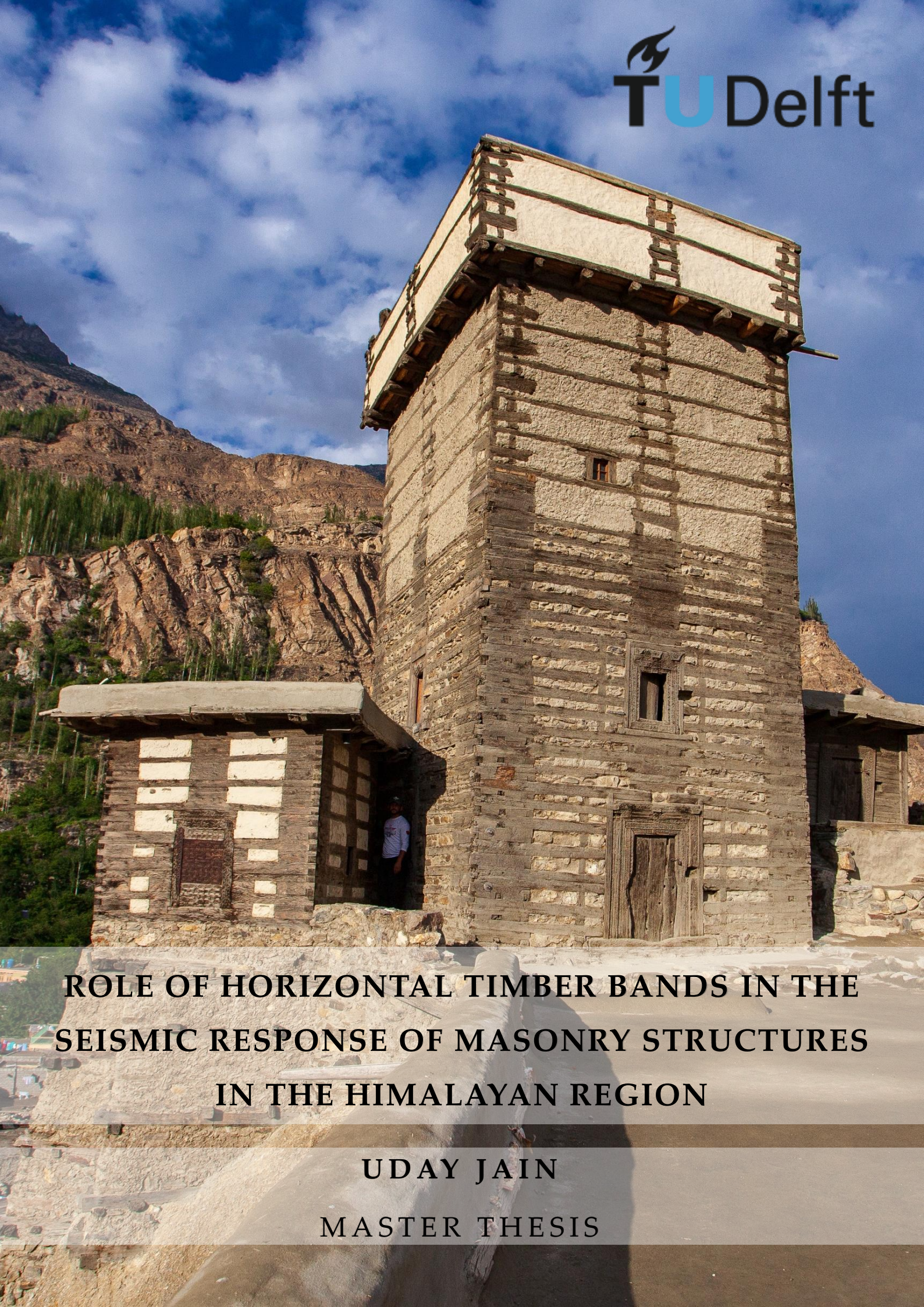

ROLE OF HORIZONTAL TIMBER BANDS IN THE SEISMIC RESPONSE OF MASONRY STRUCTURES IN THE HIMALAYAN REGION

UDAY JAIN

MASTER THESIS

ROLE OF HORIZONTAL TIMBER BANDS IN THE SEISMIC RESPONSE OF MASONRY STRUCTURES IN THE HIMALAYAN REGION

by

UDAY JAIN

October 27, 2023

In partial fulfilment of the requirements for the degree of

Master of Science
in Civil Engineering
Track: Structural Engineering

at the Delft University of Technology
Faculty of Civil Engineering and Geosciences

Thesis committee:	Dr.ir. G.J.P. Ravenshorst	Biobased Structures and Materials
	Dr. F. Messali	Applied Mechanics
	Dr.ir. M. Mirra	Biobased Structures and Materials

Student number: 5476437

An electronic version of this thesis is available at http://repository.tudelft.nl/

TU Delft

ABSTRACT

Masonry structures occupy a significant share of the current building stock due to widespread material availability and cost-effectiveness. Regions with high seismicity, like the Himalayas, have typically developed local seismic culture over the centuries. This has led to improved construction techniques providing an enhanced seismic performance, as evident from post-earthquake surveys in this area. In this framework, Bhatar is a building typology found in the greater Himalayan region, featuring embedded horizontal timber bands in masonry walls, enhancing the box-behaviour and in turn avoiding their premature out-of-plane failure.

This work aims to quantify the improvement of the out-of-plane performance of masonry walls due to the presence of horizontal timber bands. Numerical analyses were conducted in DIANA FEA software starting from the few experimental results available in literature on this typology. These were used to calibrate the properties of masonry, which was represented as a homogeneous isotropic continuum, with nonlinearities considered by means of a total strain rotating crack model.

Firstly, a U-shaped masonry wall having the same geometry and boundary conditions as the experimental tests was simulated using 3D modelling approach. Non-linear static analyses were performed exploring two different strategies, with minor variations in analysis parameters. Very good agreement was obtained with the results from literature for both strategies with one able to simulate local cracks better, while the other was able to simulate global failure mechanism better. On this basis, the calibrated numerical model was then employed to conduct sensitivity analyses considering varying factors, such as material properties, precompression load and aspect ratio.

Further refinements to the calibrated model were done. The influence of the frictional behaviour between timber and masonry was explored through discretely modelled interface elements, governed by Coulomb's friction criterion. The timber-to-timber connection was modelled as a hinge. The improvement in the behaviour of the wall due to timber bands connected throughout the frontal wall was also evaluated.

Finally, the calibrated numerical model was employed for the pushover analysis of a full-scale structure representing the geometry and configuration of a typical one-room Bhatar house. The results from the numerical analysis were then made use of for seismic assessment of the structure using Capacity Spectrum Method. The assessment demonstrated the capability of a timber-reinforced Bhatar structure to resist ground acceleration specified for the highest earthquake category defined by Indian Standard Criteria for Earthquake Resistant Design of Structures (IS Code 1893 (Part 1): 2016). On the other hand, an unreinforced masonry structure did not possess the required ductility to resist such an earthquake.

The outcomes of this study show a considerable improvement in the out-of-plane response of the masonry walls in the presence of horizontal timber bands. Inclusion of timber bands at corners of a 1:2 reduced scale U shaped masonry wall resulted in an increase of lateral

resistance by 40%. Walls with timber bands connected throughout the front wall presented a further increase of 35% in the force capacity. The corresponding improvement in force capacity for a full-scale Bhatar house was even more impressive at 109% when compared to an identical unreinforced house. There was also a noticeable increase in the ductility.

Given the limited research conducted on the Bhatar building typology in the past, this work constitutes a further step towards a better understanding of the behaviour of Himalayan masonry structures under earthquakes, promoting better seismic risk reduction strategies. This improved understanding into the role of timber in greater seismic resilience of masonry structures also informs better maintenance, conservation and preservation of heritage and historical masonry structures in the Himalayas.

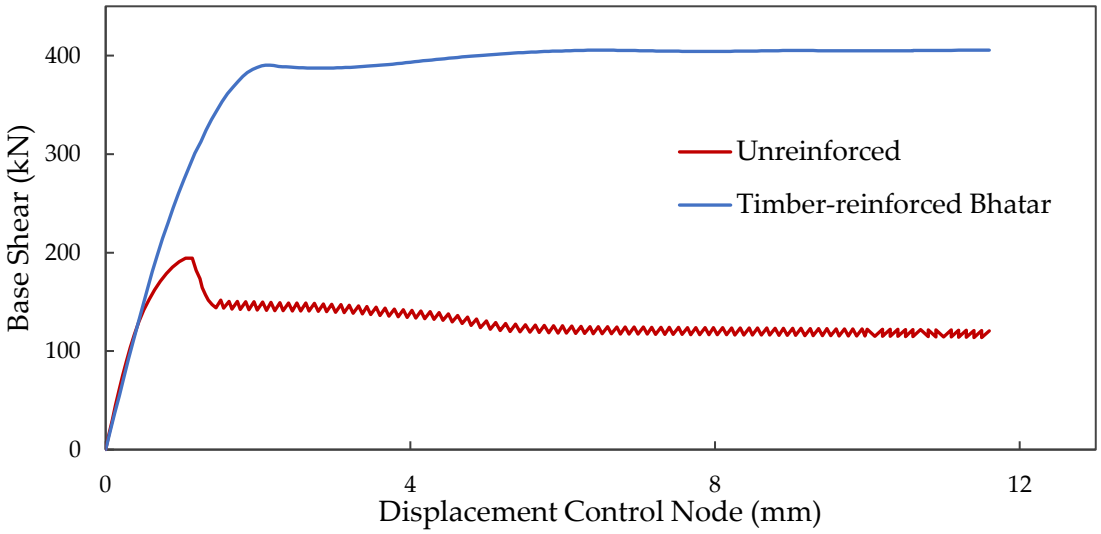

Pushover curve: unreinforced and timber-reinforced Bhatar masonry

ACKNOWLEDGEMENTS

This thesis is the culmination of my Master's in Structural Engineering at TU Delft where I investigate, through numerical analysis, how horizontal timber bands help a masonry structure survive an earthquake without collapse.

I would like to express my sincere gratitude to my supervising committee Geert Ravenshorst, Francesco Messali and Michele Mirra. I would like to thank Geert Ravenshorst for providing me the opportunity to explore a topic I deeply care about. Thank you for your practical approach, crucial insights and overall guidance. I would like to thank Francesco Messali for sharing with me his expertise on numerical modelling, seismic analysis and masonry structures. Working with him has fostered in me an enthusiasm towards numerical modelling that I hope to sustain in the future. I am grateful to Michele Mirra, whose advice, deliberation and shared passion for the seismic response of masonry structures has been instrumental. I am particularly thankful for your explanations and eagerness for discussions. Thank you for always providing prompt and apt feedback.

I am grateful to Ava for painstakingly proofreading and refining the final report. Thank you to all my friends in Delft and back home who shared with me this exciting journey. Thank you Sandeep bhai, Mahavir bhai and everyone at Hunnarshala who taught me how to place buildings in the context of communities.

To Komal, for always being there.

To my parents and sister, for their endless support, encouragement and love.

Uday Jain

Delft, October 2023

TABLE OF CONTENT

LIST OF FIGURES

LIST OF TABLES

LIST OF ACRONYMS

ADRS	Acceleration-Displacement Response Spectrum
CDP	Concrete Plasticity Damage
CGI	Corrugated Iron Sheets
CSM	Capacity Spectrum Method
DEM	Discrete Element Modelling
DBE	Design Based Earthquake
DIANA	Displacement ANAlyzer
DIC	Digital Image Correlation
DLS	Damage Limitation Limit State
DLS	Damage Limit States
ELF	Equivalent Lateral Force Method
FE	Finite Element
FEA	Finite Element Analysis
FEM	Finite Element Method
IS	Indian Standard
LVDT	Linear Variable Differential Transformers
MCE	Maximum Credible Earthquake
MRSA	Modal Response Spectrum Analysis
NCLS	Near Collapse Limit State
NDA	Nonlinear Dynamic Analysis
NDLS	No Damage Limit State
NLHTA	Nonlinear Time History Analysis
NLPO	Nonlinear Pushover Analysis
PBD	Performance Based Design
PGA	Peak Ground Acceleration
RC	Reinforced Concrete
RCC	Reinforced Cement Concrete
RE	Rammed Earth
SDLS	Severe Damage Limit State
SDOF	Single Degree of Freedom
SFLS	Shear Fatigue Limit Stress
TSC	Total Strain Crack
TSRCM	Total Strain Rotating Crack Model
URM	Unreinforced Masonry

1. Introduction

Masonry is one of the oldest and most prominent construction materials humans have used to house themselves. Evidence of the earliest forms of masonry has been reported as far as 7,500 years ago. The scientific revolution and industrialisation led to the prolific adoption of reinforced cement concrete and steel as the most used building materials in the 20th and 21st centuries. Still, brick and stone remain prevalent as walling materials due to local availability in remote regions where transporting industrialised materials such as cement and steel is difficult. This also reduces the dependence of the local populace on imported materials. Masonry continues to occupy a significant portion of the current building stock of many such remote regions with high incidences of earthquakes. Furthermore, most culturally and traditionally significant historical structures are built of masonry.

1.1. Context

The Himalayan region in the Indian subcontinent is an example of such a remote region with a high frequency of earthquakes [1]. Providing water to river basins populated by over 1.5 billion people in Northern India, Pakistan, Bangladesh, Nepal, and Bhutan, the Himalayas act as a natural climatic and physical barrier for the Indian subcontinent. They can be subdivided into four broader regions, as seen in Figure 1.1.

a) Karakoram range - Gilgit-Baltistan, Kashmir, Ladakh
b) Western Himalayas – Jammu & Kashmir, Ladakh, Himachal Pradesh, Uttarakhand
c) Central Himalayas – Nepal, Uttarakhand, Sikkim
d) Eastern Himalayas – Sikkim, Bhutan, Arunachal Pradesh, Assam

The high seismic activity in this region is the result of ongoing collision and convergence between the Indian and Eurasian tectonic plates [2]. Consequently, the region has experienced significant earthquakes during the 20th and 21st centuries (Table 1.1). Studies have predicted that due to significantly higher population density today, a future earthquake of over M 8.0 would result in casualties of well over 200,000 [3].

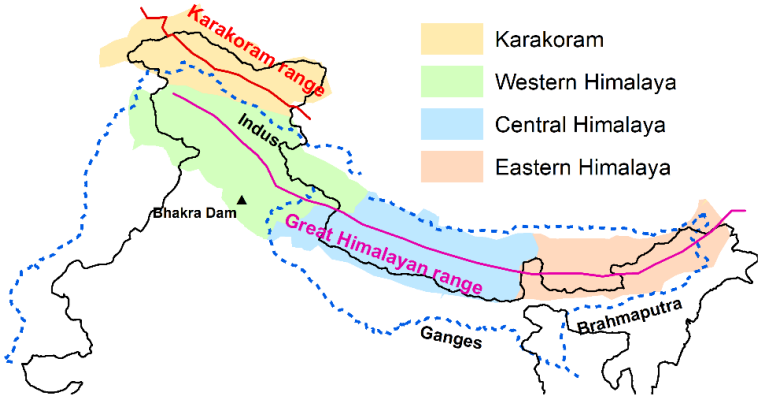

Figure 1.1: Regions of Himalayas.Map by Kulkarni et al. (2018)

Table 1.1: List of recent, major earthquakes in the Himalayan region

Year	Mw	Location	Death toll
1897, June 12	8.7	Shillong Plateau, Assam	1,542 [5]
1905, April 04	8.6	Kangra Valley (Himachal Pradesh)	20,000 [5]
1918, July 08	7.6	Assam	
1934, January 15	8.4	Nepal-Bihar	7,253 in Bihar [6] 8,500+ in Nepal [7]
1950, August 15	8.7	Assam-Tibet	1,526 in Assam 3,300 in Tibet
1975, January 19	6.8	Kinnaur (Himachal Pradesh)	60 [8]
1980, July 29	6.6	Nepal-Uttarakhand	200
1988, August 21	6.6	Bihar-Nepal	1,450
1991, October 20	6.8	Uttarkashi (Uttarakhand)	1,500 [9] 1,383 – 2,000
1999, March 29	6.6	Chamoli (Uttarakhand)	103
2005, October 08	7.6	Muzaffarabad (Kashmir)	85,000 [5]
2011, September 18	6.9	Sikkim	111
2015, April 25	7.8	Gorkha (Nepal)	9,000 [5]
2015, May 12	7.3	Nepal	218
2015, October 26	7.5	Pakistan, Afghanistan	399

Masonry still comprises a major share of the building stock in the Himalayan region, and the collapse of unreinforced masonry buildings is the leading cause of loss of human life during earthquakes. Over the past few centuries, a local seismic culture has developed in different regions of the Himalayas to enhance the seismic capacity of the masonry structures. Materials with high tensile strength, such as wood, are used to reinforce the masonry. These timber-reinforced masonry structures have shown better performance, evident from the post-earthquake reconnaissance surveys. However, scientific research into the behaviour and mechanism of these structures remains scarce, whether in the form of laboratory-based experiments or analytical modelling. Moreover, the current Indian seismic code does not mention specific criteria for assessment of timber-reinforced masonry. Improved understanding of how timber elements impart greater seismic resilience to masonry structures will:

a) Inform better maintenance, conservation, and preservation of heritage structures,
b) Assist national seismic codes to provision details regarding assessment of timber-reinforced structures,
c) Help and encourage practitioners in designing and building using techniques that have demonstrated superior performance,
d) Provide an avenue for making safer buildings using materials with a low carbon footprint as efforts to reduce the impact of building on our environment are increasing.

Past research on the buildings in the Himalayas has predominantly focussed on building typologies and spatial organisation while detailed seismic assessment of these structures has received limited attention. The present study is a step towards better understanding the seismic performance of traditional timber-reinforced masonry building typologies to preserve this vernacular heritage of the Himalayas better.

1.2. Objectives

Based on the knowledge gap identified in the previous section, the main objective of this thesis is to investigate the contribution of timber elements – specifically horizontal timber bands - to the seismic response of masonry buildings in the Himalayan region. The main research question, thus, can be postulated as:

What is the role of horizontal timber bands in the seismic response of masonry buildings in the Himalayan region?

The primary research goal in the form of the above research question is broken down further and following sub-research questions were realised:

- What is a suitable numerical modelling strategy to evaluate the response of a timber-reinforced masonry structure to lateral loads?
- Do horizontal timber bands increase the resistance of an unreinforced masonry structure to seismic loads?
- How does the failure mechanism of a masonry structure change in presence of horizontal timber bands?
- Do the timber bands affect only force capacity or do they impart ductility to the structure too?
- Does a Bhatar structure have sufficient seismic resilience to withstand an earthquake in Zone V without undergoing collapse? How does it compare to the response of an unreinforced structure?

To answer the above research questions, the following specific objectives were pursued for the thesis:

1. Identify and select a numerical modelling strategy for seismic analysis of the chosen structure.
2. Investigate the increase in the capacity of a masonry structure to resist the demands of an earthquake when reinforced by horizontal timber bands.
3. Analyse the cracking patterns and displacements, comparing them for drift levels at predefined limit states.
4. Assess the efficiency of timber bands to strengthen the masonry against horizontal loads and assess the most effective locations for timber bands across the height of a Bhatar structure.

5. Evaluate quantitatively the seismic behaviour of a representative example of Bhatar[1] building typology.
6. Propose practical recommendations towards construction of new and assessment of existing timber-laced buildings.

1.3. Organisation of thesis

First, Chapter 2 delves into failure modes of masonry and the building typologies specific to the Himalayan region. Further, state of the art experimental (Chapter 2.7) and numerical (Chapter 2.9) studies focusing on the investigation of masonry with structural timber elements are presented. It also introduces the numerical methods (Chapter 2.8) and seismic analysis and assessment (Chapter 2.11) approach adopted for this thesis. Chapter 2.10 provides information on the benchmark study used to validate the numerical modelling strategy adopted in this thesis.

Chapter 3 describes the numerical modelling strategy used along with parameters employed for the Finite Element (FE) analysis.

Chapter 4 presents the results obtained from the numerical analyses. The strength, stiffness and toughness of masonry is assessed based on maximum force capacity (obtained through the load displacement curve), ductility, failure modes, drift limits, and post-peak non-linear behaviour. First, the model is validated against the experimental and numerical benchmark in Chapter 4.1. Then. Chapter 4.2 briefly discusses the results of points of model refinement like timber-masonry interface and timber-to-timber connection. Thereafter, results from a sensitivity study are presented in Chapter 4.3 where the effect of varying material and geometrical properties is explored.

Chapter 5 presents the numerical and seismic analysis for a full-scale Bhatar building.

Finally, Chapter 6 presents a discussion and summary of the results, draws the conclusions from those results and concludes the study by summarising its main outcomes. Practical recommendations that can be applied in the field during design, construction, or assessment are provided. Finally, recommendations and future research possibilities are provided.

[1] Bhatar is a traditional building technique that uses horizontal timber bands to reinforce masonry structures against earthquake forces.

2. Literature review

2.1. Masonry: structural typologies and mechanics

Earliest evidence of masonry structures exists from more than 7,500 years ago. Material for masonry units can vary from fired clay bricks and stone to (unfired) earth-based blocks and cement-based blocks. A masonry wall is built when the masonry units are joined together by a mortar that is in *plastic* state initially but hardens with time. Masonry without any mortar is known as dry masonry. Traditionally mortar comprised materials such as soil and sand with lime as a binder. Over the past century, cement has replaced lime to become the most commonly used binder. Though similar in the way that both masonry unit and mortar have better compressive strengths than tensile, their material properties still differ considerably. Due to this composition of different materials and variations in the material properties of the constituents, masonry is characterized as being inhomogeneous and anisotropic.

2.2. Building typologies in the Himalayas

Masonry buildings occupy a large share of the current building stock in the Himalayan region. Specifically, over 70% of Nepal's [10-12] and Himachal Pradesh's [13] building stock has been reported to be masonry buildings. The majority of these are unreinforced. Since the Himalayas stretch for over 2,400 kilometres from one end to another, the building typologies differ widely from one region to the other. Like in any other region, the building typology in the Himalayas is dictated by the availability of materials in the particular region. This is evident from the diversity in vernacular architecture. Assam-type houses are popular in the Eastern Himalayas due to abundant availability of bamboo. In the Central Himalayas, due to the rich alluvial soil deposits of the Kathmandu valley, architecture is dominated by fired clay bricks. The rocky, high altitude Western Himalayas are dotted with villages built entirely out of stone masonry. In the past three decades, reinforced concrete (RC) buildings have become popular amongst locals due to the proliferation of steel and cement. However, most of these RC buildings are not engineered well and are often designed by local masons and contractors using thumb rules and their intuition and experience.

Regions such as Greece, Italy, Turkey and Portugal with high seismic activity have been reported to develop a local seismic culture [14-16]. This includes reinforcing the masonry (adept at resisting compression) with materials to resist tension and bending forces, too. Traditionally, this role was played by timber (timber-reinforced masonry) [17], however in modern times, steel and RC elements are used more commonly to reinforce masonry.

While there exist many typologies, the scope of this literature review is kept limited to masonry buildings that use timber structurally. Himalayas are covered with alpine, evergreen, temperate, coniferous, and tropical forests depending on the altitude and region. Logically, wood finds copious use in a range of construction applications - from structural applications such as beams, columns, joists, and planks to non-structural elements such as doors and windows.

Most of the typologies described below have a strip foundation of shallow stone masonry and the roof is mostly constructed through wooden beams, rafters, and purlins upon which either a flat mud roof is made or iron sheets for a sloping roof are laid. Therefore, only walling systems are elaborated.

2.2.1. Bhatar (Taq)

This timber-laced stone (or brick) masonry has horizontal timber bands at different levels to assist the structure in resisting tensile and bending stresses (Figure 2.1). The timber bands also connect the lateral and frontal wall, providing better resistance to out-of-plane movements [18]. Stone or brick masonry walls are laid in either mud mortar or cement mortar (in more recent times). However, dry stone masonry without any mortar is commonly seen in more remote regions, too. A detailed description of the *Bhatar* structure follows in Chapter 2.6.

2.2.2. Dhajji Dewari

Indicating its resemblance to a quilt, *Dhajji* and *Dewari* meaning patchwork quilt and wall in Persian, this construction technique is also known as *half-timbered* construction in Europe and *brick-nogged timber-frame construction* in Indian building codes. The timber frame acts as the vertical and lateral load carrying system infilled with either dry or mud-mortar masonry. Figure 2.2a shows how the infill is further divided into smaller sections by diagonal timber elements connecting the corners and junctions of the timber frame [19]. While pinned mortise and tenon joints or locking pegs were traditionally used to connect the timber elements; of late metal straps are also found with the dearth of knowledge of sophisticated joinery and skilled craftspeople. The larger dissipation capacity of the system can also be attributed to the pinned connections [20].

This technique is often found on the upper floors of buildings where the lower floor is constructed with the Bhatar (Taq) construction technique as can be seen in Figure 2.2b. This is done to take advantage of its lighter weight and thus reducing the seismic weight of the structure with increasing height. The relatively better performance of this system compared to other conventional building systems, including RC frame structure, has been reported after the 1967 and 2005 earthquakes. Non-uniform braces with random lengths can be found occasionally to maximise the locally available lengths of wooden pieces.

2.2.3. Thathara

Named after the local term for wooden planks, this construction system uses a 500 mm x 500 mm column, *thola,* made from wooden planks placed orthogonally in each alternate layer (Figure 2.3a). Perpendicular planks are connected vertically to each other by timber dowels to prevent displacement in in-plane or out-of-plane direction. The column is occasionally filled with either dry or mud-mortar stone masonry (Figure 2.3b). The columns and beams have no moment-bearing connections [21].

2.2.4. Kath-Kuni (Koti Banal)

The walls of Kath-Kuni have two horizontal timber cross-sections, one at the outer face of the masonry, another at the inner face. The beams are connected to the corresponding transverse beams in vertical directions through timber dowels, called *kadils*. The parallel cross sections at the same level are connected to each other by dovetail connections known as *maanwi* [22]. *Kadil* and *maanwi* are illustrated in Figure 2.4b. The capacity of these connections ensures sufficient shear transfer from the top of the building to the foundation. The space between the timber beams is infilled by stone masonry, such that the wall has alternating layers of stones and timber beams as seen in Figure 2.4a.

2.2.5. Newari

Developed due to the suitability of the rich alluvial soil of the Kathmandu valley for fired clay bricks, this vernacular has two variants for the composition of the wall. One has a cavity between the inside and outside leaves, filled by broken brickbats. The other has trapezoidal bricks known as *dachi aapa*, that taper from the outside to the inside, giving the appearance of no mortar while having enough clearance for mortar on the inside surface (Figure 2.5). The openings are usually constrained by two timber frames on each surface of the masonry and connected by transverse timber pieces. In recent times, the vertical expansion of the structures invariably involves extensive use of RC especially for the frame and slabs on the top floors in buildings with load bearing brick masonry walls on the lower floors [23].

2.2.6. Ikra (Assam-type house)

Evolved as a part of local seismic culture in the Eastern Himalayas, this building technique exploits the local abundance of bamboo [24]. The main timber frame with vertical posts and horizontal members is clamped onto the foundation without inserting it into the foundation. Figure 2.6a shows a typical Ikra house with no diagonal braces and the connections are either mortise and tenon or groove and wedge [25]. The infill wall panels are made of woven Ikra (a local river reed) or bamboo mesh. Traditionally Ikra was also used in the thatch roof, however, nowadays corrugated iron is used as roofing sheets [26]. The details of a typical wall of an Assam-type house can be seen in Figure 2.6b.

a

b

Figure 2.1: Bhatar structure : a) With dry stone masonry [27], and b) Timber band (photo: Schildkamp ()

a

b

Figure 2.2: Dhajji Dewari a) A modern house [29], and b) with Bhatar on ground floor [30]

a

b

Figure 2.3: Thathara house : a) Thola columns, b) With stone masonry infill [21]

a

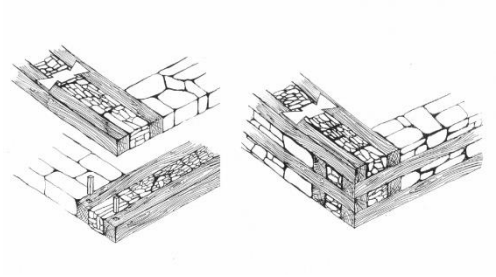

b

Figure 2.4: Kath-Kuni house a) [31], and b) Connections showing *maanwi* and *kadil* [32]

a

b

Figure 2.5: Traditional Newari houses : a) Picture by Francisco Anzola under Creative Commons Attribution 2.0 Generic, b) 300 year old Newari house [33]

a

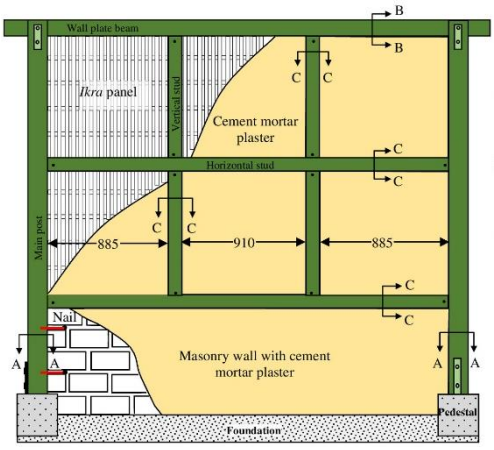

b

Figure 2.6: Ikra house : a) Typical Ikra house (photo: Sheth (), and b) Details of an Ikra house [25]

2.3. Mechanical behaviour of masonry

The behaviour of masonry is generally anisotropic and the properties in each direction depend on the properties of the constituents – mortar and unit, arrangement of the units, and orientation of mortar joints. Both constituents of masonry – mortar and unit, have much higher compressive strength than tensile strength. Consequently, while masonry resists gravity loads (from self-weight or overburden on walls) well, it behaves quite poorly when lateral loads are imposed. As a result, masonry cracks sooner when subjected to tensile or bending. These cracks, more often than not propagate through mortar joints, but depending on the boundary conditions and loads applied, might also go through the masonry units. On the other hand, the shear strength of the masonry is dependent on the friction between the masonry units and the bond strength of the mortar. Under tensile or lateral loading, masonry also behaves in a brittle manner with lesser capacity to deform plastically than conventional materials like steel and concrete. This includes failing without significant warning of distress in the masonry component or wall. This is also one of the major reasons of high vulnerability of unreinforced masonry walls to seismic actions. However, at a micro level, and under certain conditions, the masonry behaviour can be classified as quasi-brittle. The increase in stress results in microcracks in mortar joints or the interface between masonry unit and mortar. These microcracks propagate and coalesce under increasing stress denoting limited non-linear strain softening behaviour before failure.

2.4. Failure mechanisms of masonry

Unreinforced Masonry (URM) suffers failure through different types of failure mechanisms (Figure 2.7). Most of these failure mechanisms can be categorized into in-plane and out-of-plane failures. This chapter briefly describes the various ways of failure of masonry.

2.4.1. In-plane failure

A structure undergoing in-plane failure is able to dissipate a significant amount of energy, utilising the inherent capacity of the wall to undergo damage. In-plane behaviour of a wall can be activated if the structure can be prevented from failing through out-of-plane or local failure mechanisms. In-plane failures are preferred as larger forces, anssd consequently higher accelerations are needed to activate them compared to out-of-plane failures. However, once the in-plane failure is activated, the structure might suffer collapse of comparably larger portions after achieving the ultimate displacement capacity as the floors are generally connected to or rest upon walls undergoing in-plane collapse. Therefore, some in-plane failure modes, such as diagonal shear, are more brittle than others. The behaviour of a masonry wall under lateral load can be described by two basic behaviours – shear and flexural. Both, shear and flexural, have associated failure modes. The in-plane capacity of a masonry wall is affected by the mechanical properties of the material, slenderness of the wall, boundary conditions, and the vertical load on the wall [35].

The two flexural in-plane failure modes, rocking and toe-crushing, are influenced by the ratio of the vertical load on a masonry wall to its compressive strength. In the case of this ratio

being low, tensile flexural cracks occur at the corners. The behaviour of a typical wall with openings can be discretised into piers and spandrels. If slender piers have low overburden stresses and large aspect ratios, the masonry wall acts like a rigid body, rotating around the compressed toe (rocking) [36]. This results in tensile cracks at either top or bottom of the corners of the pier [37] and leaves the pier with no capacity in resisting further lateral loads [38]. Contrarily, if the ratio is high, the compression strength of the toe region of the wall is exceeded leading to toe-crushing. This also occurs under multiple cycles. Galvez (2016) provides a graphical overview of the relationship between the shear strength and the overburden stress on the wall in Figure 2.8. Shear failure in a masonry wall under lateral load is manifested in two primary modes – sliding shear and diagonal shear. Flexural cracks at the corners reduce the cross section resisting the load resulting in sliding shear failure. The cracks propagate either in a stepped diagonal manner or over a horizontal bed plane, also known as bed joint sliding. Diagonal shear cracks, on the other hand, occur when the tensile strength of the masonry is exceeded. They start at the centre of the low aspect, squat masonry piers with a large vertical load and propagate towards the corners in an X pattern [40].

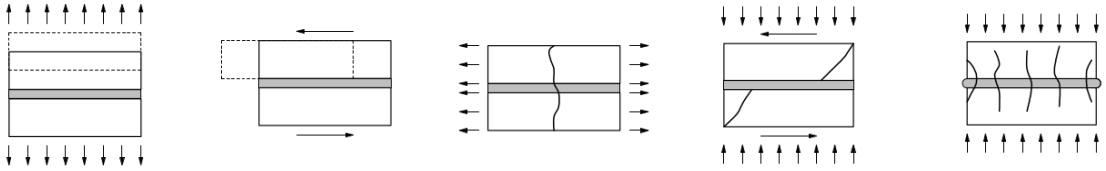

Figure 2.7: Masonry failure mechanisms – (a) tensile cracking of joint, (b) slipping of joint, (c) unit direct tensile cracking, (d) unit diagonal tensile cracking, (e) crushing of masonry from [39]

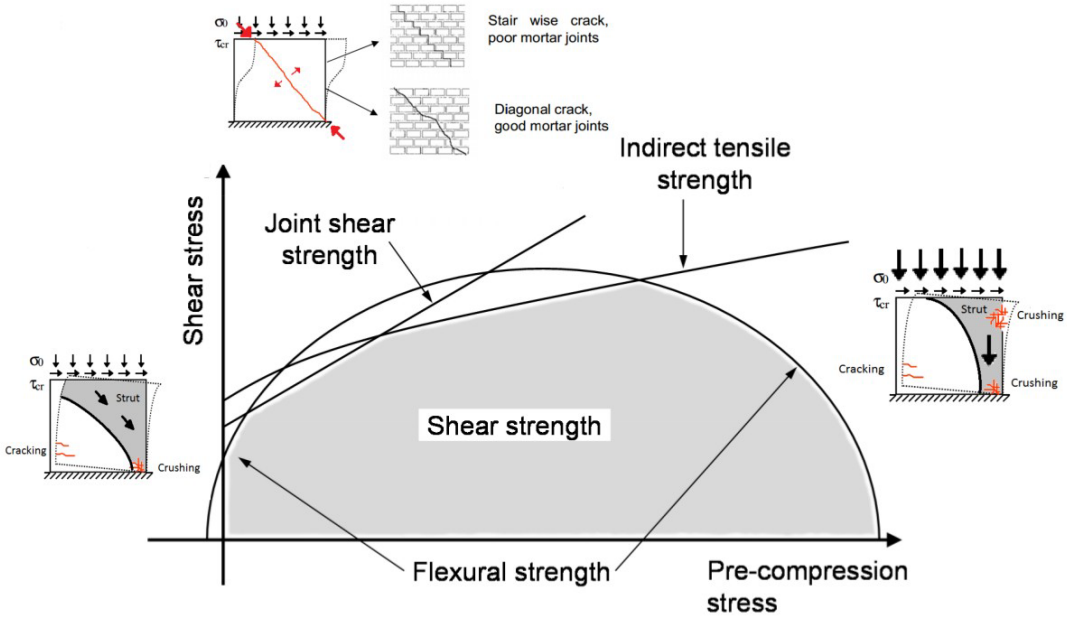

Figure 2.8: Shear stress vis-à-vis Pre-compression stress from [39]

2.4.2. Out-of-plane failure

When a wall is subjected to out-of-plane horizontal bending due to lateral loads and the structure is unable to behave in a box-like manner, it undergoes out-of-plane failure. The inability of the horizontal diaphragms to adequately connect the orthogonal walls also contributes to the inability of the structure to resist the inertial force developed in the walls due to the seismic action [41]. Certain out-of-plane failure modes such as one way bending are more ductile than others. However, when brittle, out-of-plane failures can result in sudden collapse of parts of the structure. This can be avoided by design and detailing that activate in-plane capacity of lateral walls during seismic events. Since traditional floors with timber joists rest on the walls involved with in-plane failure, the out-of-plane failure of walls does not trigger progressive collapse. Slender walls are more vulnerable to out-of-plane failure as the top section of the wall acts as a cantilever leading to collapse. The extent of supported edges influences the internal stresses developed at the mortar-masonry unit interface by dictating the crack pattern and thus, failure mechanism [42]. Long walls without effective support at the edges behave like one-way spanning walls undergoing one-way bending, while those with effective support at the edges undergo two-way bending. As a result, the out-of-plane failure occurs at a lower ground acceleration than in-plane failure. Lawrence and Page (2013) in their *Manual 4: Design of clay masonry for wind and earthquake*, present different crack patterns that develop in a masonry wall depending on the boundary conditions and aspect ratios Figure 2.9.

More importantly, sufficiently connected transversal walls lead to the inertial forces being transferred from façade walls to the lateral walls, thereby activating the in-plane capacity of the lateral walls. Here, timber elements act as excellent connectors for orthogonal walls.

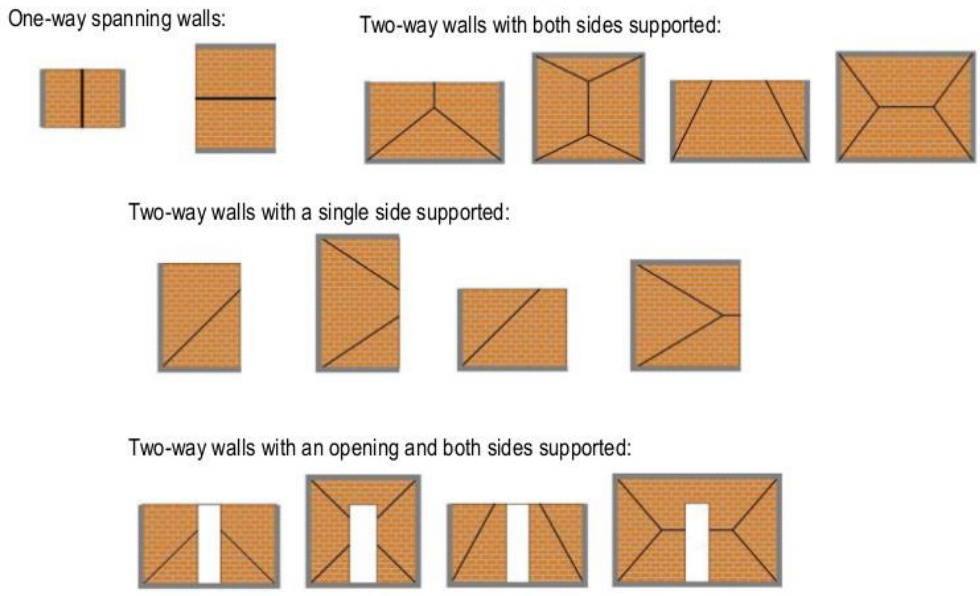

Figure 2.9: Failure of out-of-plane masonry walls from [43]

2.5. Failure mechanisms observed in URM structures in the Himalayan region

The past earthquakes in the Himalayan region have led to significant damage to Unreinforced Masonry (URM) structures and subsequent loss of lives [13, 44-46]. Post-earthquake surveys have demonstrated the performance of timber-reinforced structures to be better than conventional construction techniques throughout many regions with high seismicity [47]. Specifically in the Himalayas, this has been observed after earthquakes in Anantnag (1967) [48], Assam [30, 49], Kashmir (2005) [50], Uttarakhand and Himachal Pradesh [51] and Gorkha, Nepal (2015) [52]. This chapter describes various failure mechanisms observed in URM after earthquakes in the Himalayan region.

2.5.1. In-plane failures

Many of the failure modes described in 2.4.1 have been seen in post-earthquake surveys. Diagonal cracks start at the corner of the opening and propagate towards the top or bottom corners of the wall (Figure 2.10). Diagonal shear failure in piers between openings can also be commonly seen (Figure 2.11). Multiple ventilators beneath the roof leads to insufficient connection of the diaphragm to the wall and reduction in volume available to resist the in-plane shear forces (Figure 2.12). Horizontal cracks can be seen at the top and bottom of piers between openings as a result of rocking motion (Figure 2.13).

2.5.2. Out-of-plane failure

Overturning of gable walls has been observed as one of the most common failure mechanisms to develop in URM structures, essentially behaving like a parapet wall [12]. Gable overturning happens due to several reasons, the major ones being - insufficient connection to transversal walls, lack of vertical load on top of the gable wall, and lack of tying and bracing to the roof (Figure 2.14). Asymmetrical plans, protrusions or long façade walls without regular transverse walls are other characteristics that lead to out-of-plane failure (Figure 2.15). Insufficient connections between orthogonal walls leads to separation of the two walls [53, 54] (Figure 2.17). Severe damage is also seen when an ineffectively connected roof exerts thrust on the gable or wall, or the timber joists are simply resting on the top of the wall without a proper connection (Figure 2.16). When a diaphragm is not able to effectively transfer the forces (acting on the structure due to lateral load) to the lateral walls, out-of-plane failure often leads to complete collapse of the masonry.

Figure 2.10: Diagonal cracks from openings [54, 55]

Figure 2.11: Diagonal shear failures of masonry piers [40]

Figure 2.12: Damage due to multiple ventilators and openings below roof [40]

Figure 2.13: Horizontal flexural cracks due to rocking [40]

Figure 2.14: Out of plane collapse and overturning of gable masonry [46, 56]

Figure 2.15: Out of plane damage due to asymmetrical plan or protrusion [53]

Figure 2.16: Inadequate connections to the diaphragm [53, 57]

Figure 2.17: Separation of orthogonal wall [53, 54]

2.6. Bhatar – a closer look

The vernacular construction method known as the Bhatar technique is widely employed in regions such as Gilgit-Baltistan (Pakistan), Kashmir (India, Pakistan), Himachal Pradesh, Uttarakhand (India) and Nepal. Though this particular typology is from the Himalayas, similar building typologies (masonry interspersed with horizontal timber bands) are prevalent in many seismic-prone regions throughout the world – Turkey, Italy, Portugal, and Greece to name a few.

As described in Chapter 2.3, masonry often behaves in a brittle or quasi-brittle manner. Inclusion of reinforcing elements like timber limits the brittle nature of the masonry by enhancing the ductility and energy dissipation capacity of the wall. Thus, timber has been a prevalent reinforcing material in masonry buildings in seismic regions. Traditional stone walls possess inherent weaknesses stemming not only from inconsistent quality but also from irregular mortar application. Due to manual lifting, stones at the base are larger than the ones used as the wall rises. To counter these vulnerabilities, timber lacing is frequently integrated into the wall for reinforcement. The tensile and elastic properties of timber reinforcement in walls make it invaluable. In seismically active regions, timber lacing has been a preferred choice of reinforcement because of its ability to withstand dynamic forces such as earthquakes. 50 to 120 mm, square or rectangular sections are embedded into walls at various vertical intervals. These are interconnected by crossbeams for enhanced stability. Along with the inherent advantages, timber lacing has few limitations such as combustibility and sensitivity to moisture and decay.

The history of timber lacing as a wall-strengthening method goes as far back as the Bronze and Iron ages as found in archaeological sites across Europe. Its utilization has also been observed in countries such as Greece, Macedonia, Syria, and Yemen [58]. Building typologies similar to Bhatar have been found in seismic regions across the world as part of the local seismic culture. Horizontal wooden beams have been used for reinforcing earthen or stone masonry construction in Anatolia (Turkey) for many millennia [59]. Like Bhatar, two timber runner beams, *hatıls,* aligned with external and internal surfaces of the wall, are connected by outward extending crossbeams, *peştivanm,* also referred to as *düğme*, translating to "button". Therefore, these types of houses are called "button houses" or *pişt*uvanlı in the local vernacular meaning *wall with beams*. These runner beams are present every 50-60 cm across the height of the wall section, while *peştivan* extends approximately 25 cm from the wall, doubling as integrated scaffolding [60]. Similar stone masonry interspersed with horizontal timber beams is also part of the seismic culture of Greece [61].

Notable examples of Bhatar masonry are Baltit Fort and Shigar Fort in Gilgit-Baltistan. This technique incorporates timber-laced structures that use stone masonry, reinforced with horizontal timber bands or beams at the sill, lintel and roof/floor level to enhance confinement. The rubble stone masonry provides compressive strength, while the timber beams contribute to tensile and bending resistance. The timber also facilitates more robust corner joints, providing resistance to out-of-plane movements, making this method more resilient against wall cracking [18].

a b

Figure 2.18: Timber-reinforced masonry : a) Ibradi button house in Turkey. Photo by Erarslan (2020), and b) Typical horizontal timber tie in stone masonry in Greek [61]

Bhatar building typology is an element of the local seismic culture in the Himalayas that has developed over centuries as local craftsmen, guilds, and builders fostered over generations, a construction with relatively better seismic behaviour. Over the previous millennia, this vernacular architectural approach has been employed for various purposes and scales, from religious temples and military forts to civilian houses. Several structures built with this method have survived major earthquakes, suggesting the Bhatar system's seismic resilience. Timber has been increasingly used as seismic bands after earthquakes in the Central Himalayas as observed by Khadka (2022). The variance in the survival rate of these buildings could be attributed to numerous factors, including materials used, the location selected for construction, and, importantly, the differences in techniques passed down through generations.

It is popular and often employed to a larger extent in remote areas with less affluent populations where utilisation of local materials is essential. This makes the construction system both cost-effective and practical and avoids reliance on industrialised materials that must be imported from distant regions – which is particularly challenging due to the strained infrastructure usable only during certain seasons. Construction of a building with this technique requires neither expensive materials, equipment or machinery, needed in the case of modern RC frame construction, nor highly skilled artisans, essential to specific traditional construction techniques.

Furthermore, extensive research on climate change has shown the detrimental environmental impact of industrialised building materials on the planet. A large proportion of CO_2 emissions result from the cement and steel industry, respectively. In contrast, the Bhatar building typology has a particularly low carbon footprint as both major materials involved in the construction – wood and stone/brick - are local (avoiding transport) and natural (avoiding energy intensive manufacturing processes).

Figure 2.19: Stone masonry in mud mortar with horizontal timber bands observed after the 2015 earthquake in Nepal observed by [62]

The practicality, cost-effectiveness, minimal environmental impact and structural durability make the Bhatar system a viable option for alternative building systems and post-disaster reconstruction, especially in developing countries. On the other hand, the Bhatar system has a significant disadvantage regarding its seismic behaviour - the substantial weight of the structure. Since seismic forces acting on a structure are proportional to its weight, and Bhatar structures are heavy due to thick masonry walls often built out of stone, its high seismic weight is a drawback. Thus, further research is crucial to understand better the seismic response of structures built using the Bhatar technique, focusing on the constraints and integrity during earthquakes.

2.6.1. Geometry

2.6.1.1. Foundation

The foundation of these buildings usually comprises a strip foundation constructed from stone. It is shallow in rocky areas and deep in areas with less stability in the soil. The width of the foundation is usually between 60 and 75 centimetres depending on the thickness of the wall.

2.6.1.2. Walls

The walls are usually 45 cm thick, but in certain structures, the thickness can reach as much as 60 cm. The masonry consists of either stone or brick masonry depending on the region. Stone masonry is found in the Upper Himalayas with an abundance of stone and little soil. On the other hand, the valleys, for example, Kathmandu Valley in Nepal, are rich in soil, leading to the prevalence of brick masonry. The masonry is bound in mud mortar, with some regions also practising dry stone masonry. In recent times, cement mortar is also used.

2.6.1.3. Timber bands

The walls incorporate two horizontal wooden beams, 8-10 cm deep and wide, one flush at the inner surface of the wall and the other at the outer surface of the wall. These beams are connected with cross pieces to create a ladder-like timber frame, present at the ground, sill, lintel, and roof or floor level as seen in Figure 2.20.

2.6.1.4. Roof

Timber floor joists span opposite walls and rest on timber roof beams at the roof level. These joists are covered with planks, twigs, and compacted earth, resulting in a significantly heavy roof. The details of the roof can be seen in Figure 2.21.

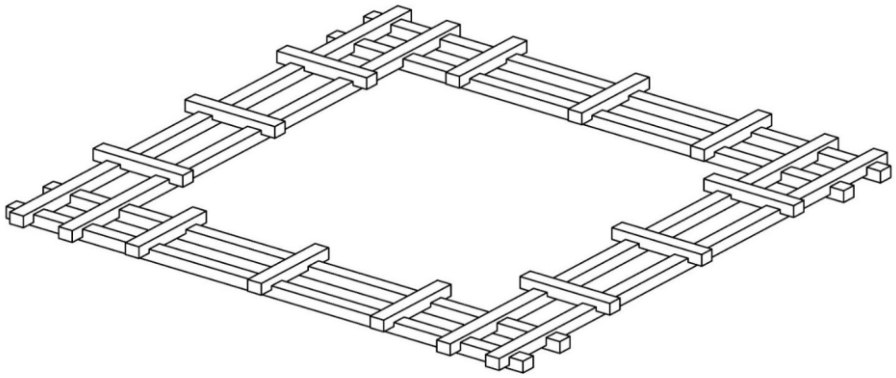

Figure 2.20: Timber band [63]

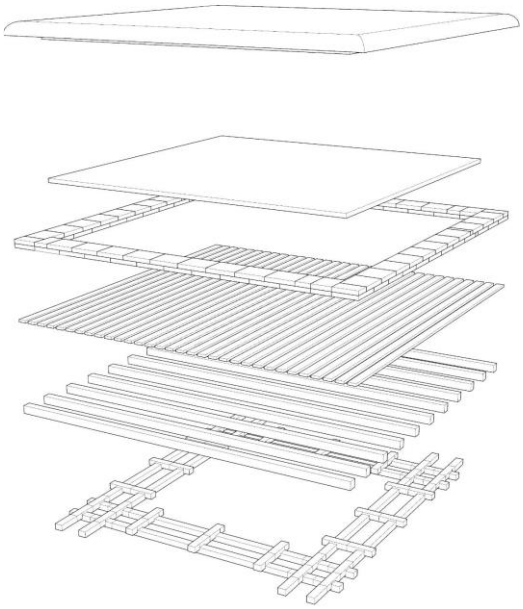

Figure 2.21: Roof details [58]

Conclusion

Masonry structures, especially when unreinforced, are prone to both in-plane and out-of-plane failures. In-plane failures, which are preferred due to higher acceleration needed to activate them, can be understood through shear and flexure behaviours, leading to diagonal and sliding shear cracks or rocking and toe-crushing. On the other hand, out-of-plane failures arise from horizontal bending in walls, exacerbated by inadequate connections to orthogonal walls, with slender walls being especially vulnerable. The presence or absence of proper support on wall edges and the use of materials such as timber that connect the orthogonal walls can significantly influence these failure mechanisms.

Earthquakes in the Himalayan region have extensively damaged Unreinforced Masonry (URM) structures in the past, leading to loss of life. Timber-reinforced constructions have demonstrated better resilience during these seismic events compared to traditional building methods. Within the purview of URM failures, in-plane failures, although ductile, manifested as diagonal cracks from openings, diagonal shear failures between apertures, and horizontal cracks due to rocking motions. In contrast, out-of-plane failures led to abrupt, global collapses. Commonly observed mechanisms include overturning of gables or façade walls because of insufficient connections, lack of vertical load, and inadequate bracing. Asymmetrical designs and inadequate wall connections further exacerbated these failures, sometimes resulting in the complete collapse of masonry structures.

In the Himalayan region, masonry buildings constitute the dominant building stock, the majority being unreinforced. The diversity in building typologies across the vast stretch of the Himalayas is influenced by the availability of local materials. Assam-type houses, popular in the Eastern Himalayas, leverage bamboo abundance, while fired clay bricks characterize the valleys, and stone masonry dominates the rocky Western Himalayas. Modern trends have seen a rise in non-engineered, often poorly built reinforced concrete (RC) buildings. Historically, regions with high seismic activity, such as parts of Europe, have integrated reinforcement materials such as timber, steel, and RC, into their masonry for better resilience. This literature focuses on masonry buildings incorporating structural use of timber, such as Bhatar (Taq), Dhajji Dewari, Thathara, Kath-Kuni (Koti Banal), Newari, and Ikra (Assam-type house), each utilizing different combinations of masonry and timber, influenced by regional resources, and building practices.

The Bhatar technique, a vernacular construction method, is prevalent in Himalayan regions and has parallels with other seismically active global areas, such as Turkey, Italy, Portugal, and Greece. Characterized by stone masonry reinforced with horizontal timber bands at key structural points, this technique combines the compressive strength of rubble stone with the tensile and bending resistance of timber. The Bhatar method of building has showcased resilience against major earthquakes and remains a cornerstone of local seismic culture. Despite its seismic weight drawback, its adaptability in remote, less affluent areas makes it cost-effective, environmentally sound, and reliant on local, natural materials. The construction comprises a stone strip foundation, thick masonry walls, ladder-like timber frames within the walls, and heavy timber-reinforced roofs.

2.7. Experimental studies

Brittle nature of masonry along with anisotropic properties, make it crucial to evaluate its response to lateral loads for safe design and construction. Several experimental campaigns have been conducted in the past to assess the response of unreinforced masonry to lateral loads. However, this chapter presents a selection of few experiments that focus on the inclusion of horizontal timber elements within thick masonry walls since they are representative of the Bhatar building typology relevant to the Himalayan context using timber for structural reinforcement.

The variation between the tests ranges from the configuration (single walls, U-shaped walls, full structures), and the scale of the walls to the method of testing (cyclic, quasi-static, shake table) to the application of load (in-plane, out-of-plane). A "pushover" test subjects a structure to incremental load through a hydraulic jack or actuator until a predefined damage level or collapse, in order to assess nonlinear behaviour, determine the ultimate load capacity and associated displacements of the structure. Strain gauges, linear variable differential transformers (LVDTs), accelerometers or displacement transducers measure different parameters during testing. Load-displacement curves provide information about the yielding point, peak load capacity, and post-peak behaviour. While monotonic loading determines the maximum load-bearing capacity, cyclic loading also sheds light on the energy dissipation and hysteresis behaviour of masonry. Pushover tests are useful to evaluate the performance of masonry structures, validate or refine analytical models, design, or validate retrofitting techniques and inform guidelines or codes.

2.7.1. In-plane tests

Cyclic or quasi-cyclic in-plane tests conducted on adobe [64], earthen [65] or stone masonry [66] walls with and without embedded timber bands or beams have revealed higher ductility and greater energy dissipation for the timber-reinforced versions. Some studies use the Digital Image Correlation (DIC) technique to assess the displacement and crack patterns [64, 65]. Yadav et al. (2021) note the increased energy dissipation in timber-reinforced walls due to limiting of the vertical cracks while allowing horizontal cracks to propagate, activating a sliding mechanism. The authors also present a correlation between the dissipation energy and the crack opening area, demonstrating that the wall with a timber band has a lower fissure surface area and hence smaller cracks and greater structural integrity. On the other hand, Wang et al. (2019) found that the timber bands increase the flexural strength and structural integrity of stone masonry while also distributing the seismic load, delaying the cracking and local failure during initial deformation stages.

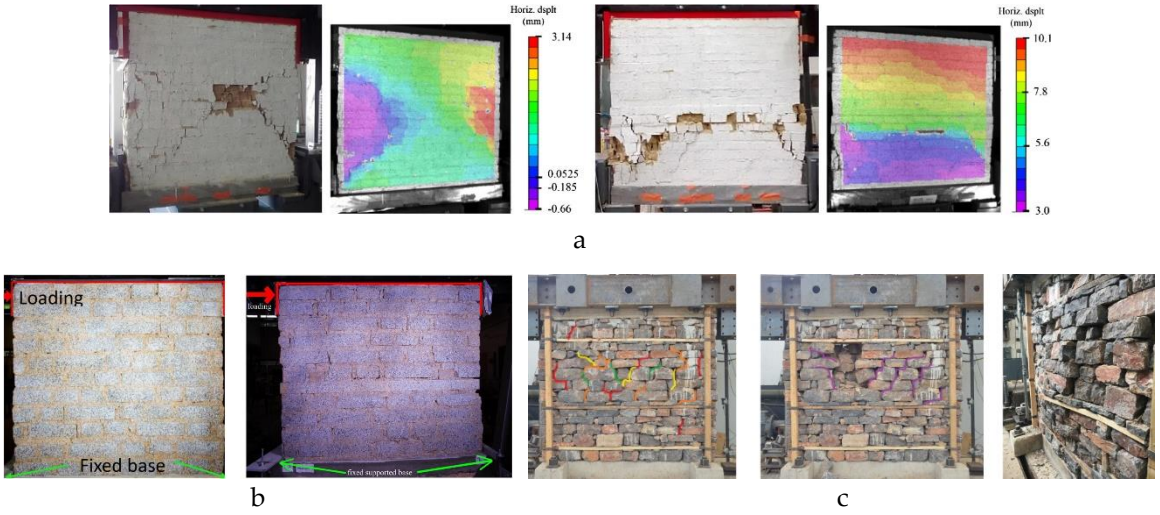

Figure 2.22: In-plane tests for masonry with embedded timber beams – (a) by [65], (b) by [67], and (c) by [66]

2.7.2. Out-of-plane tests

Pull down tests have been employed on unreinforced and reinforced rammed earth (RE) walls to find a 59% increase in their pull-down load after strengthening of wooden beams [68]. However, more popular are out-of-plane horizontal loads on façade walls. Misir et al. (2022) conducted quasi-static cyclic tests (Figure 2.23b) on large-scale U-shaped stone masonry wall specimens and suggested damage limits to be used in performance-based evaluations. The experiments were done on three specimens – a) drystone double-leaf masonry, b) double-leaf mortar bonded masonry and c) three-leaf with rubble infill layer. Of these, the double-leaf mortar bonded specimen (Figure 2.23a) is of interest as its geometry and masonry correspond closely to the other benchmark test. The crack evolution observed in this experiment closely relates to the damage evolution observed in the unreinforced masonry numerical analysis for this thesis, see Chapter 4.

2.7.3. Shake table tests

Shake table tests have been a popular experimental method to assess the out-of-plane response of masonry structures. Candeias et al. (2017) conducted shake table tests on two U-shaped masonry structures with openings – one with brick and one with stone. Mouzakis et al. (2018) conducted shake table tests on two-storey timber-laced three-leaf stone masonry buildings and drew the conclusion that the presence of timber laces at regular intervals along the height of the building led to limited detachment between the leaves of the masonry. Additionally, the timber laces were found to limit the occurrence of in-plane cracks while also distributing the vertical load more evenly.

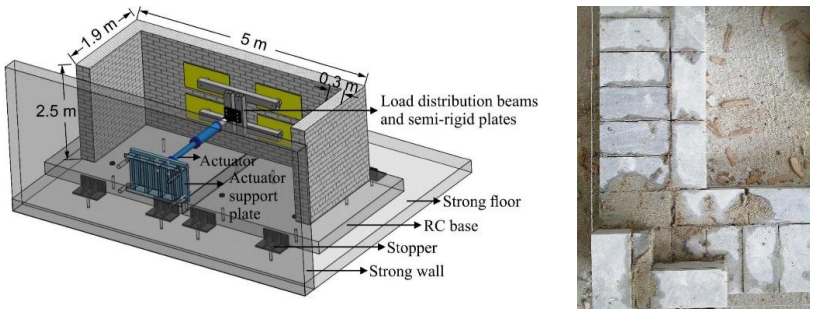

a b

Figure 2.23: Out-of-plane experiment details of (a) experiment setup, (b) masonry bond as explained in [69]

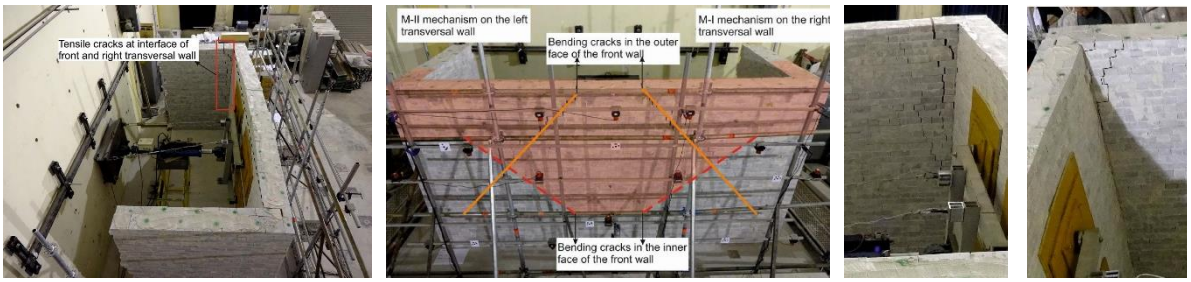

a b c d

Figure 2.24: Observed damage – a) Deformation and damage at the connection, (b) the overturning mechanism, (c) and (d) close-up damage details of corners as detailed in [69]

Wang et al. (2019) conducted shake table tests to assess the performance of two-storey dry stone masonry building and observed that timber laces considerably improved the performance of the masonry buildings by distributing the seismic load evenly, confining the cracks to local areas and preventing collapse of entire walls. The 4500 x 4500 mm structure was scaled by 0.55 to fit the shake table, while the thickness was 450 mm. The prototype model also had timber laces at ground, sill, and lintel levels while having corner braces at roof and middle levels. This makes the experiment similar to the Bhatar structure in Chapter 5 to a large extent, with key differences being two storeys, floor between the two storeys and sloping roof. The authors also found that the timber laces contribute to the structure by improving the structural integrity and providing the structure higher ductility rather than increasing initial stiffness. For the unreinforced wall, the authors report separation of lateral walls through vertical cracks at the corners at PGA 0.31 g, with collapse of the wall at 0.40 g. On the other hand, a similar structure with timber laces did not suffer collapse though undergoing local failure at 0.51 g.

Yadav et al. (2023) conducted shake table tests on 1:2 reduced scale earth block masonry houses with and without horizontal timber bands. It was found that the timber band limited the out-of-plane deflection and allowed lower acceleration amplification at the top of the wall. Furthermore, the seismic band limited the crack propagation and prevented corner separation.

a b c

Figure 2.25: Shake table tests on U-shaped walls – (a) brick masonry, and (b) stone masonry [70], and c) two-storey timber laced masonry [71]

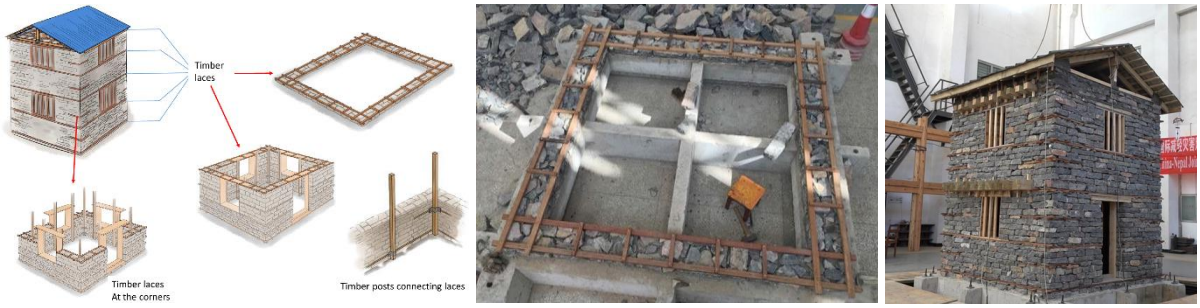

Figure 2.26: Shake table test of timber-laced dry stone masonry structure [72]

Figure 2.27: Shake table testing for timber-reinforced earth block masonry [73]

Conclusion

Experimental studies have extensively evaluated the performance of unreinforced masonry under lateral loads. Pull down tests examined the out-of-plane response of RE walls and found rapid decrease in load capacity after minimal deflection [68]. In-plane tests utilized DIC, revealing the timber's role in enhancing ductility, energy dissipation, and structural integrity [65-67]. Out-of-plane pushover tests, crucial in assessing masonry response under lateral loads, evaluated performance, validated analytical models, and guided seismic design principles. Such tests have emphasized the importance of bond types in masonry performance [69]. Shake table tests, another experimental method, demonstrated masonry's seismic performance [70, 71]. Notably, few tests conducted on masonry with embedded timber highlight timber's positive impact on masonry in confining cracks, distributing loads, enhancing structural integrity, and preventing total collapse [72, 73].

2.8. Numerical methods

Masonry, unlike reinforced concrete or steel, has very low tensile strength. This renders a linear elastic approach ineffective in assessing its response. Nevertheless, as computational capabilities have grown exponentially in modern times, there has been an increase in the application of nonlinear analyses. The choice of numerical models varies widely, contingent on the intent of the analysis, from computational-based simplified strategies such as the lumped mass method for dynamic analysis, to the equivalent frame method using truss and beam components, to macro-element modelling.

Advanced nonlinear Finite Element (FE) analyses are competent in predicting and studying the response of a masonry structure. However, results from FE models need to be validated and calibrated by experiments. It should also be noted that FE models are particularly sensitive to boundary conditions, local mechanisms and loading conditions.

2.8.1. Finite element modelling

The Finite Element Method (FEM) allows a more detailed analysis, with different methodologies and modelling strategies for different structures depending on varying geometry, material, and scale. Two predominant alternative strategies are the discontinuous and the continuous models. The former, also known as discrete crack models, exhibits a non-continuous displacement field. Conversely, the continuous model prohibits any separation between elements. Instead, the crack is *smeared* along the elements. While the FEM facilitates the representation of a structure's complex geometry, more comprehensive models invariably increase the time required for both model construction and subsequent analysis. Thus, establishing appropriate levels of model simplification is critical before starting the analysis.

According to Lourenco (2009), numerical characterisation of masonry can be done using two predominant approaches, micromodelling and macromodelling. The former examines the discrete components, such as brick and mortar. In contrast, the latter perceives masonry as a composite material. Thus, three primary modelling strategies emerge as shown in Figure 2.28 – detailed micromodelling, simplified micromodelling and macromodelling.

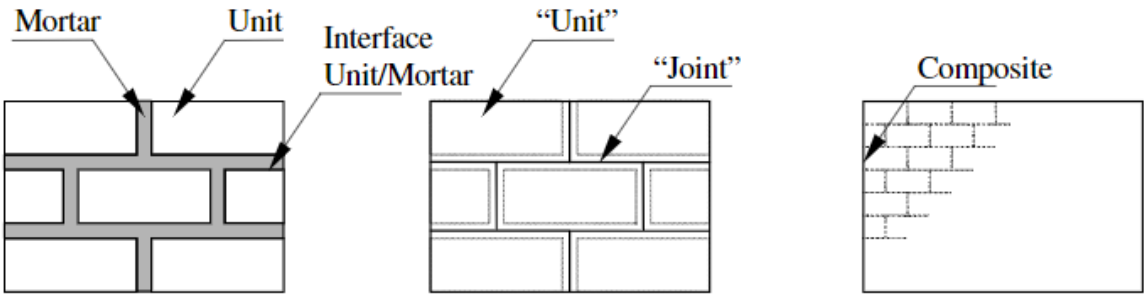

Figure 2.28: Modelling strategies for masonry structures: (a) detailed micromodelling; (b) simplified micromodelling; (c) macromodelling as detailed in [74]

A universally optimal modelling approach does not exist; the selection of a modelling technique depends on the available computational time and resources, demands of the analysis and balancing of accuracy and simplification. Each strategy has unique advantages tailored to the specific use cases.

2.8.1.1. Micromodelling

Individual bricks (or units) and the mortar present in the joints are represented through continuum elements. The interface between a brick and its accompanying mortar is expressed through discontinuum elements. Since each unit is modelled discretely, it allows the model to capture the real geometry of the wall. This framework has the possibility to incorporate both the physical properties of the brick and the mortar, such as Young's modulus, Poisson's ratio, and inelastic properties. The role of the interface is noteworthy, as it is a potential location for crack development or slippage. This strategy allows to scrutinise the interaction between the brick, mortar, and their shared interface. Notably, micromodelling is more equipped at describing and capturing local behaviour of masonry [74].

2.8.1.2. Simplified micro (Meso) modelling

Simplified micromodelling describes each masonry unit as an individual unit and the interaction between the masonry units and the mortar is also explicitly modelled. The masonry units are expanded in geometry such that the representation of brick-mortar interfaces and the mortar can be lumped into one single discontinuum interface element at the joint, which is also the location of potential fracture and slip. The material properties of the combined unit is associated with the properties of both mortar and the masonry unit. A limitation of this method is the exclusion of the effect of Poisson's ratio of the mortar [74]. Simplified micromodelling is a balanced compromise between the higher accuracy of detailed micromodelling and computational efficiency of macromodelling.

2.8.1.3. Macromodelling

Continuum-based models in macromodelling focus on the representation of the masonry as a homogeneous material without specifying individual discontinuities. This approach does not differentiate between discrete masonry units, mortar and interface, but considers masonry as a homogeneous continuum with either orthotropic or isotropic properties [74]. Due to the approximation of material models, the computational demand of the analysis is significantly reduced. Since the entire wall is considered to be a homogenous block, the damage is spread throughout the continuum element.

Macromodelling has another significant advantage in its ability to auto-generate a mesh independent of unit dimensions. Mesh sizes can be adjusted according to either the required accuracy of the result or the computational cost. While significant computational resources and time is needed for intricate structures, for symmetrical, simple structures as the one used for this study, it offers a suitable choice. Moreover, as macromodelling is a simplified

approach with lesser demands placed on computational resources and time taken to build the model, it is more suited to practical applications in engineering.

2.8.2. Constitutive models

Constitutive models help predict the response of materials under varying conditions by describing the relationship between two physical quantities, such as stress and strain. Simpler constitutive models based on linear elastic behaviour of the material do not capture the nonlinear response of masonry occurring due to its composite nature. Many constitutive models have been developed to incorporate the varying strengths and softening natures of the masonry due to its orthotropy. These models are based on three major approaches – plasticity, smeared cracking, and damage mechanics. Amongst these, the numerical model developed for this study is based on the smeared cracking approach.

2.8.2.1. Total Strain Rotating Crack model (TSRCM)

The *smeared crack* approach is a material model that distributes the displacement differences on both sides of a crack within the element width. Traditional crack models start with an isotropic assumption for the material, shifting to orthotropic post-cracking and with the crack direction fixed to the initial direction. An alternative cracking model is the total strain crack model (TSC), which allows cracks in two perpendicular directions. This approach, however, encounters *shear locking* issues that can be prevented by employing rotating crack models. The cracking in this material model starts when the maximum principal stress just exceeds the tensile strength of the material. Initially, the crack orientation is normal to the strain, however in the TSRCM, it rotates along with the principal strain axes. Due to this mechanism, the approximation of the crack direction is better finally, if erred at the start. TSRCM does not require user definition input for shear behaviour.

2.8.3. Shell 2D v/s Solid 3D elements

2D elements have been employed by many researchers to conduct numerical analysis of masonry structures [75]. 3D elements, though computationally heavy, are utilised specifically for examining out-of-plane behaviour [76].

Conclusion

Masonry, distinct from materials such as reinforced concrete or steel, possesses low tensile strength, making linear elastic analyses unsuitable. The rise in computational capabilities has, however, facilitated the application of nonlinear analyses. Numerical models for masonry vary, including simplified strategies such as the lumped mass method, to advanced techniques like macro-element modelling. The Finite Element Method (FEM) is widely used, with choices between discontinuous (discrete crack models) and continuous models. Masonry can be numerically characterized using micromodelling, which examines discrete components like brick and mortar, and macromodelling, which views masonry as a composite material. Each method has its advantages depending on computational resources, desired

accuracy, and specific requirements. Constitutive models explain the relationship between material attributes such as stress and strain. The chosen model for the discussed study uses the smeared cracking approach. Researchers have frequently used 2D elements for numerical analysis of masonry structures, while 3D elements, though more computationally intensive, are essential for studying out-of-plane behaviours.

2.9. Numerical studies

Many researchers have investigated the response of masonry walls through FE modelling. The approaches used vary from micro, simplified micro (meso) to macromodelling. Wangmo et al. (2019) developed a macro and micro FE model to predict the response of a rammed earth (RE) block structure and both closely simulated the crack patterns observed in the pull down tests. The validated macromodel was used for a parametric study to examine the influences of material and physical properties on the response of the wall. It was found that the elastic modulus affected the pre-cracking phase while the density of the RE wall affected the post-peak response, the tensile strength of the RE had minimal effect on the response. Additionally, it was found that increasing the physical characteristics, such as the thickness of the wall and the vertical load on top of the wall, enhanced the rocking resistance capacity of the wall.

Chácara et al. (2017) conducted FE modelling using macro continuum and simplified micromodelling numerical approaches to evaluate the structure and compare the response of the numerical model with the experimental response obtained from shake table testing. Static nonlinear (pushover) analyses were performed to assess the out-of-plane response due to incremental loading, and dynamic non-linear analyses were conducted to evaluate the collapse mechanism. Both techniques of modelling simulated the in-plane experimental response well. The numerical study also concluded that when the macromodelling approach is used in conjunction with the cracking model, rotating crack formulation should be used instead of the fixed crack formulation.

2.9.1. Timber elements in masonry

Many researchers have explored the use of timber as horizontal bands, braces or beams in masonry structures to improve the global seismic performance. Angulo-Ibáñez et al. (2012) found that merely placing timber braces at the corners of an earth-based wall increased the collapse load by 48%. Timber ring beams were found to be the best option to reinforce earth-based walls against horizontal loads as they enhanced the connection between orthogonal walls and achieved better distribution of the horizontal load, increasing the collapse load of the structure by 118%.

Khadka et al. (2023) conducted 3D FE numerical analysis on unreinforced stone masonry buildings (Figure 2.29a) of Nepal and compared them with a reinforced version (Figure 2.29b). Engineering masonry model was used with a combined cracking, crushing, shearing behaviour. The results of the static pushover analysis indicated an improvement of 73.5% in lateral strength compared to the unreinforced version (Figure 2.29c). Though this improvement includes the combined contribution of all three improvements – buttresses,

timber bands and roof-to-wall connections, it still provides a promising insight into capacity increase due to timber bands. Lourenço et al. (2019) conducted a seismic assessment to find that after strengthening (Figure 2.30), the retrofitted Church Kuno Tambo (in Peru) met the performance criteria and local seismic demand (Figure 2.31a). The authors also found that the strengthening led to the distribution of seismic load between lateral and transversal walls (Figure 2.31b) and increased energy dissipation. The nonlinear material properties of the numerical model were calibrated and informed by pull-out tests conducted on adobe masonry with embedded timber bands.

Parajuli (2009) conducted a numerical analysis to find that horizontal wooden bond beams effectively confined the walls and improved the seismic response of dry and mud-bonded stone masonry houses of different configurations to low acceleration earthquakes (Figure 2.32). Misir and Yucel (2023) simulated quasi-static out-of-plane experimental tests by conducting static pushover analyses on a FE model using the Concrete Plasticity Damage (CDP) material model in the ABAQUS software. The maximum principal strain profile was found to be similar to the experimental crack pattern in terms of damage distribution throughout the wall (Figure 2.33). Ortega et al. (2018) compared a two-storey rammed earth structure with and without timber laces to find that the inclusion of timber laces almost tripled the maximum capacity of the building and delayed the crack propagation (Figure 2.34).

Studies have also been conducted on the ability of macromodelling to simulate the experimental out-of-plane response of masonry walls and comparing that to micromodelling. [85] used detailed FE micromodelling, FE macromodelling and discrete element modelling to simulate the experimental response of a drystone U-shaped masonry wall and a similar specimen but with mortar-bound masonry. The study revealed that macromodelling was able to identify the areas of the wall with maximum damage even if it was not able to capture the asymmetrical cracking. Al Qablan et al. (2019) also employed micro and macromodelling techniques to understand the influence of the embedded wooden beams in stone masonry by using both, tied and frictional surfaces to depict the relationship between the two surfaces. The authors use a continuum, plastic-based, damage constitutive model (CDP) to represent the behaviour of the masonry walls and found that the shear stress in the stone masonry reduced by 33%.

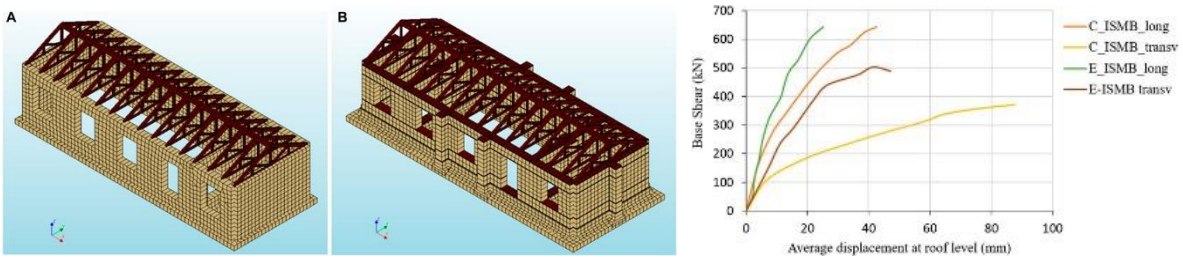

a b c

Figure 2.29: Numerical modelling of stone masonry buildings in Nepal - (a) unreinforced, (b) enhanced, (c) comparison of results as detailed in [80]

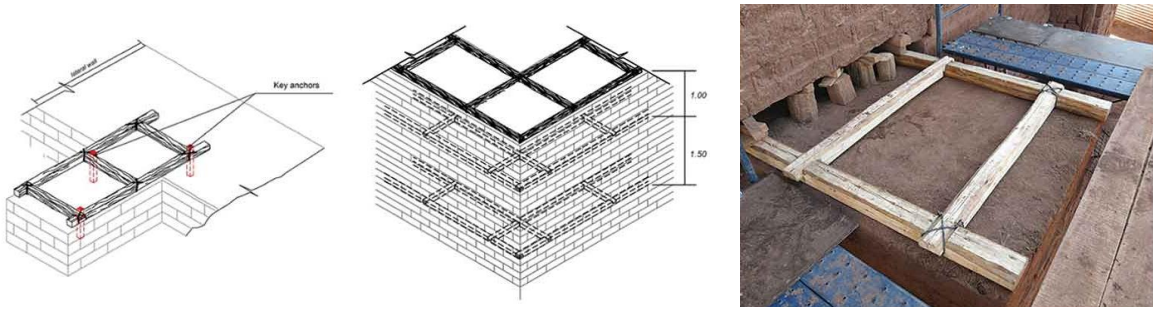

Figure 2.30: Traditional strengthening techniques applied in the Church Kuno Tambo by [81]

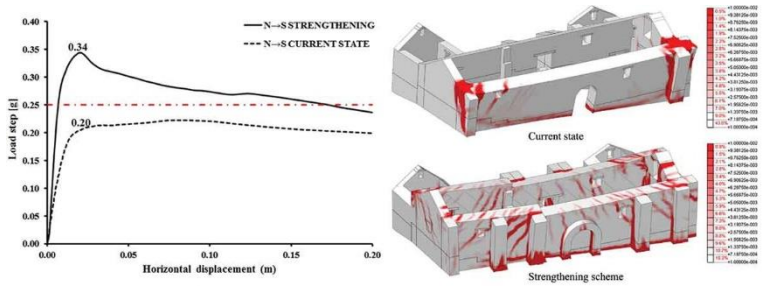

a b

Figure 2.31: Church Kuno Tambo : (a) load-displacement diagram, (b) maximum principal tensile strain distribution [81]

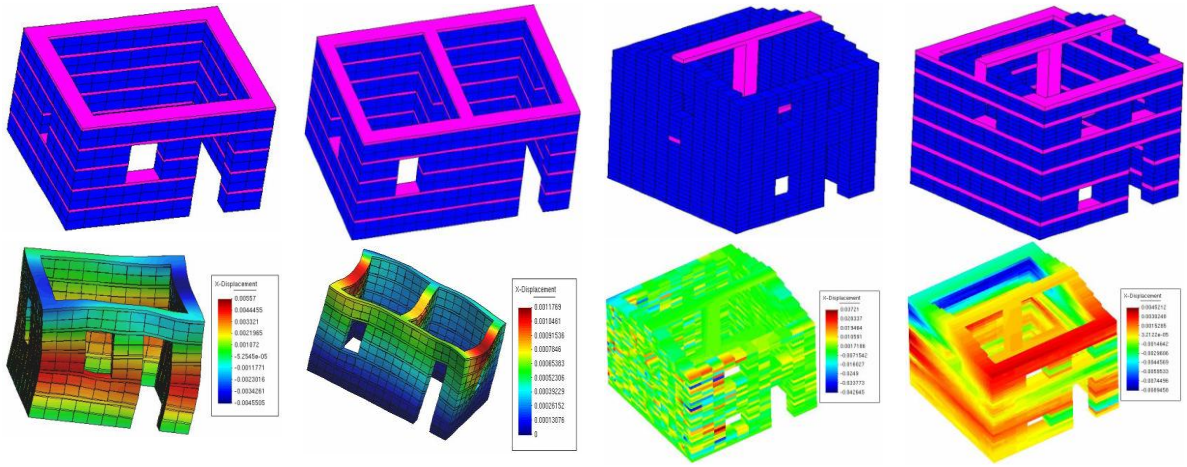

Figure 2.32: Numerical models and deformations for dry and mud-bonded stone masonry [82]

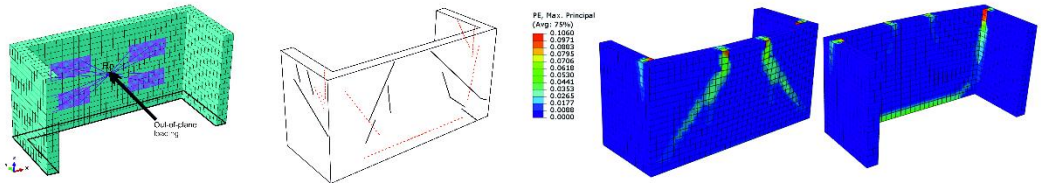

a b

Figure 2.33: Double-leaf masonry - (a) Numerical model in ABAQUS, and (b) Maximum principal tensile strain distribution [83]

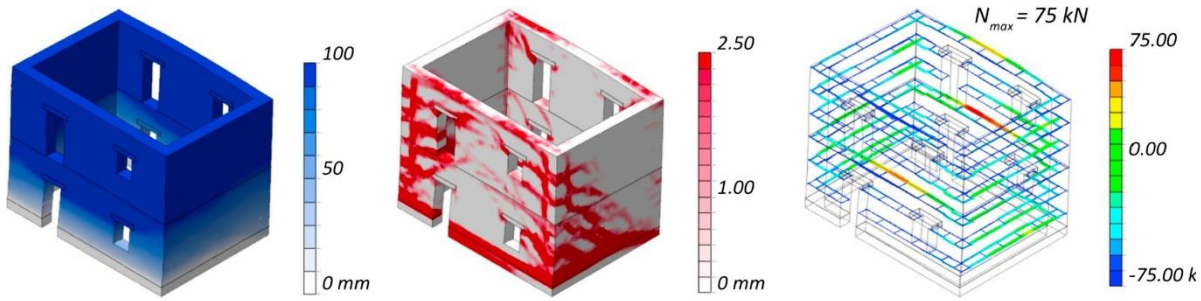

a b c

Figure 2.34: Results from numerical analysis of timber-reinforced rammed earth building – (a) maximum displacements, (b) crack width, and (c) stress in timber elements from [84]

2.9.2. Timber-masonry interface

Although timber has been used with stone masonry for centuries, not many studies have investigated the behaviour of the interface between timber and stone masonry. Therefore, the literature review was expanded to include the behaviour of timber with other masonry units as well, such as brick, adobe, rammed earth, etc. Some studies have also explored the numerical modelling of buildings with masonry and timber in combined action. While some of these studies are done on half-timbered walls with a timber frame and masonry infill, fewer are done on timber-laced masonry. The key difference between the two is the load-carrying mechanism. While timber frame resists both, the vertical and the horizontal load in the former; load-bearing masonry plays the role of the vertical load bearer in the latter while timber resists the lateral loads. However, these studies provide insight into the frictional behaviour at the interface of timber and masonry.

Mirra and Ravenshorst (2019), in their study, report a timber joist-masonry connection (Configuration A in the study, Figure 2.35a) that was characterised mainly by frictional behaviour and peak and post-peak friction values were reported. Almeida et al. (2020) conducted extensive cyclic friction tests for mortar-timber and timber-timber triplets (Figure 2.35b) to find that the average static friction coefficient values varied between 0.6 and 0.8. Endo and Goda (2023) conducted pull-out tests (Figure 2.36a) to characterize the frictional behaviour between a timber beam and brick masonry. The authors also conducted a numerical analysis (Figure 2.36b) to simulate the pull-out test using a combined cracking-crushing-shearing interface material at the bed joint between timber and masonry which presented similar results to the experiment. Dimovska et al. (2022) modelled the interface between timber beams and masonry vaults in a floor (Figure 2.37a) using conservative frictional values. Costa et al. (2015) made use of multi-body dynamics concentrating the nonlinearities at contact regions to study local mechanisms (Figure 2.37b). One of such contact regions modelled as interface elements was between masonry and timber beams. Coulomb friction model has also been used to model the interface between masonry and lumber [92]. Endo and Hanazato (2022) defined the connections between a masonry wall and timber beams by a nonlinear elastic friction model defined only by friction angle and cohesion without any tension failure (Figure 2.38a). Al Qablan et al. (2019) conducted micro- and macromodelling to prove the shear stress reducing role of embedded wooden string courses as an anti-seismic device in sandstone masonry. The authors used tied and frictional surfaces to localise the

occurrence of slipping while using a continuum, plastic-based damage model in the ABAQUS software to model the behaviour of masonry walls (Figure 2.38b). AlShawa et al. (2022) simulated the non-linear dynamic response from shake table tests (Figure 2.39a) of a half-scale masonry building by conducting 3D FEM-DEM modelling on LS-DYNA (Figure 2.39b). The shear response of the contact surface between timber and masonry was governed by a Mohr-Coulomb model with shear failure limit stress (SFLS) being the cohesion. Illampas et al. (2014) modelled a scaled adobe masonry structure to simulate the response from shake table testing (Figure 2.40). The interface between timber and masonry was modelled by assigning timber members as the master surface due to higher stiffness than masonry.

a b

Figure 2.35: a) Timber joist and brick masonry, frictional behaviour from [87], and b) Cyclic friction triplet test setup between mortar and timber from [88]

a b

Figure 2.36: Mud mortar masonry and timber – (a) Pull-out test, and (b) Numerical model from [89]

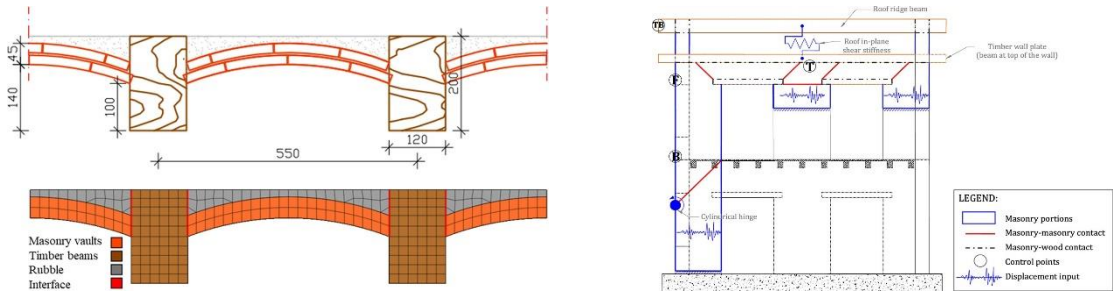

a b

Figure 2.37: a) Finite element model Jack arch floor with timber beams and masonry vault from [90], and b) Numerical model representation from [91]

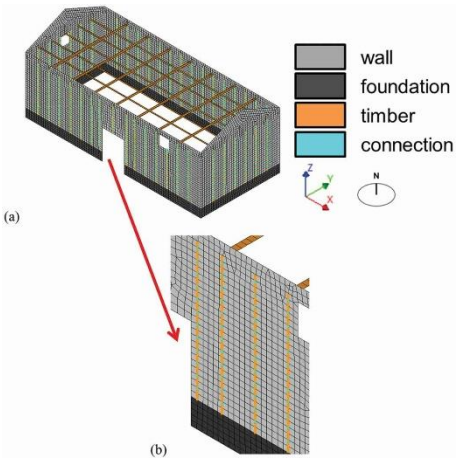

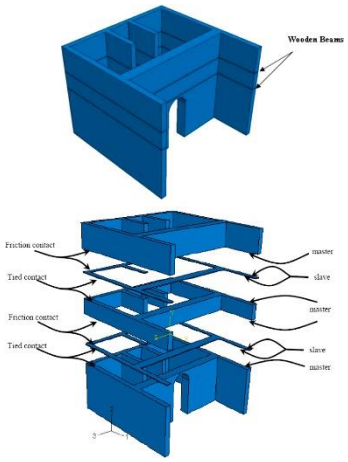

a b

Figure 2.38: Numerical model of a) Kobayashi warehouse from [93], and b) Qasr el-Bint Palace from [86]

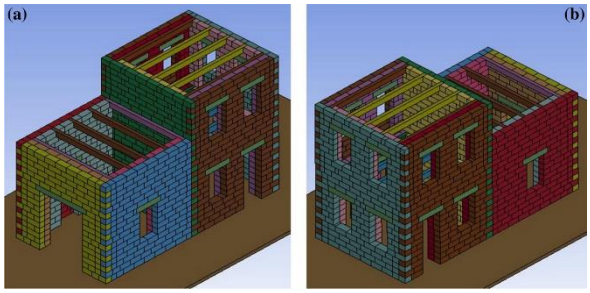

a b

Figure 2.39: Stone masonry building – (a) Physical model, and (b) FEM-DEM model from [94]

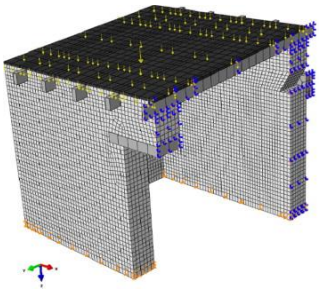

a b

Figure 2.40: 1:2 scale adobe masonry building – (a) Physical model, and (b) Numerical model from [95]

Conclusion

Researchers have investigated the response of masonry walls through Finite Element (FE) modelling techniques. These investigations span various approaches from micro to meso to macromodelling. Few studies have been conducted with a focus on the enhancement of masonry structures using timber. Timber, when introduced in masonry as braces, bands, or beams, substantially improves seismic performance. The incorporation of timber elements, such as laces, has also shown to considerably increase the load-bearing capacity of structures, delaying collapse. Meanwhile, fewer studies have focused on the interaction between timber and masonry, especially the frictional behaviour at their interface. Most investigations indicated friction coefficients between 0.5 and 0.8 for the masonry-timber or mortar-timber interface. Furthermore, there is a notable difference in load-carrying mechanisms between half-timbered walls and timber-laced masonry, with the latter relying on masonry for vertical loads while utilizing timber for lateral loads.

In light of the literature review conducted and the insights generated by the previous studies, for the Bhatar building typology with stone masonry and timber bands, an appropriate modelling strategy can be devised. Within the scope of this thesis, macromodelling is chosen for the computational efficiency and time requirements. Furthermore, rotating crack formulation available in DIANA FEA – Total Strain Rotating Crack Model (TSRCM), is used to represent the behaviour of masonry under vertical and horizontal loads.

2.10. Benchmark study

From the literature, a study was identified that represented a good benchmark for this thesis. This chapter elaborates on the chosen set of studies at the University of Minho. [96] present results from an experimental campaign where the stone masonry walls were subjected to out-of-plane load using airbag pressure in the controlled environment of a laboratory. Three specimens of the walls were tested, a) unreinforced, b) reinforced with steel ties, c) reinforced with timber laces (Figure 2.41a). The specimen with steel ties is not included here as it is not pertinent for the scope of this thesis. While the construction of the wall was done according to Portuguese vernacular architecture, it closely resembles the Bhatar technique. This is the reason for choosing this group of studies as the benchmark tests. Besides the out-of-plane test, the authors also simulated the experimental response of the wall through numerical analysis, conducted on DIANA FEA. The study found that vernacular strengthening techniques such as steel ties and timber laces substantially improved the seismic performance compared to the unreinforced specimen.

2.10.1. Experimental assessment

Direct and indirect sonic tests were done on the walls to generate first approximations of the elastic properties (Young Modulus and Poisson Ratio) of the masonry. Then, dynamic characterization tests were carried out using ambient vibrations to determine the natural frequencies of the walls. Finally, the out-of-plane uniform horizontal load was applied to the rear façade of the frontal wall through airbag pressure in order to simulate lateral load during an earthquake (Figure 2.41b and Figure 2.41c). To mimic the dead-load of a timber roof, vertical load was also applied to the lateral walls (Figure 2.41d). The displacements were measured through linear variable differential transducers (LVDTs).

2.10.2. Analysis of experimental response

The authors analysed the response of the wall to cyclic load by capacity curves, visual observation of damage, drift limits and energy dissipation. The lateral force capacity of timber-reinforced wall was found to be 52% higher than the unreinforced one. From the cracking patterns, it was observed that the unreinforced wall's failure was governed by the detachment of the lateral walls from the frontal walls even though bending of the frontal wall was observed. On the other hand, the authors attributed the lack of vertical cracks at the junction of transversal walls on the inner corners of the timber-reinforced wall to the improved connection between the orthogonal walls due to the timber laces. Also, the higher number of cracks in the timber-reinforced masonry wall was credited to the damage being distributed to a larger portion of the surface rather than higher localised damage and eventual failure as in unreinforced masonry (Figure 2.42). Furthermore, for an equal drift level, 53% higher dissipation energy was observed in the timber-reinforced wall than the unreinforced wall. Comparing the drift limits of both walls, it was found that the reinforced wall attained higher forces for the corresponding lateral drift.

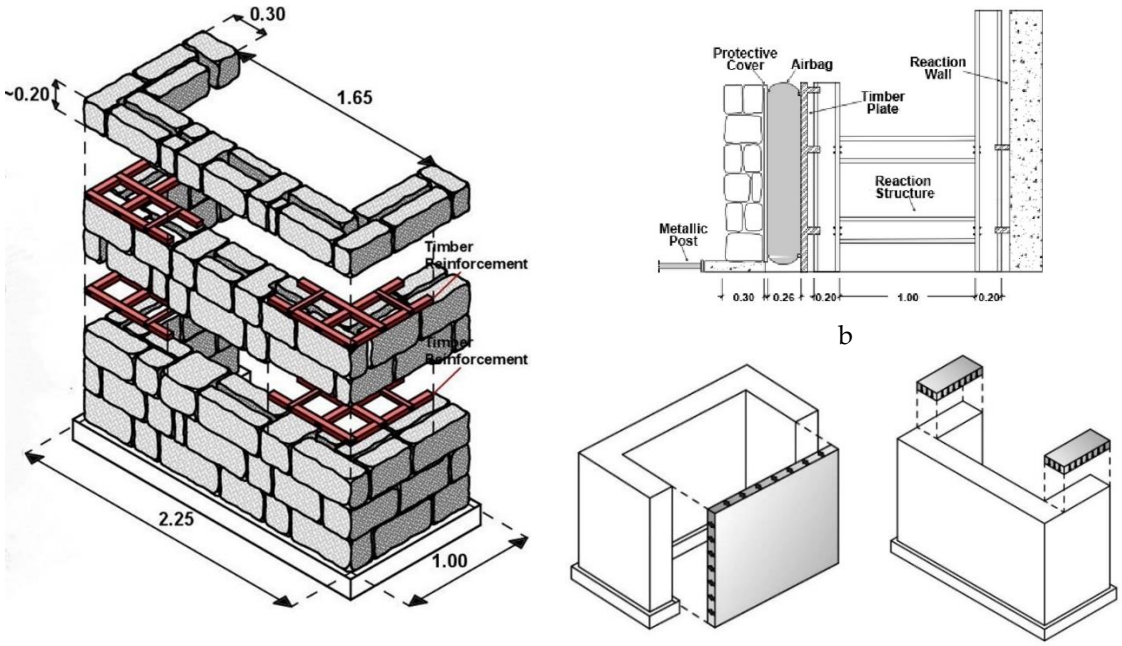

a b c d

Figure 2.41: Experiment details (a) Timber-reinforced masonry details, (b) Test set-up, (c) Vertical load configuration, (d) Horizontal load configuration from [96]

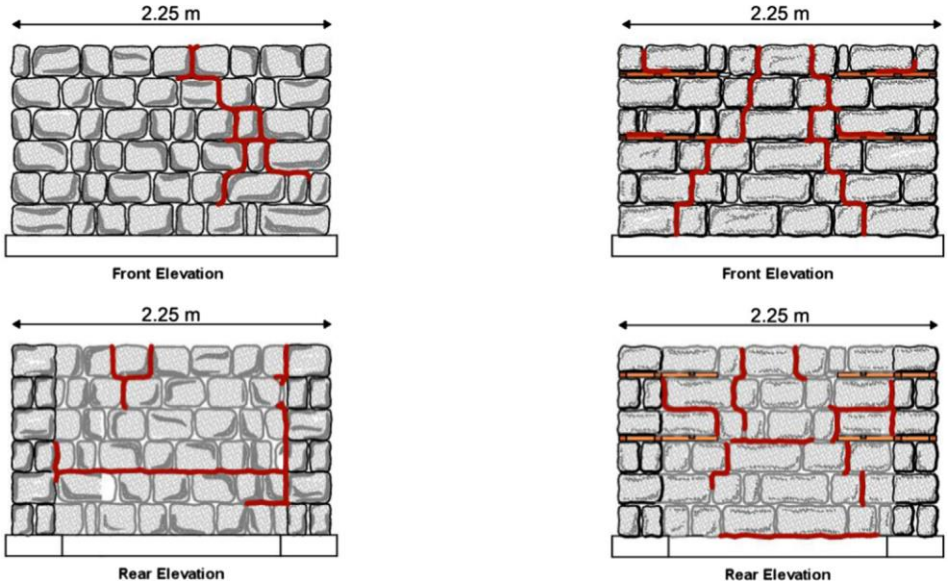

a b

Figure 2.42: Experimental crack patterns in - (a) Unreinforced masonry, and (b) Timber-reinforced masonry from [96]

2.10.3. Numerical analyses

Finally, a pushover analysis was conducted to compare the numerical and experimental results (Figure 2.43). The 3D numerical model was created in the DIANA FEA software with the Total Strain Rotating Crack model used to define the non-linear behaviour of stone masonry. The numerical modal analysis allowed the authors to calibrate the elastic properties predicted from the sonic tests. Non-linear properties were defined using the capacity curves from experimental out-of-plane tests.

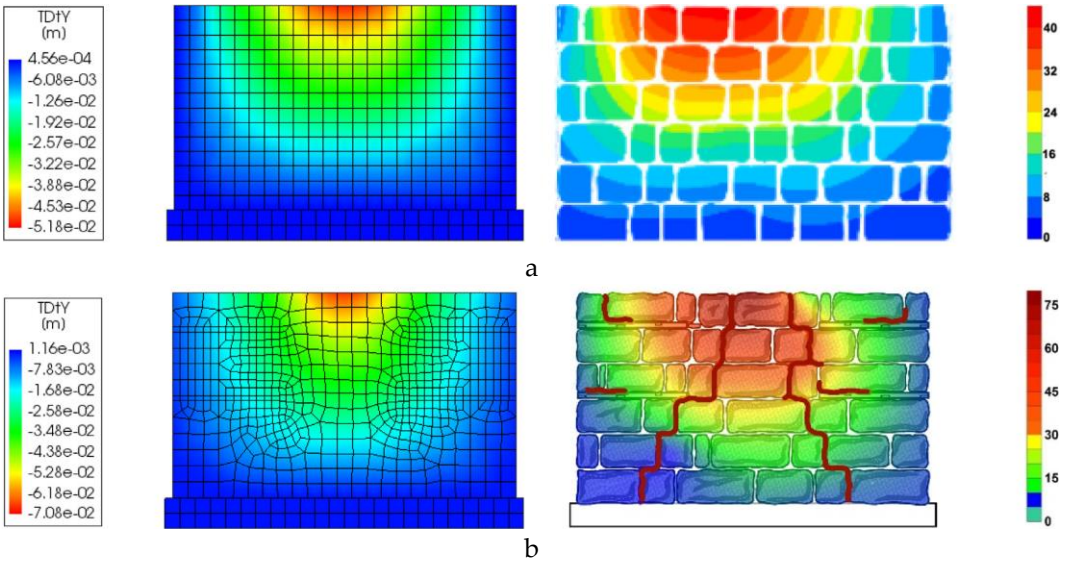

Figure 2.43: Comparison of Numerical and Experimental displacement contours from [96] – (a) Unreinforced masonry, and (b) Timber-reinforced masonry

The stiffness properties of the base interface were also calibrated. The numerical models were subjected to the boundary and load conditions corresponding to the experimental tests. The numerical models were able to attain maximum load values close to the experimental ones, but post-peak, the numerical model showed increased softening compared to the experimental curve. Expectedly, the maximum displacements were noted at the top of the frontal wall mid-section and the base of the frontal wall experienced extensive damage due to rotation. The results obtained through numerical analyses are further elaborated in Chapter 4.1 and are compared to those found in the literature mentioned in this chapter.

Conclusion

An experimental and numerical study investigated the seismic performance of stone masonry walls [96]. The walls were tested under out-of-plane load using airbag pressure in a controlled laboratory setting. Three wall specimens were evaluated: unreinforced, steel-tie reinforced, and timber-lace reinforced, with the steel-tie variant omitted from this report. The construction mirrored Portuguese vernacular architecture, comparable to the Bhatar technique. Experimental tests assessed the elastic properties of the walls and their response to simulated seismic loads. The timber-reinforced wall exhibited a 52% higher lateral force capacity than the unreinforced one, with the timber lacing resulting in better energy dissipation and crack distribution. Numerical analyses using DIANA FEA were conducted, comparing experimental and modelled results. While the models approximated maximum load values well, post-peak they showed increased softening compared to experimental observations. This study, due to the resemblance of the masonry wall to a Bhatar structure, and the detailed experimental and numerical results, was chosen as the benchmark study for this thesis. Comparison of numerical results with the benchmark will be further discussed in the subsequent Chapter 4.

2.11. Seismic analysis and Assessment

An evaluation of seismic performance of a structure is predicting how a structure behaves under earthquake-induced forces. This prediction in turn ensures a structure's ability to safeguard human life, protect property, and maintain function during and after seismic events. Performance-Based Design (PBD) is a design methodology used to achieve seismic performance where instead of merely satisfying prescriptive code-based requirements, the design aims for specific outcomes such as life safety, immediate occupancy, or collapse prevention under different seismic intensities. Seismic demand represents the forces, deformations, and other dynamic responses imposed on a structure due to an earthquake. It is essentially what the earthquake "demands" of the structure. In order to be considered *safe*, the seismic capacity of the structure should exceed the seismic demand that the earthquake imposes on the structure. It describes the maximum earthquake-induced force (force capacity) or deformation (displacement capacity) that a structure can withstand without experiencing a specified level of damage or failure. Force and displacement capacity dictate limit states of a structure – or its ability to perform safely or functionally, beyond which it signals a potential for damage or failure. Different limit states might include serviceability (normal use without excessive deformation or damage) or ultimate (point of imminent or actual collapse).

In summary, a structure should be designed according to PBD to handle the seismic demand placed on it by earthquake loads in the local area, without exceeding the prescribed limit states.

2.11.1. Seismic analysis

A seismic analysis predicts the response of structures to earthquake-induced loads. It depends mainly on two factors – (i) loading condition, and (ii) material properties. Straightforward analyses such as linear elastic analysis operate on the premise that the response of the structure lies in the linear elastic phase, implying that the structure reverts to its original state without residual deformations while the inelastic component is accounted for by applying force reduction through a behaviour factor. However, this neglects the nonlinear behaviour of masonry which rules that the structure does not return to its original state after an earthquake. Due to the very low tensile strength and quasi-brittle nature of masonry, it becomes pertinent to choose the appropriate way to analyse the structure.

The Equivalent Lateral Force Method (ELF) provides a simplified procedure using static lateral forces to capture the structure's maximum expected earthquake response, influenced by factors like weight and seismic conditions. The building is often idealized as a Single Degree of Freedom (SDOF) system for the primary mode of vibration, making the analysis relatively accurate and tractable for structures that are regular in both plan and elevation and that do not have significant contributions from higher vibration modes. For more complex and irregular buildings, this simplification is less accurate.

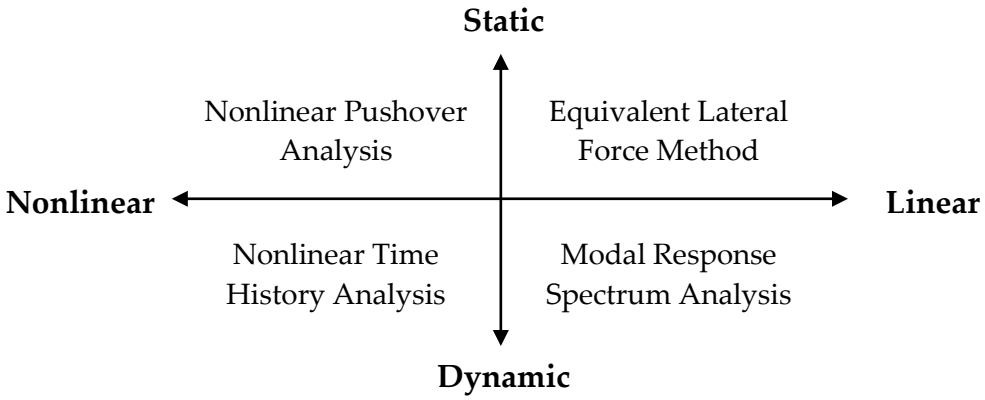

Figure 2.44: Overview of analyses for the evaluation of seismic response of structures , from [97]

Modal Response Spectrum Analysis (MRSA) decomposes the structural response into several modes of vibration treating each mode as an independent SDOF system. The responses of each of these modes are combined to get a total response. MRSA captures the dynamic effects of higher modes, significant especially in tall or irregular structures. However, since this method assumes linearity, if a structure undergoes significant changes in properties (such as stiffness) during the earthquake or experiences significant inelastic (beyond elastic limit) behaviour, then nonlinear analyses are more appropriate.

Ideally, nonlinear analysis acknowledging inelastic behaviour mimicking dynamic, time-varying earthquake load would predict the response of the structure precisely. Nonlinear Time History Analysis (NLTHA) integrates specific recorded or artificial ground motion histories to evaluate a structure's time-dependent response. NLTHA describes the detailed sequential response of a structure, therefore providing better understanding of progressive damage. However, it is also computationally demanding, presenting with limited practical applications for complex and large structures. This leads to its limited practical application in the field.

A solution to this problem is the nonlinear pushover approach subjecting the structure to progressively increasing lateral loads, essentially *pushing* it until failure. The selection among these methods invariably hinges on factors such as expected seismic loading conditions, the desired balance between computational efficiency and accuracy, and the inherent characteristics of the structure and its materials.

2.11.1.1. Static Nonlinear (Pushover) Analysis

Pushover analysis is a static, nonlinear procedure to assess the performance of structures subjected to seismic loading. It estimates a structure's vulnerability to seismic activity by characterizing its strength and deformation capacities. It involves applying an incrementally increasing lateral load pattern to a structural model until a predefined level of damage or target displacement is achieved. The relationship between applied lateral load (base shear) and the resulting displacement at a control point (example, roof) can be plotted to produce a capacity (or pushover) curve. The lateral load pattern is defined based on an assumption of

the distribution of the inertial forces over the height of the structure during an earthquake – either based on proportional mass distribution or on the first mode of vibration.

Pushover analysis provides insight into the failure mechanisms, most damaged regions, and sequence of yielding in a structure. It also predicts the inelastic behaviour and vulnerability of the structure. It is often used for performance-based design, where a specific performance level is targeted. However, it assumes the load increment to be monotonic, which does not capture the dynamic effects of multiple loading-unloading cycles during an actual earthquake. Moreover, it does not accurately capture the distribution of inertia forces during a real earthquake as it considers a single mode of vibration. However, multi-modal pushover (Modal Pushover Analysis) methods consider more than one mode of vibration.

Pushover analysis offers a more detailed understanding of a structure's seismic performance than a linear static analysis but requires fewer computational resources than a full nonlinear dynamic analysis. However, using pushover analysis implies two assumptions to be made for the structure. First, the structure should be sufficiently regular, in order to be approximated with the first mode. Second, the out-of-plane failure mechanisms should be effectively prevented so that the response can be quantified with the in-plane behaviour.

2.11.1.2. Modal Pushover in DIANA

DIANA [98] uses a generalized mode shape dependent load as input load for modal pushover analysis given by the below equation:

$$f_{push} = \sum_{j} a * M * \phi_i * x_j$$

where a is the specified acceleration,

M is the mass matrix,

ϕ_i is the ith eigenvector (normalized with respect to the mass matrix),

x_j is the earthquake direction j

The distribution of the inertial forces is based on the equivalent lateral force (ELF) modal distribution, approximately proportionate to the first mode shape.

The load capacity of a structure without box behaviour evaluated by Pushover analyses proportional to the first mode shape has been found to be in good correspondence with Nonlinear Dynamic Analysis (NDA) [99]. Another study has found the mass-proportional Pushover analysis to have the closest correspondence for force distribution and maximum shear capacity with NDA [100]. However, many authors have highlighted the limitation of a pushover analysis to predict the out-of-plane behaviour of the structure. In this study, an approach is attempted combining 3D elements along with pushover analysis to capture out-of-plane failure mechanisms and compare them with experimental failure mechanisms found in literature.

2.11.2. Seismic Assessment

Seismic assessment is essential in understanding how structures respond to earthquake-induced forces, ensuring their safety and functionality during seismic events. Relevant methods used for seismic assessment of the Bhatar structure are presented in this section.

2.11.2.1. Capacity Spectrum Method

The Capacity Spectrum Method (CSM) is a further development of the pushover analysis to compare the pushover curve (capacity curve) with a demand curve (response spectrum) in a graphical format. By comparing the intersection points of demand and capacity, information about performance points and expected behaviour during a seismic event is provided. CSM is an analytical approach used to evaluate the seismic performance of structures. It combines aspects of both nonlinear static (pushover) analysis and dynamic response spectrum analysis to provide an estimate of a structure's likely behaviour under seismic loading conditions.

The capacity curve, showing the capacity of the structure to resist the seismic load, and demand spectrum, also known as the Acceleration-Displacement Response Spectrum (ADRS), are used to evaluate the structure in this method. CSM allows for the evaluation of a structure's performance under different seismic intensities, making it a valuable tool in performance-based seismic design. The method can also be used to assess the effectiveness of different seismic retrofitting strategies. While in Eurocode, a spectral reduction factor is provided to reduce the demand of the Acceleration-Displacement Response Spectrum, in IS code (Indian Standard Code), the reduction of demand is done through a slightly different method explained in Chapter 5.4. This analysis is based on the procedure described in IS 1893 (Part 1) : 2016 [101]. This method has been found to have good performance for symmetrical structures. As the one-room Bhatar structure evaluated in this study is a simple, symmetrical structure, Capacity Spectrum Method in combination with Pushover Analysis is used to conduct the seismic analysis.

2.11.2.2. IS 1893:2002

IS 1893:2002 has two criteria for the seismic design. Maximum Credible Earthquake (MCE) represents the most extreme earthquake effects defined by the code, while Design Based Earthquake (DBE) refers to the earthquake effects that are likely to be experienced by the structure at least once during the design lifespan. The standard stipulates that the design of the structure should be such that the structure is able to endure DBE without major structural damage and should survive MCE without collapsing. However, unlike Eurocode 8, the IS 1893:2002 does not specify a return period associated with DBE or MCE.

2.11.2.3. Limit States

The Eurocode specifies limit states for design and evaluation of structures. For seismic design, Eurocode 8 (EN 1998) employs three Damage Limit States (DLS) to classify the extent and type of damage a structure may experience during a seismic event.

No Damage Limit State (ND): This limit state represents the serviceability limit state for seismic design at which a structure is expected to remain virtually undamaged after an earthquake. The structure should remain operational, and only minor non-structural damage is considered acceptable. The structure response remains on the linear elastic spectrum. This limit state is associated with more frequent, lower magnitude earthquakes.

Damage Limitation Limit State (DL): At this limit state, slight structural damage is permissible, but the overall safety of the structure should not be compromised, and the structure should be repairable while retaining most of its stiffness and strength. This LS is associated with either the change in stiffness or the load-displacement curve. This state is associated with a 10% probability of exceedance in 50 years.

Severe Damage Limit State (SD): Severe Damage limit state is associated with the lateral drift corresponding to the maximum out-of-plane strength of a building, also defined as life safety limit state. The building cannot be used after the earthquake even if it does not collapse.

Near Collapse Limit State (NC): Near Collapse represents the ultimate limit state and is associated with the lateral drift that corresponds to the 20% decrease in the maximum lateral resistance of the structure in the post-peak phase. Structure should not collapse, ensuring that the occupants' safety is preserved. However, due to significant structural damage it is not economically feasible to repair the building. The NC limit state can be located by the lateral drift corresponding to the lateral resistance reduced by 20% relative to maximum load attained. This limit state is associated with a rare but strong seismic event, typically with a 2% probability of exceedance in 50 years.

Conclusion

Seismic analysis encompasses methods such as linear elastic, pushover analyses, and nonlinear time history, each catering to different structure complexities and desired accuracies. The Equivalent Lateral Force Method (ELF) simplifies dynamic earthquake effects into equivalent static loads, whereas Modal Response Spectrum Analysis (MRSA) captures dynamic effects from various vibration modes. Pushover analysis analyses the inelastic behaviour, by identifying potential failure points. Nonlinear Time History Analysis (NLTHA) is the most detailed, evaluating the dynamic response to time-varying loads but is computationally intensive. Seismic assessment tools, such as the Capacity Spectrum Method (CSM), evaluate structural performance by juxtaposing demand and capacity curves. Eurocode 8 classifies potential structural damage into limit states such as No Damage (ND), Damage Limitation (DL), Severe Damage (SD), and Near Collapse (NC), each indicating the extent of allowable damage.

Given the constraints and limited computational resources available for this study, Pushover analysis was deemed apt to assess the seismic response of the Bhatar structure typology. Further research conducting NDA and the subsequent comparison of NDA and Pushover analysis would result in a better assessment of the Bhatar typology. However, for the purpose of this study, the scope is limited to Pushover analysis.

3. Numerical model

To assess the seismic resilience of the structure, multiple pushover analyses were conducted. The performance of unreinforced masonry is compared to that of timber-reinforced masonry. A phased methodology was used, wherein the initial analysis was focused on a U-shaped wall for horizontal load and the results were compared to the experimental response found in literature. After a good correspondence was achieved with the benchmark tests, the numerical model was extended to a full-scale Bhatar building.

This section introduces the methodology used to develop the numerical model which is then used for the pushover analysis. The linear and non-linear material properties are derived from literature. The choice of element model, material model, cracking model and mesh is discussed. Further, the solution method and analysis parameters used for numerical analyses are presented. DIANA (DIsplacement ANAlyzer) Finite Element Analysis (FEA) software is an extensive multi-purpose 3D finite element simulation tool which is often used for advanced nonlinear analysis of masonry structures. For the purpose of this thesis, a detailed 3D finite element model (FEM) was developed in DIANA version 10.5 [98] with the intent to accurately simulate the structural behaviour of a masonry wall subjected to out-of-plane loads.

3.1. Finite element model

DIANA has three options for three-dimensional structural elements – tetrahedrons, pentahedrons and hexahedrons. The number of nodes depends on the interpolation functions for the displacement field. For linear, quadratic, and cubic interpolation, each edge has two, three and four nodes, respectively. A tetrahedron 3D element based on quadratic interpolation, leading to a twenty node element (CHX60 [98] shown in Figure 3.1a) was chosen to model concrete, masonry and timber elements. This element uses a 2 x 2 x 2 integration scheme. It should be noted that unlike a shell element, for a solid element the integration points are located within the element, not on the external surface. Therefore, the cracking has a delay rather than beginning the moment stresses on the surface exceed the tensile strength of the material.

The connection between the concrete base and the floor was modelled using three-dimensional plane quadrilateral interface elements (CQ48I [98] shown in Figure 3.1b) based on quadratic interpolation and using 3 x 3 Newton-Cotes integration scheme [98]. The connection between the concrete base and the masonry wall on the other hand is considered to be fully connected. The interface between the timber band and masonry has been modelled using two approaches – fully connected and interface elements. For the interface element, the frictional behaviour between stone and brick is represented by the Coulomb's friction model in DIANA (Figure 3.2).

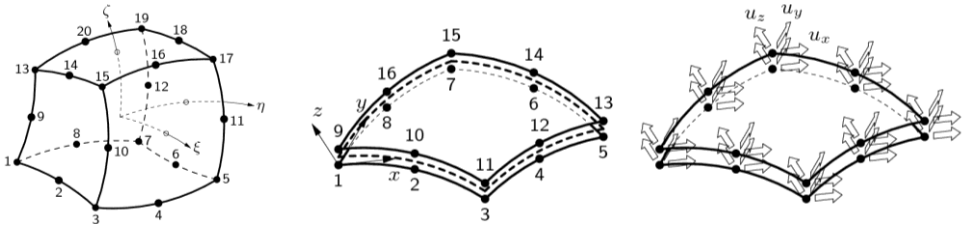

a b

Figure 3.1: Elements used for analyses – a) Solid 3D element used for masonry, concrete and timber, and b) 3D Interface element between concrete and floor [98]

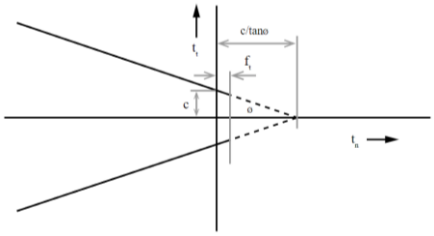

Figure 3.2: Coulomb friction criterion according to [98]

3.1.1. Geometry

The details and dimensions of the experimental wall provided by Murano et al. (2019) inform the geometry of the model. The geometry details of the numerical model constructed in DIANA are given in Table 3.1 and subsequently is shown in Figure 3.3.

Table 3.1: Dimensions of the masonry wall

Member	**Length**	**Width (Thickness)**	**Height (Depth)**
	(m)	(m)	(m)
Frontal wall	2.250	0.300	1.350
Lateral wall	1.000	0.300	1.350
Longitudinal timber beam	0.700	0.050	0.035
Transversal cross piece	0.200	0.035	0.025

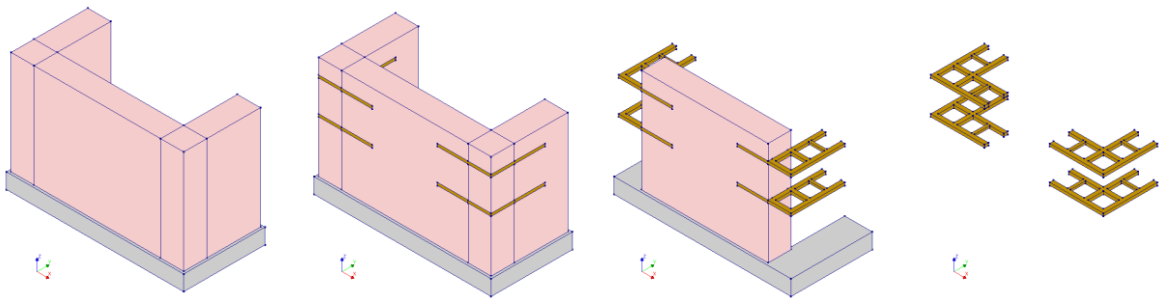

a b c d

Figure 3.3: Masonry walls model – (a) Unreinforced masonry, (b) and (c) Timber-reinforced masonry, and (d) Timber laces

3.1.2. Material model

Many material models are available to simulate the behaviour of brittle materials such as masonry, however, considering the literature, a smeared crack approach using the Total Strain Rotating Crack model (TSRCM) was used to model the non-linear behaviour of stone masonry. TSRCM has been found suitable to analyse primarily the cracking and the crushing response of the material. It is also relatively robust and reliable. TSRCM adopts a smeared approach for fracture energy. It provides multiple approaches to model the tensile and compressive behaviour. However, for the purpose of this research, exponential softening (Figure 3.4a) and parabolic curves (Figure 3.4b) describe the tensile and compression behaviour of the masonry, respectively.

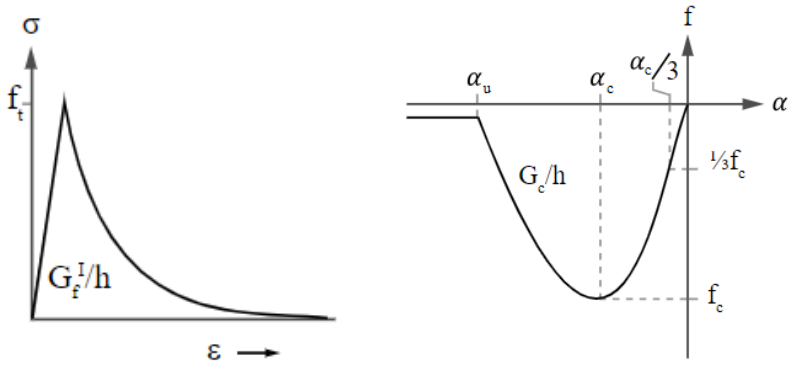

(a) (b)

Figure 3.4: Behaviour of masonry – (a) exponential softening tensile behaviour, and (b) parabolic compressive behaviour [98]

In the referenced literature, the timber elements did not show damage, hence all non-linearity is assumed to occur in masonry. It is anticipated that timber remains in linear range throughout the analysis. Therefore, timber and concrete are assumed to have linear elastic behaviour. However, the stresses developed in the timber elements are verified against the material strength in the post-processing phase.

3.1.2.1. Material properties

Since the model is validated through the benchmark experimental and numerical study, the material properties are taken from the study conducted by Murano et al. (2019). They are listed in Table 3.2. Properties of timber and concrete are given in Table 3.3.

Table 3.2: Calibrated material properties of masonry wall from [96]

Model	**Poisson ratio**	**Density**	**Young's Modulus**	**Strength**		**Fracture energy**	
				Compressive	**Tensile**	**Compressive**	**Tensile**
		kg/m³	MPa	MPa	MPa	N/m	N/m
Unreinforced	0.39	2495	3600	3.6	0.07	5760	12
Timber-reinforced	0.25	2482	2974	2.97	0.07	4760	12

Table 3.3: Material properties of concrete and timber from [96]

Material	Poisson ratio	Density	Young's Modulus
		kg/m³	MPa
Timber	0.2	600	10000
Concrete	0.2	2400*	31000

**Density of concrete was assumed*

3.1.2.2. Poisson's ratio

Total strain based models provide three choices for input parameters to include the lateral influence – a) Cracking, b) Confinement, and c) Poisson's ratio reduction. One key difference between the two iterative techniques described later in Chapter 3.2.1.1 is the input choice for the Poisson's ratio reduction parameter. DIANA FEA version 10.5 offers two choices for the reduction of Poisson's ratio through the Total Strain Rotating Crack model – a) No reduction, and b) Damage based reduction. For the former the behaviour under lateral cracking remains the same, while the former pertains to decrease of Poisson's ratio resulting in increased damage as cracking progresses. This is based on the behaviour of a cracked material, where extension in the cracked direction does not result in contraction in the perpendicular direction. This model provides a rate of Poisson's ratio reduction that is equal to the reduction of secant modulus after cracking. The effect of these choices is presented in the results in Chapter 4.

3.1.3. Loads

DIANA FEA calculates the self-weight from the density of the material and the geometry of the elements. Apart from self-weight, two loads were imposed on the wall. A vertical load was applied during the experiment to represent the weight of a heavy timber roof. A corresponding uniformly distributed vertical load was applied to the lateral walls as shown in Figure 3.5a. The horizontal load applied in the experiment through the airbag in the test setup shown in Figure 2.41b is simulated by a uniformly distributed horizontal load on the rear façade of the frontal wall as shown in Figure 3.5b.

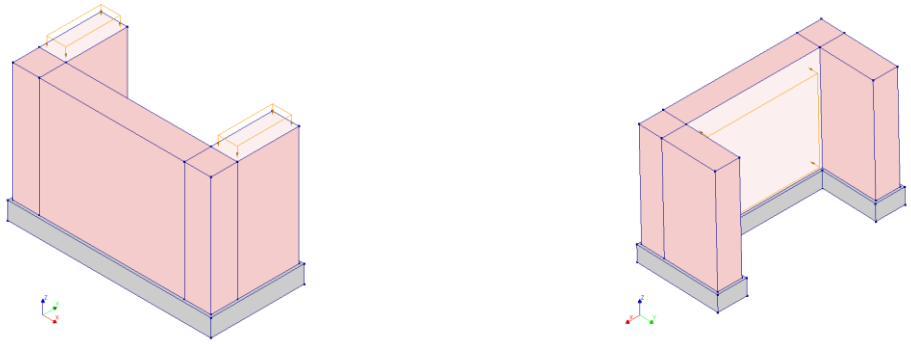

a b

Figure 3.5: Loads applied to the walls – (a) Roof load to the lateral walls, and (b) Pushover load to the frontal wall

3.1.4. Mesh size

The mesh size was considered to be 0.10 m for masonry and concrete, while timber elements were meshed with a size of 0.05 m. A sensitivity analysis was also done to assess the difference in accuracy with coarser and finer mesh. A meshed model of both wall specimens can be seen in Figure 3.6. The generated mesh includes 11,158 nodes and 2,403 elements for the unreinforced model. However, with the inclusion of the timber-masonry interface elements, the number of elements increases. The mesh is more refined the closer it is to the timber elements, and coarser (0.10 m) away from the timber braces, as the stress concentrations are expected to be high in this region. This results in 34,691 nodes and 10,828 elements for the timber-reinforced model. This provides a balance between reliable results and computational needs and time. Since quadratic interpolation is used for the elements adopted, the displacement field is expected to have a reasonable degree of approximation.

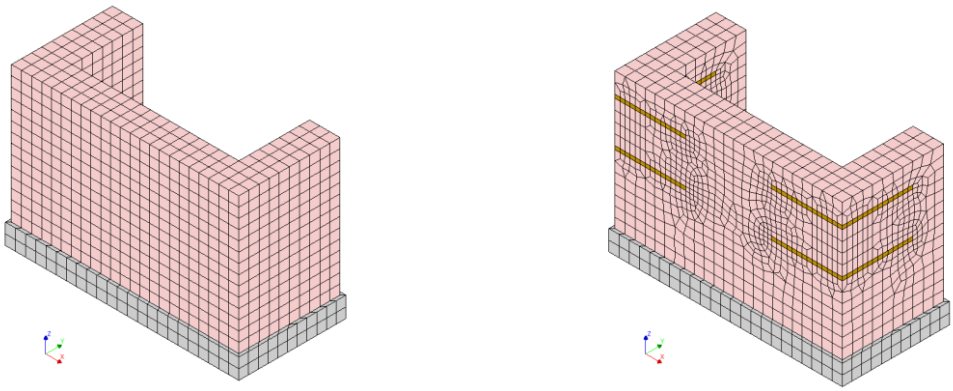

a b

Figure 3.6: Meshed model - (a) Unreinforced masonry, and (b) Timber-reinforced masonry

3.1.5. Interaction between structural components

Along with the response of individual materials, consideration has been given to the behaviour at the contact of two different materials. The interface between the masonry wall and the concrete base was considered to be fully connected, and the interaction between other interfaces is discussed in the following sections.

3.1.5.1. Between the concrete base and the floor

The interface between the concrete base and the floor has been modelled using the boundary interface elements properties provided by Murano et al. (2019). They are listed in Table 3.4 and can be seen in Figure 3.7a.

3.1.5.2. Between masonry wall and the timber bands

The interface between embedded timber elements and the masonry are modelled in two manners. Most models were simulated with timber elements having a perfect connection to the masonry wall, meaning that common nodes share the same degree of freedom. In turn,

this leads to no slip and relative displacement between the timber and masonry. In reality, however, there would be slip at the interface of timber and masonry. An attempt was made to accurately simulate this behaviour.

3.1.5.3. Timber-masonry Interface

Interface elements were modelled at the contact surfaces of masonry and timber as seen in Figure 3.7b. The behaviour of these elements is governed by Coulomb friction law. From the studies reviewed in Chapter 2.9.2, a range of 0.337-0.730 radians has been indicated for the frictional angle [86-95, 102]. For cohesion, the same value was indicated to be in the range of 0.1-0.233 MPa [89, 90, 93, 94]. An overview of frictional coefficient and cohesion values from literature is presented in Table 3.6. From this, a conservative cohesion value of 0.15 MPa and frictional angle of 0.600 radians was chosen for the interface element between timber and masonry. The friction properties used for the timber-masonry interface are presented in Table 3.5.

Table 3.4: Interface stiffness between concrete base and floor from [96]

Wall specimen	**Direction**	**Unit**	**Value**
Unreinforced masonry	Tangential	N/mm^3	0.397
	Normal	N/mm^3	0.992
Timber-reinforced masonry	Tangential	N/mm^3	0.257
	Normal	N/mm^3	0.640

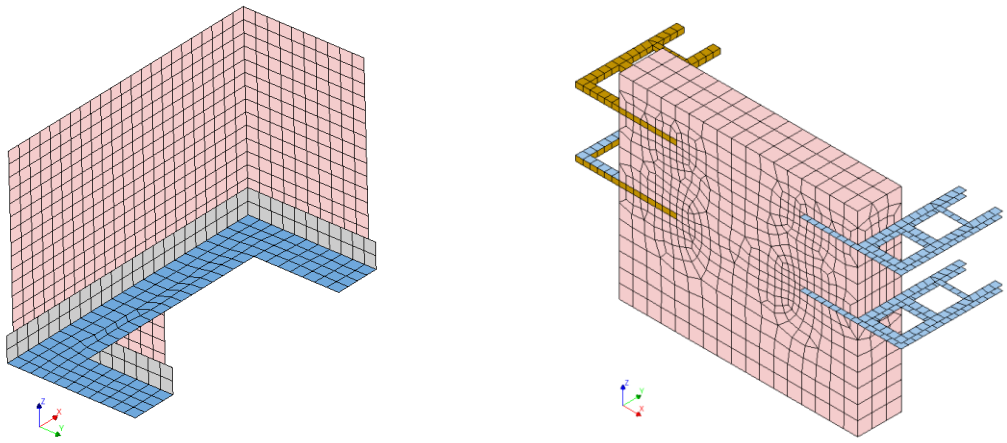

Figure 3.7: Interface: a) Between concrete base and floor, and b) Timber and masonry

Table 3.5: Material properties of timber-masonry interface

Interface Property	Value	Unit
Normal stiffness (z)	200	N/mm^3
Shear stiffness (x)	100	N/mm^3
Shear stiffness (y)	100	N/mm^3
Cohesion	0.15	N/mm^2
Friction angle	0.6	radians
Dilatancy angle	0	radians

Table 3.6: Friction and cohesion values for timber-masonry interface from literature

Type of building	Interface		Frictional coefficient	Friction angle	Cohesion	Reference study
			μ	radians	MPa	
Single-leaf clay brick masonry	Brick masonry - Timber joist		0.800			[87]
	Mortar – modern sawn timber		0.77			[88]
	Brick masonry - Timber beam	Experimental		0.600	0.150	[89]
		Numerical		0.730	0.178	
Masonry vault	Masonry arch - Timber beam			0.54	0.1	[90]
Double-leaf stone masonry	Stone masonry - Timber beam		0.4 – 0.7			[91]
Masonry with timber band	Brick masonry - Timber lumber		0.64			[92]
Welded tuff masonry with timber frames	Brick masonry - Timber frame			0.5	0.15	[93]
Stone masonry with embedded timber beams	Sandstone cut veneer - Timber beam		0.35			[86]
Undressed Stone masonry	Stone masonry - Timber beam		0.80		0.233	[94]
Adobe masonry	Adobe masonry - Timber lintels		0.50			[95]
Half-timbered	Masonry infill - Timber frame –		0.50			[102]
Pombalino	Masonry infill - Timber frame		0.1 – 0.4			[103]

3.1.5.4. Timber-to-timber connection

The connection between timber elements was considered to be perfect. This is, though, a simplification of the actual connection that exhibits a partial connection behaviour. However, to assess the effect of the connection on the global behaviour, a scenario has been assumed where all four connections between the longitudinal beam and transverse beam are considered to be hinged connections. The numerical model construction is presented in Figure 3.8.

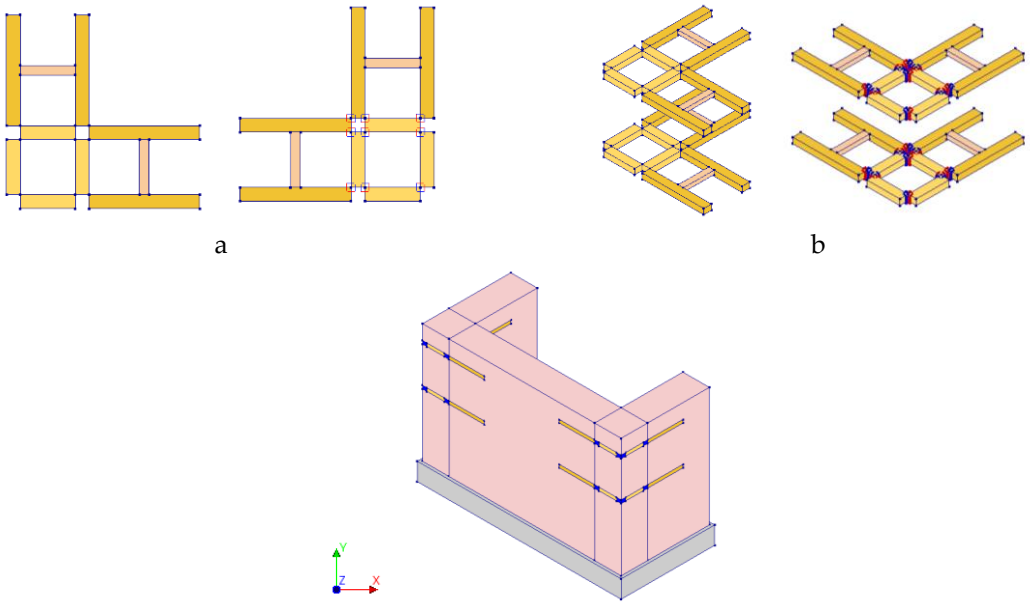

Figure 3.8: Hinged connections between orthogonal timber braces : (a) Plan view, (b) Overview, (c) Model overview

Conclusion

In this chapter, the numerical model used for the pushover analysis was introduced. The model incorporates both linear and non-linear material properties sourced from literature. It explains the chosen element model, material model, cracking model, and mesh size. DIANA FEA software (version 10.5) is used for the simulation, aiming to represent the structural behaviour of masonry walls under out-of-plane loads. The study employs a twenty-node tetrahedron 3D element for modelling concrete, masonry, and timber elements, with interfaces modelled using quadratic interpolation. The geometry of the model is based on an experimental wall, with stone masonry modelled using the Total Strain Rotating Crack model (TSRCM) due to not just its efficacy in analysing cracking and crushing responses but also robustness and reliability. While timber is assumed to have linear elastic behaviour, the stresses in timber elements are verified in the post-processing phase. Two loads are applied, roof and pushover load, and the mesh size varies, being denser near the timber elements. Interactions between different structural components, such as concrete, timber, and masonry, are carefully detailed, with some interfaces modelled with perfect connections and others reflecting frictional behaviours. Timber-to-timber connections are simplified as perfect, but the potential impact of hinged connections is also considered.

3.2. Numerical analyses

When the relationship between the load applied and the response (displacement) of the system is not linear, it leads to convergence problems, especially for structures that experience significant deformations. This section briefly presents the different analysis approaches and iterative techniques used for FE nonlinear analyses. The solution methods and analysis parameters are also described. Physical and geometrical both nonlinearities were accounted for the analysis with 'Total Lagrange' type specified for the geometrical nonlinearity.

3.2.1.1. Iterative techniques

To achieve accurate results for a nonlinear analysis, the step sizes have to be very small. This leads to very long runtimes in explicit solvers. However, in an implicit solver with an iterative procedure, the step size can be larger. The iterative procedure depends on the incremental, sequential recurrence of four predefined steps – (i) increasing the external load applied on the system; (ii) calculating the out-of-balance force; (iii) predicting the change in displacement; and finally (iv) calculating the revised internal force. The analysis for this thesis was chosen to be a force-based analysis rather than the imposed displacements used more often for pushover analyses. The predefined convergence criteria help the solver to assess whether to continue with the iteration for the current increment or to end the increment and move on to the next increment.

DIANA FEA [98] supplies multiple incremental-iterative solution procedures for nonlinear analysis, however only the relevant ones are discussed in the following sections.

Newton-Raphson

Newton-Raphson method is used as an iterative technique to find solutions to nonlinear equations and hence, determine the equilibrium state at each load step. However, the Newton-Raphson method has convergence issues, especially when the load-displacement curve has points of inflection or turning points.

Two Newton-Raphson methods are specified – Regular and Modified. The location of stiffness matrix determination signifies the difference between the two. While the stiffness relation is evaluated every iteration in the former, it is evaluated only at the start of the increment in the latter. This results in two different kinds of predictions of the relation between the force vector and the displacement vector. In Regular Newton-Raphson, this relation is based on the previous prediction, regardless of the equilibrium state. On the other hand, the prediction of the force-displacement vector relation is always based on the converged equilibrium state for Modified Newton-Raphson.

The implication of this difference is that each iteration of Regular Newton-Raphson is time-consuming, but convergence is achieved within fewer iterations, while on the contrary, Modified Newton-Raphson has faster iterations but needs more of them to reach the solution.

Secant (Quasi-Newton)

The Secant method depends on the out-of-balance force vectors from the previous iteration for approximation of the solution, eliminating the need of setting up a stiffness matrix with every iteration.

Number of iterations

The number of iterations was set at 100. If the solution does not converge after a limit of 100 iterations, it was set to continue the analysis instead of terminating. The effect of number of iterations had a significant impact on the pushover curve of the unreinforced masonry. A limit of 30 iterations was found to present a significantly more ductile response for the Secant (Quasi-Newton) iterative technique than when 100 iterations were specified. The convergence with 30 iterations was also found to be very low. On the contrary, the force envelope for the Newton-Raphson iterative technique did not seem to be sensitive to the number of iterations. Further detailed results of this sensitivity analysis are provided in Appendix A.

3.2.1.2. Solution control

For each increment in solution, the solution can be specified by either load control (increasing the load in small steps) or displacement control (increasing displacement in small steps). The choice of the force control depends on the experimental setup or the numerical modelling strategy. When load control is applied, the solution is not able to correctly approximate the next step after the maximum force has been reached ('limit point' as described in [104]). Displacement control, while able to overcome the limit point, is unable to overcome the 'turning point' [104]. Arc length control is the third choice of increment control described in the following section.

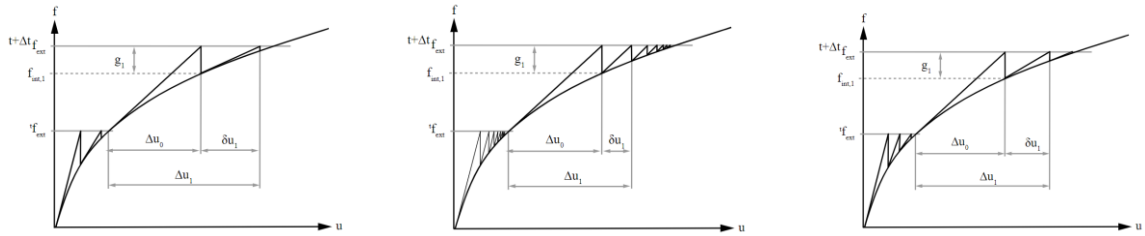

Figure 3.9: Incremental-iterative solution procedures available in DIANA FEA 10.5 - (a) Regular Newton-Raphson, (b) Modified Newton-Raphson, and (c) Secant (Quasi-Newton) from [98]

Arc length control

When the numerical model prescribes a fixed load increment, as prescribed by the numerical model in this thesis, there exists a strong possibility that the prediction of the displacement becomes very large. This problem can be solved by the Arc length control method that juxtaposes a displacement control factor onto the load control prescribed by the numerical model. Arc length control helps in arriving at the stable solution, especially for materials with distinctively nonlinear behaviour of softening in the post-peak phase, by achieving a snap-through behaviour. Additionally, this method is also able to achieve snap-back behaviour (overcoming the turning point as described in [104]). The loading-unloading determination,

i.e., the choice between increment or decrement for the incremental analysis is made via *Negative pivots*. 'Updated normal plane' is chosen as the method for constraining the incremental displacement vector linearly. The term is a result of the fact that the new solution is normal to the solution in the previous iteration.

3.2.2. Convergence Criteria

As the last step of the iterative method, the solver concludes to end the current iteration by comparing the out-of-balance values for energy, force or displacement to the prescribed convergence tolerance norms for the same. Prescribing the convergence tolerance values can be a balancing act as stricter-than-required values might lead to a drastic increase in computational demands while not improving the results appreciably. On the other hand, too relaxed a convergence would yield results not representative of the actual response.

The analysis used in this study was chosen to have convergence criteria for either force or displacement with the convergence norm chosen to be 1%.

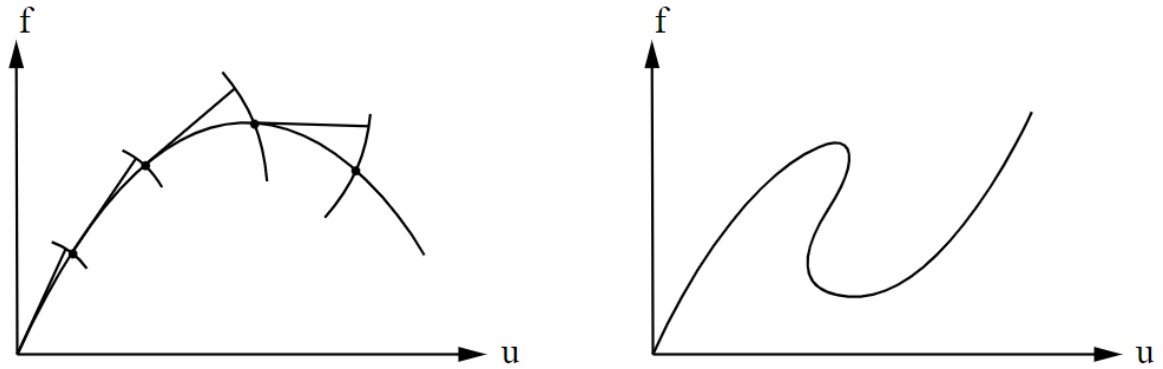

Figure 3.10: Arc length control in DIANA FEA 10.5 - (a) Snap-through, and (b) Snap-back, from [98]

Finally, four models were simulated, as described in Table 3.7.

Table 3.7: Variations of the four models

Model	Wall	Iterative technique	Poisson's ratio reduction model
Model U1	Unreinforced	Regular Newton-Raphson	Damage-based reduction
Model T1	Timber-reinforced		
Model U2	Unreinforced	Secant Quasi-Newton	No reduction
Model T2	Timber-reinforced		

Conclusion

In the discussed numerical analyses, different approaches and iterative techniques for nonlinear analysis are elaborated. Implicit solvers with iterative procedures allow for larger step sizes. These iterative methods encompass a set sequence: loading increase, out-of-balance force calculation, displacement change prediction, and revised internal force computation. DIANA FEA software offers several iterative solutions, notably Regular and Modified Newton-Raphson, and the Secant (Quasi-Newton) iterative methods. Regular Newton-Raphson iteratively reevaluates the stiffness matrix, making it time-intensive but quick to converge. Meanwhile, Modified Newton-Raphson is swifter per iteration but needs more iterations overall. The convergence criteria, based on energy, force, or displacement, determines when the iteration should cease. Force or displacement convergence criteria with a norm of 1% were chosen for this study. Pushover analyses were executed to assess the structure's seismic response, contrasting unreinforced masonry with timber-reinforced variants. Initial tests on a U-shaped wall corresponded with experimental responses in literature, leading to an extensive model analysis of a Bhatar building.

4. Results

This chapter presents the results of the replication study conducted for a 1:2 reduced scale U shaped masonry wall. The model validation was conducted by comparing the pushover curves, crack patterns, displacement contours and principal strains to the experimental and numerical benchmark study by Murano et al. (2019). Thereafter, results of alternate modelling approaches adopted for the interaction between different structural components and materials are discussed. Finally, outcomes of a sensitivity study, assessing the influence of geometrical parameters, material properties and loading conditions, is presented.

4.1. Model validation

To validate the two numerical modelling strategies adopted for the masonry wall, the eigenfrequencies, capacity curves, strains and displacement contours are compared to the experimental values in the following sections.

4.1.1. Eigenfrequencies

As the first step to validating the numerical model, the eigenfrequencies found in literature were compared to those found through Structural Eigenvalue analysis in DIANA. The comparison can be seen in Figure 4.1 and Figure 4.2 for unreinforced and timber-reinforced masonry, respectively.

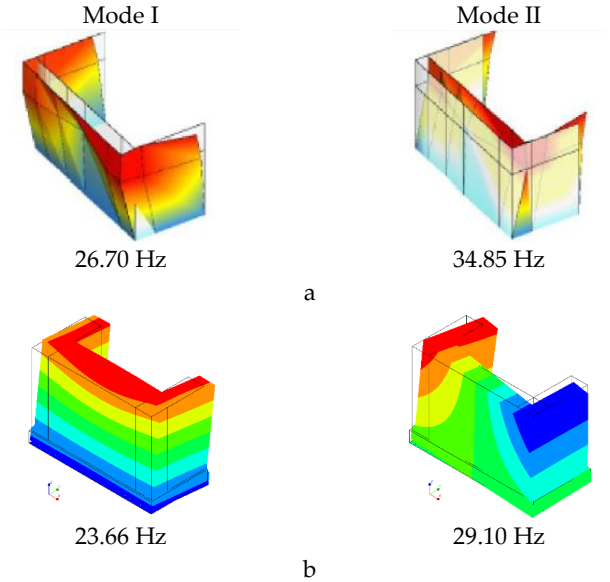

Figure 4.1: Natural frequencies for unreinforced masonry - (a) Dynamic characterization tests by Murano et al. (2019), and (b) Numerical model (this study).

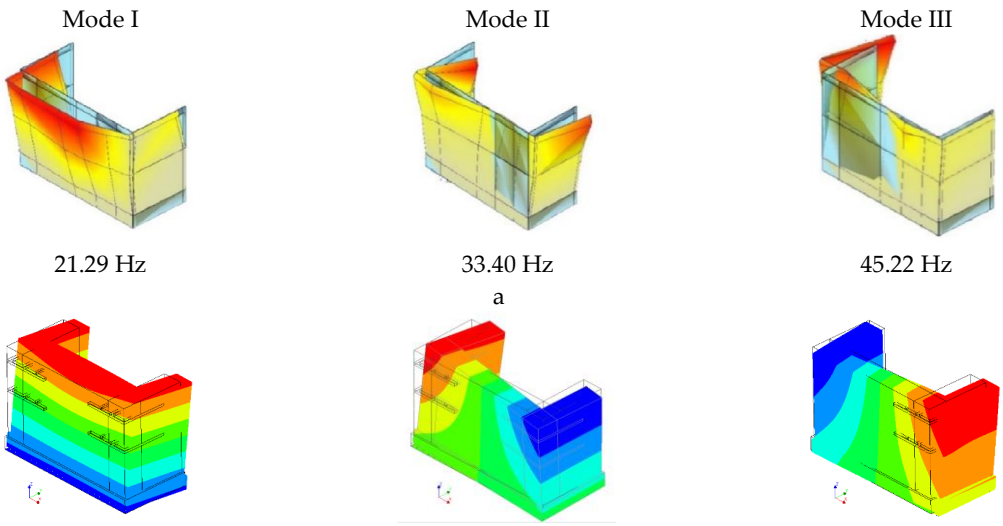

Figure 4.2: Natural frequencies for timber-reinforced masonry - (a) Dynamic characterization tests in Murano et al. (2019), and (b) Numerical model (this study).

4.1.2. Force capacity

The base shear is plotted against the displacement at the control node (top-mid node of frontal wall) to present the pushover curves for the unreinforced masonry for both the iteration procedures in Figure 4.3. It can be seen that both curves follow closely. The peak value of the base shear has almost no difference (45.77 kN and 45.68 kN). Model U2 has slightly lower resistance values for the same displacement after the softening period ends. However, this is after a displacement of over 20 mm, far beyond the Near Collapse Limit State.

Figure 4.4 shows the same pushover curve for timber-reinforced masonry. Model T1 curve shows greater brittleness in the softening phase soon after reaching the maximum resistance which is expected since it applies the influence of lateral cracking through Damage-based Poisson's ratio reduction model which also results in more discernible reduction in stiffness. However, the maximum resistance for the timber-masonry wall is very close for both iteration methods. Figure 4.5 combines the pushover curves from Figure 4.3 and Figure 4.4. The increase in lateral resistance capacity is clearly visible.

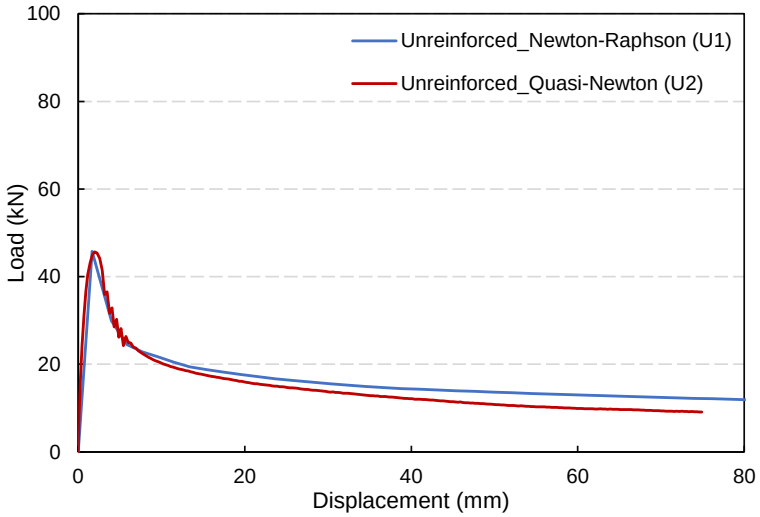

Figure 4.3: Pushover curves for unreinforced masonry

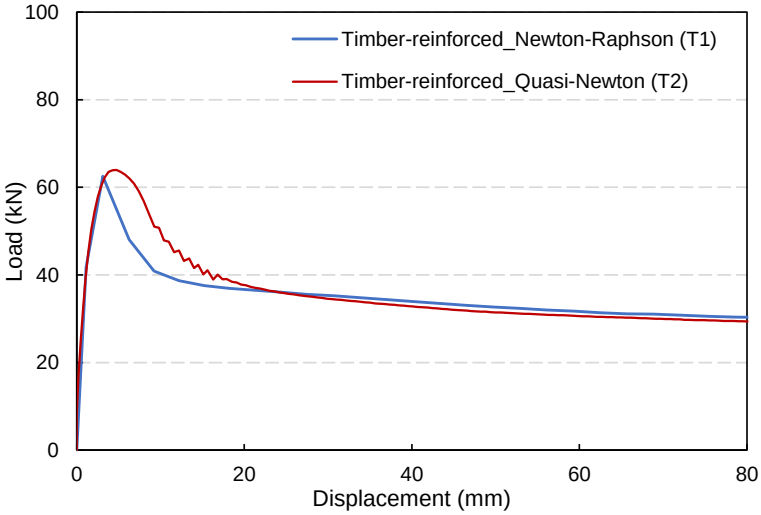

Figure 4.4: Pushover curves for timber-reinforced masonry

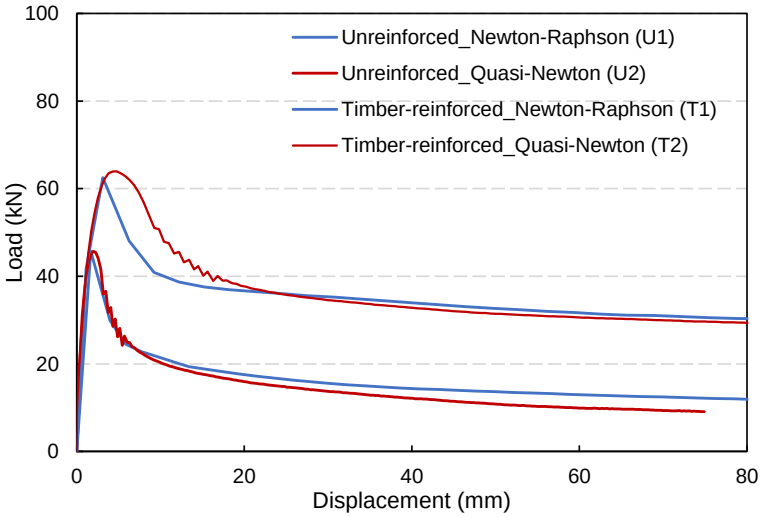

Figure 4.5: Pushover curves: Unreinforced and timber-reinforced masonry

These curves can be compared to the experimental and numerical capacity curves presented in Murano et al. (2019). Figure 4.6 and Figure 4.7 illustrate that the maximum lateral load capacity shows good correspondence with the experimental and numerical benchmark values for both unreinforced and timber-reinforced masonry. The post-peak behaviour shows noteworthy softening, unlike the more gradual reduction of force in the experimental study in benchmark. However, the results have an agreement to a reasonable degree. Moreover, the post-peak softening phase closely corresponds to the numerical results from the benchmark study.

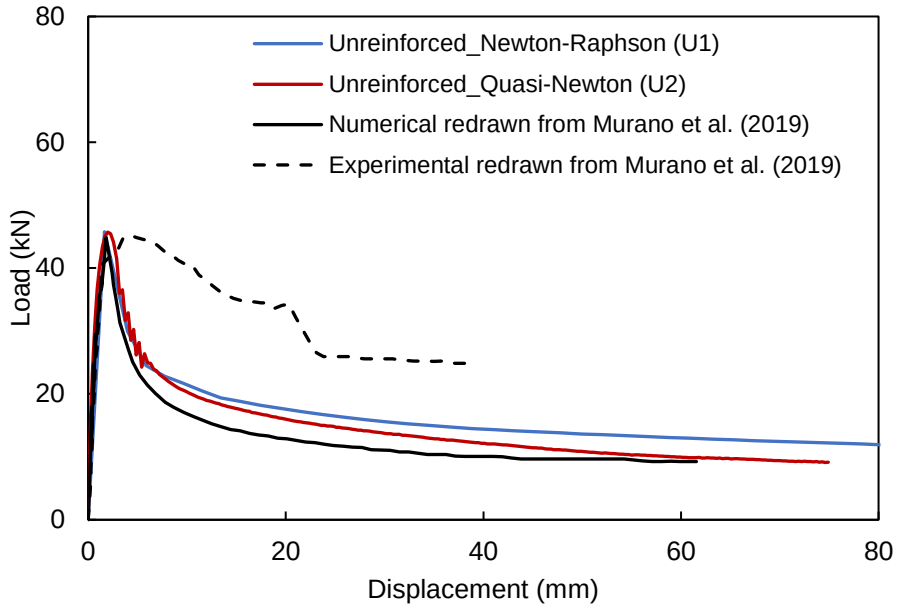

Figure 4.6: Comparison of Capacity curves for unreinforced masonry : benchmark and this study

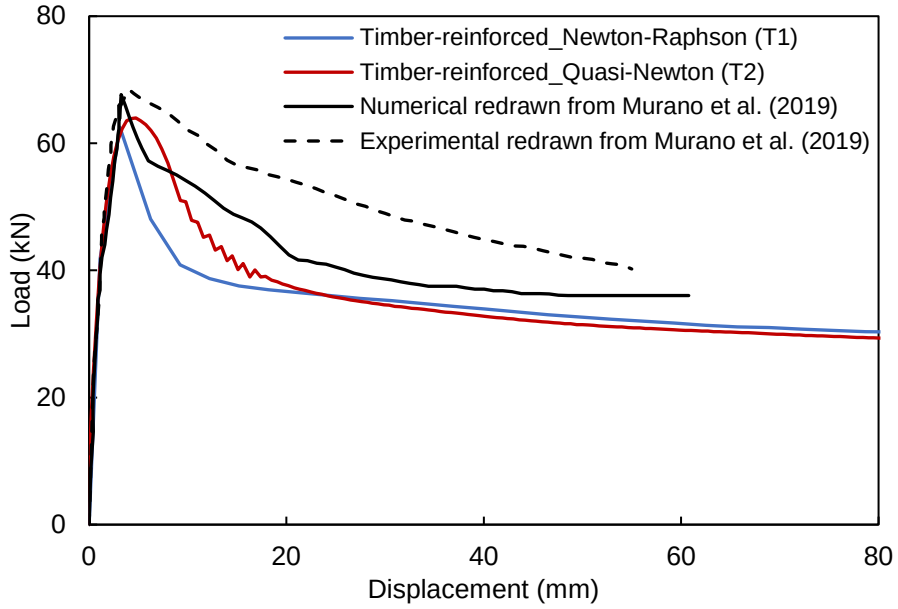

Figure 4.7: Comparison of Capacity curves for Timber-reinforced masonry : benchmark and this study

The maximum lateral resistance values obtained in this numerical study are compared with those obtained in the benchmark study in Table 4.1. The timber-reinforced masonry (63.95 kN) shows an increase of 40% in maximum resistance over unreinforced masonry (45.68 kN).

Table 4.1: Maximum lateral resistance values from the benchmark and this study

	Maximum lateral resistance (kN)			
	Murano et al. (2019)			
Wall	Experiment	Numerical	Model U1	Model U2
Unreinforced	45.64	45.04	45.77	45.68
	Experiment	Numerical	Model T1	Model T2
Timber-reinforced	68.91	67.50	62.51	63.95

4.1.3. Displacement contours

This section presents the displacement contours obtained from the numerical study and compares them to those present by Murano et al. (2019) in their study. Figure 4.8 compares the contour plots for the displacements in Y direction obtained through numerical modelling in DIANA FEA against the displacement contour plots obtained from experimental and numerical investigations by Murano et al. (2019). Both iteration methods are considered – Newton-Raphson and Quasi-Newton.

The comparison reveals that the displacements calculated by the numerical model provide a reasonable correspondence with those found in the benchmark studies. The asymmetry seen in displacements in Figure 4.8a and Figure 4.8b cannot be replicated by macro numerical models as the geometry of each stone in the model is not modelled separately. Moreover, since macromodelling is a continuum approach, the cracks are assumed to 'smear' evenly across the surface of the wall. In contrast, physical construction of the wall for out-of-plane load in the experiment, has irregularities related to construction, mortar joints, thickness, etc. This leads to the difference in the response of the so-called 'stronger' parts of the wall to the 'weaker' parts.

There is a distinct contrast between the failure mechanisms observed from the results of the two different displacement contours obtained from the two different iteration methods. While Models U2 and T2 are able to achieve the failure mechanism of horizontal flexure (Figure 4.8e and Figure 4.8f), Model U1 fails through separation of orthogonal walls (Figure 4.8g). This separation is avoided in Model T1 (Figure 4.8h) which can be attributed to the presence of timber laces, however since the laces are present only at the corners, the failure is concentrated at the centre portion of the frontal wall.

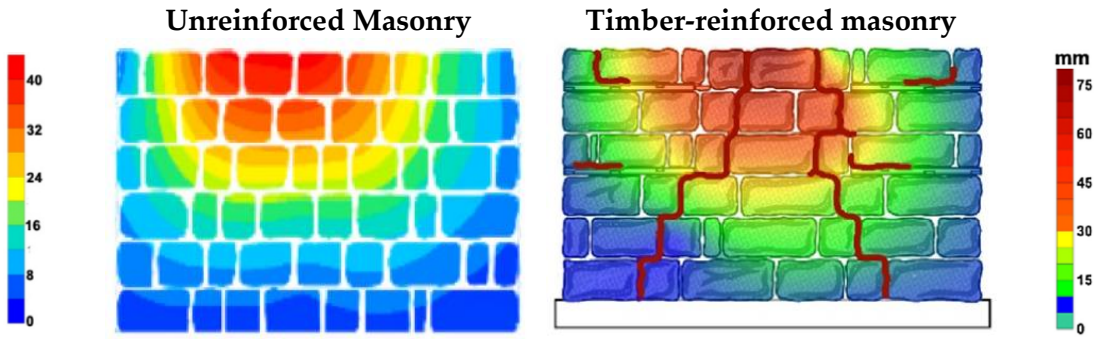

a b

Experimental from benchmark Murano et al. (2019)

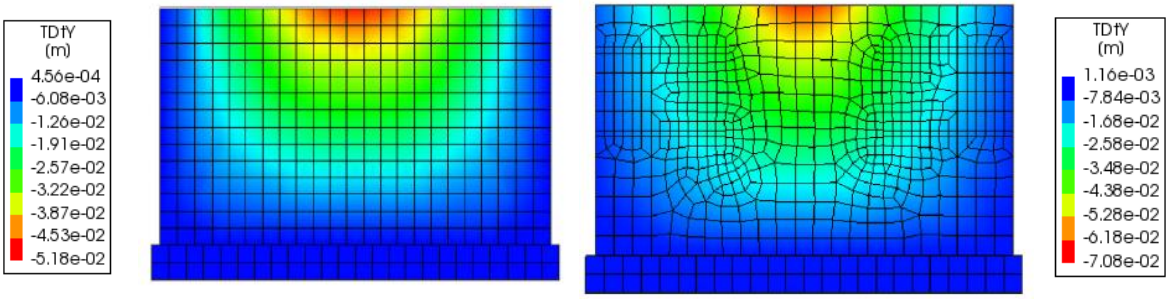

c d

Numerical from benchmark Murano et al. (2019)

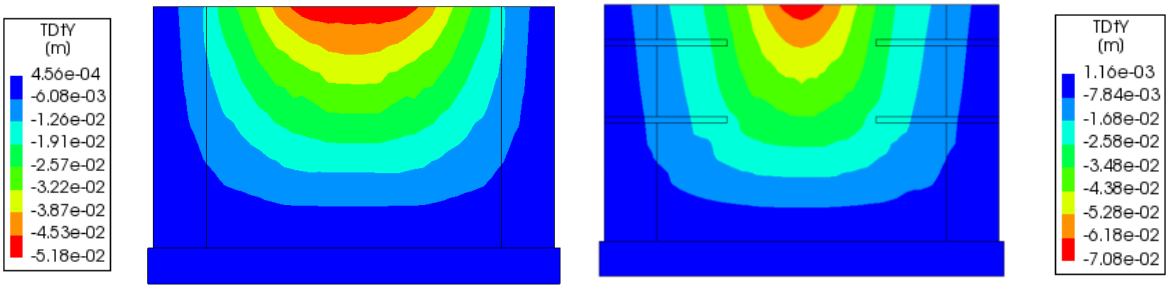

e
Model U2

f
Model T2

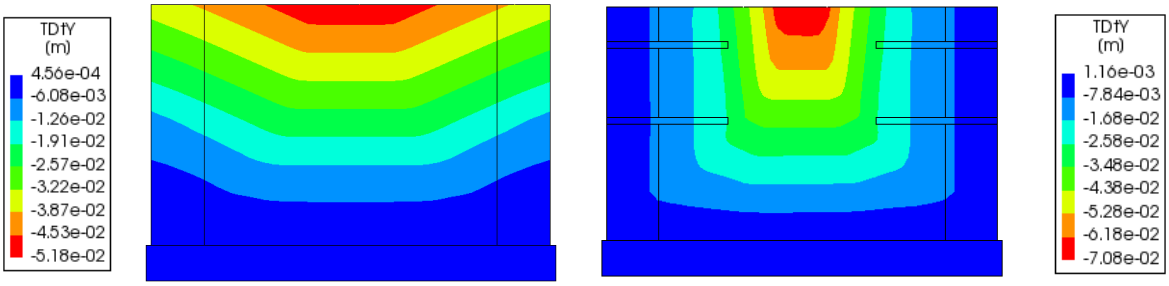

g
Model U1

h
Model T1

Figure 4.8: Comparison of displacement contours in Y direction for unreinforced and timber-reinforced masonry

Maccarini et al. (2018) conducted an experimental investigation into the out-of-plane response of irregular and regular stone masonry walls. The *regular wall* in the experimental campaign by Maccarini et al. (2018) is the same as the *unreinforced masonry wall* by Murano et al. (2019). Displacement contours provided by Maccarini et al. (2018) are also compared to relate the displacement at various stages in Figure 4.9. Only Model U2 was compared and the resemblance of the numerical displacement profiles to the experimental ones further validates the modelling strategy.

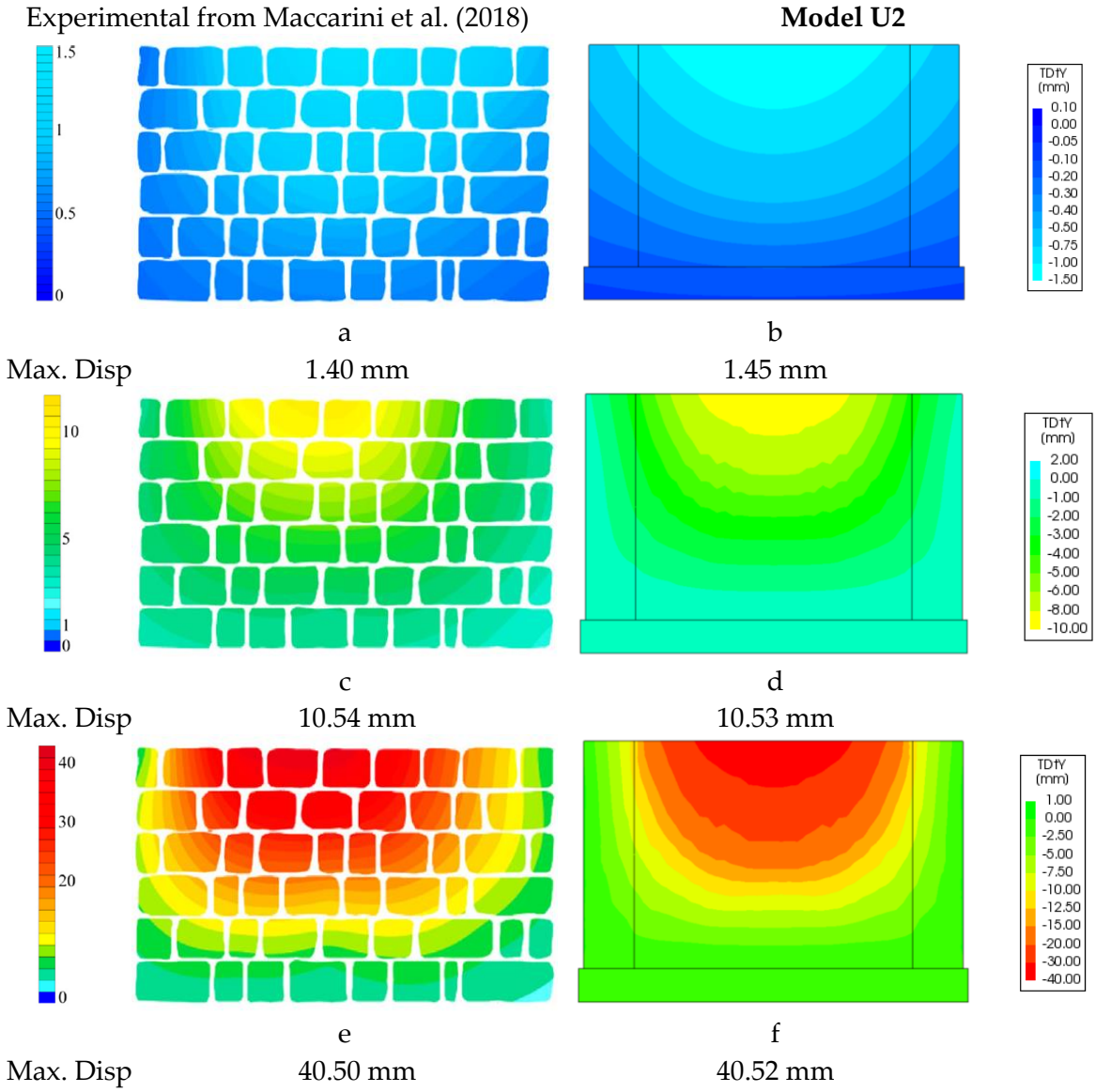

Figure 4.9: Comparison of displacement contours for unreinforced masonry wall from Maccarini et al. (2018)

The difference between the two models in simulating varying failure mechanisms can be observed in Figure 4.10. Both contour plots are reported when the displacement of the control displacement node (top-mid of the frontal wall) has reached 40 mm. It can be seen clearly that while Model U1 (Figure 4.10a) exhibits separation of the frontal wall from the returning walls; the Model U2 (Figure 4.10b) exhibits horizontal bending under out-of-plane loading conditions.

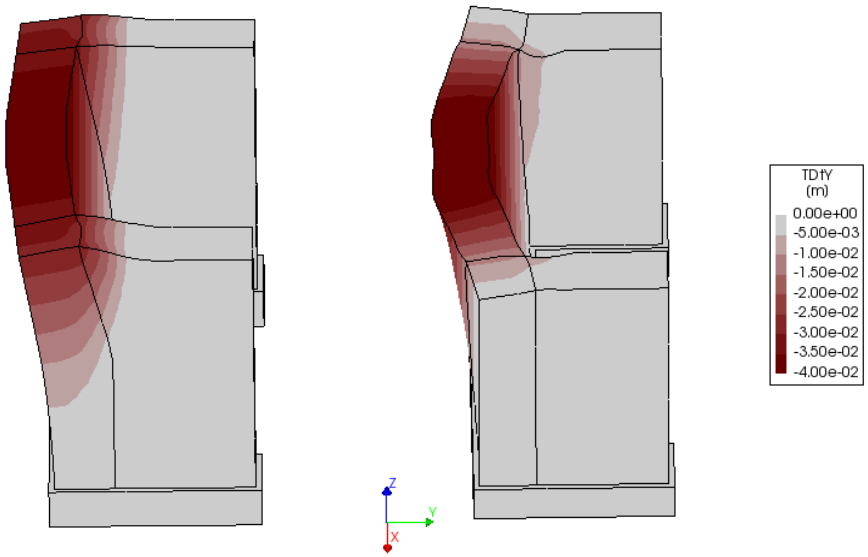

a b

Figure 4.10: Side view of displacement in Y direction : (a) Model U1, (b) Model U2

4.1.4. Strains

Strains represent the deformation of a material when subjected to an external force. Principal strains are the maximum and minimum values of normal strain at a point within a deformable body. Cracking in a brittle material such as masonry is associated with exceeding a strain (or stress) beyond the material's capacity. Principal strains also provide an indication of cracking in case of exceedance of the material's tensile strain capacity. Cracks initiate along principal strain directions as they represent the path of maximum extension. Maximum principal strain is denoted as E1 in DIANA. The strains from [96] are compared with those obtained from the numerical analysis using two iteration techniques for unreinforced and timber-reinforced masonry in Figure 4.11 and Figure 4.12, respectively.

While Model U2 (Figure 4.11b and Figure 4.11d) shows a good correlation with the strains obtained from the numerical study conducted in the benchmark [96] (Figure 4.11a and Figure 4.11c), Model U1 shows considerable difference. Model U2 exhibits the spread of strain (and hence damage) across the frontal wall, whereas the strain in the Model U1 is concentrated at certain locations. Similarly, the rear overview shows that the strains are concentrated at the connection of lateral and orthogonal wall for the Model U1 along with horizontal strains at the base of the masonry wall. Interestingly, another distinct horizontal strain is observed approximately two courses from the bottom of the masonry wall (Figure 4.11e).

Similar to Model U2, the Model T2 also shows a good match with the strains from the benchmark study for timber-reinforced masonry. Model T1 shows greater distribution of strains compared to the Model U1. A marked difference is the absence of strain at the inner corner – the location of orthogonal wall connection. While the Model U1 showed the highest concentration of strains at this location, the Model T1 shows no strain at this location, possibly due to the tying effect of corner timber braces in keeping the lateral and frontal walls.

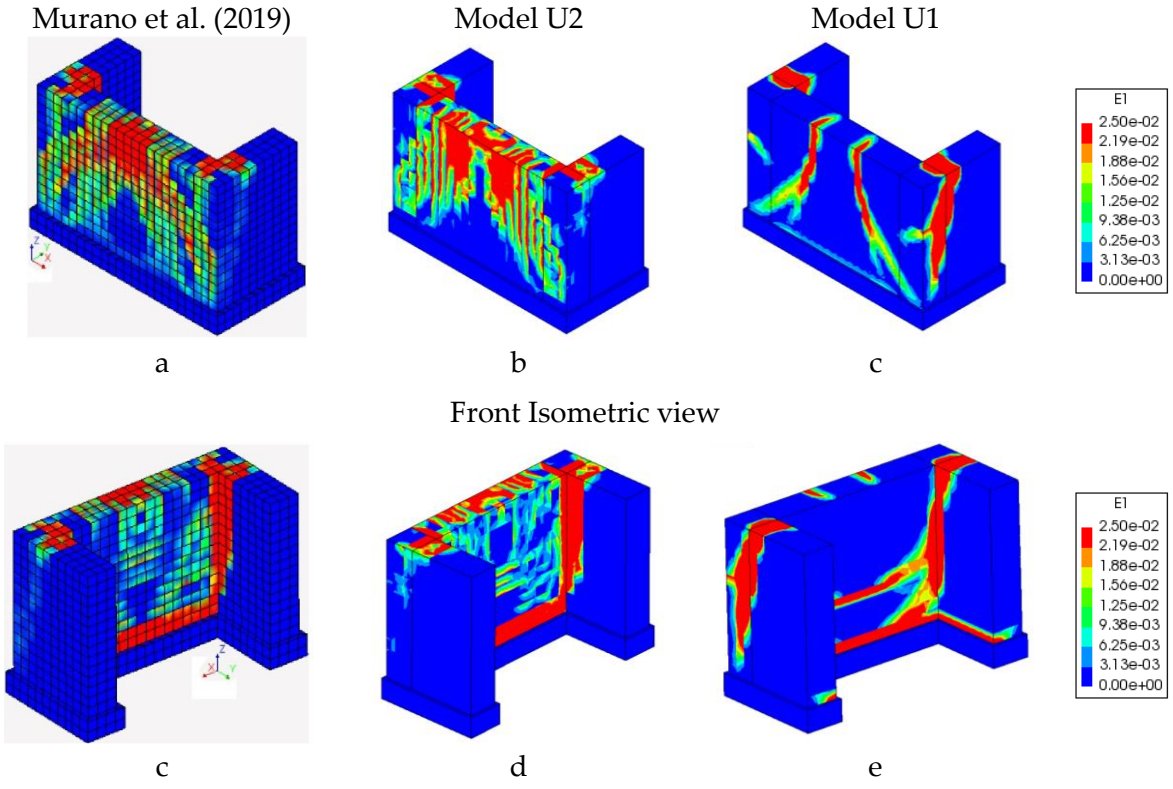

Figure 4.11: Comparison of principal strains E1 for unreinforced masonry

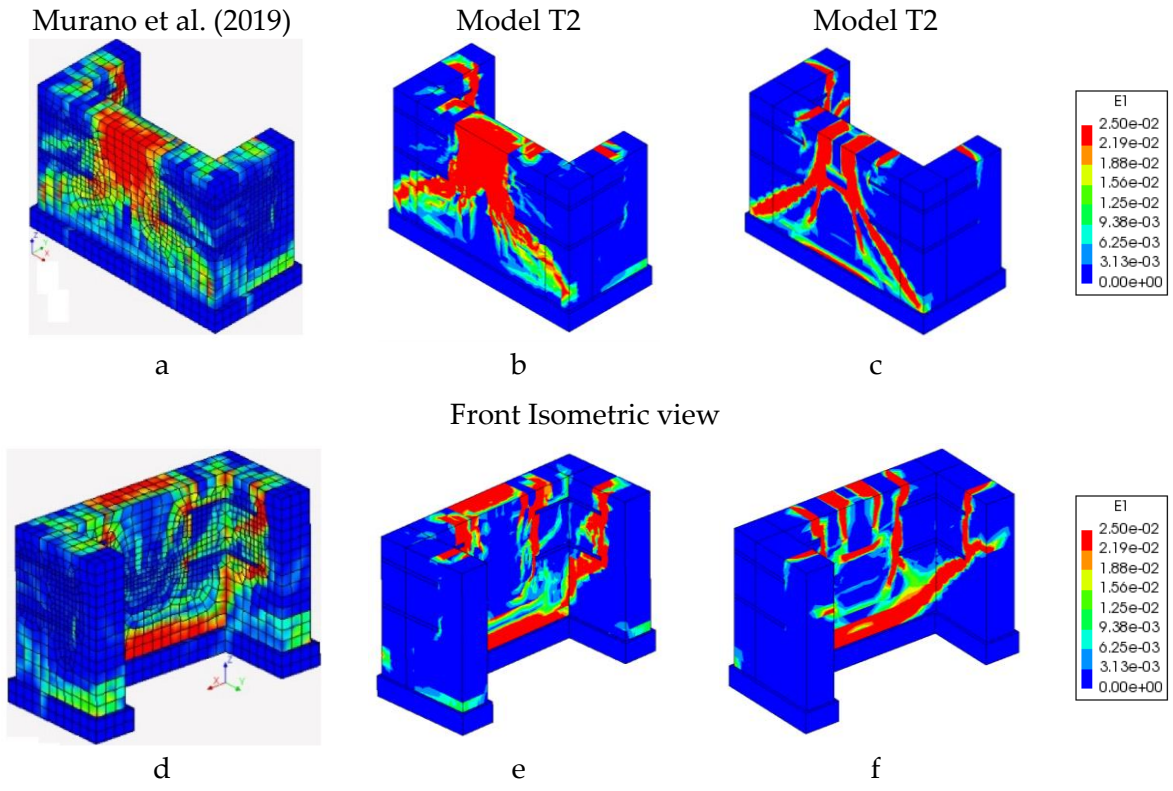

Figure 4.12: Comparison of principal strains E1 for timber-reinforced masonry

4.1.5. Crack pattern

To assess the damage, principal crack widths are plotted and presented. The extent of damage evolution is varied in the two models used to analyse the masonry walls. First, Figure 4.13 shows a comparison for crack patterns in the unreinforced masonry wall provided in [105]. Model U1 simulates the experimental crack pattern very closely. It shows a very localised damage evolution at distinct locations, including the horizontal crack in the rear façade of the frontal wall, two courses from the bottom of the masonry wall (Figure 4.13b). The diagonal crack on the frontal wall is also simulated, albeit the numerical model shows a symmetrical crack on both sides (Figure 4.13d), unlike the experiment that shows a crack only on one side (Figure 4.13a). The experimental crack on the outside wythe of the lateral wall (Figure 4.13c) is also simulated well. Model U2 also simulates the experimental diagonal cracks on the front façade well, albeit with more 'smearing' of the cracks – true to the smeared cracking approach. Though, it fails to represent any cracks on the lateral wall. Both models depict most significant cracking at two locations – (i) base of the frontal wall at the rear façade, due to overturning action, and (ii) corner connection of frontal and lateral walls, due to separation action.

a b c

Crack pattern from experiments by Maccarini et al. (2018)

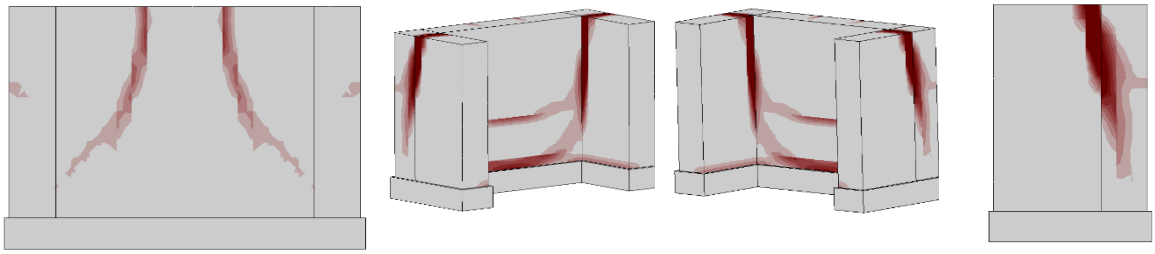

d e f

Crack width contour plot from Model U1

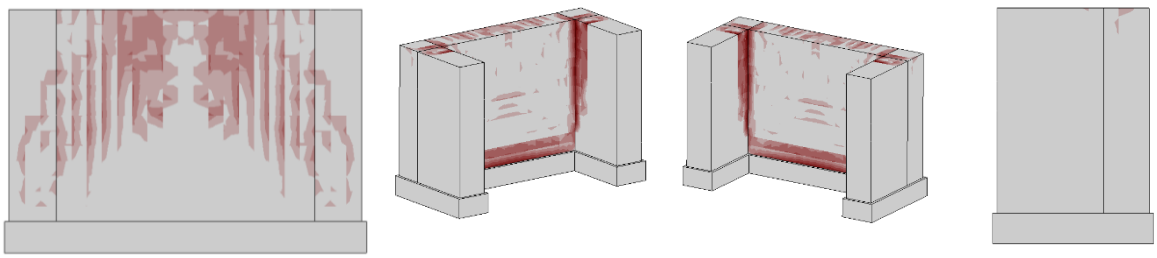

g h i

Crack width contour plot from Model U2

Figure 4.13: Cracking pattern comparison with experiments Maccarini et al. (2018)

The cracking pattern for the timber-reinforced masonry wall from the experiment in Murano et al. (2019) is compared to the numerical model in this study in Figure 4.14**.** The crack plots are taken at 40 and 57 mm top node displacement for unreinforced and timber masonry, respectively. In addition to the observations above, it can be seen from Figure 4.14e that the Model T1 is able to accurately simulate the cracks observed at the rear surface of the frontal wall (Figure 4.14d). Along with the two horizontal cracks described above, the vertical crack at the corner is also represented. Model T2 is able to simulate the cracks well for unreinforced masonry though with more distribution of the cracks across the surface in contrast to better localisation achieved by Model T1.

The above observations for unreinforced masonry apply to timber-masonry as well. A point to note is the clear horizontal crack visible at mid-height of the rear façade (experimental in Figure 4.14j and numerical in Figure 4.14k). Another point of significance is the local cracks above the timber bands, at its interaction with mortar, are not modelled in the macro numerical model.

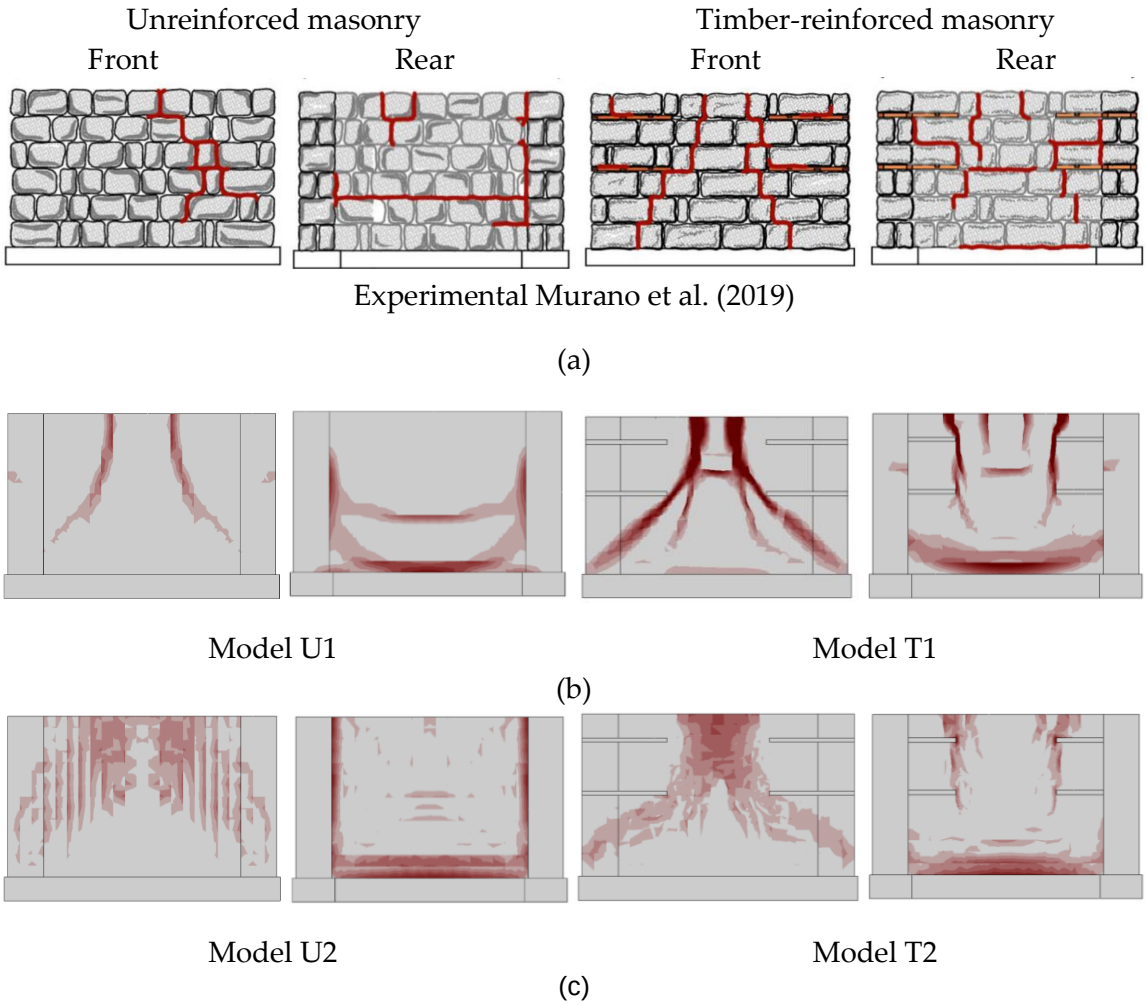

Figure 4.14: Experimental [96] and numerical cracking pattern comparison for unreinforced and timber-reinforced masonry

4.1.6. Convergence

Figure 4.15 shows the variation in convergence norms. As described in Chapter 3.2.2, force and displacement were chosen for convergence criteria with a tolerance of 1%. The out-of-balance force and displacement variations are well within the tolerance norms indicating the trustworthiness of the results obtained from the analysis. Figure 4.16 shows the number of iterations at each load-step. A few load-steps did not converge in the softening phase, indicated by the limit of 100 iterations on the plot. However, after those load-steps, the analysis converges again. Moreover, except between load-step 25 and 45 (out of 150 load-steps), all load-steps reach convergence. This also suggests that the modelling strategy and the results of the analyses are reliable, validating the model. Henceforth, the developed numerical modelling strategy will be used to investigate other influences on the masonry wall.

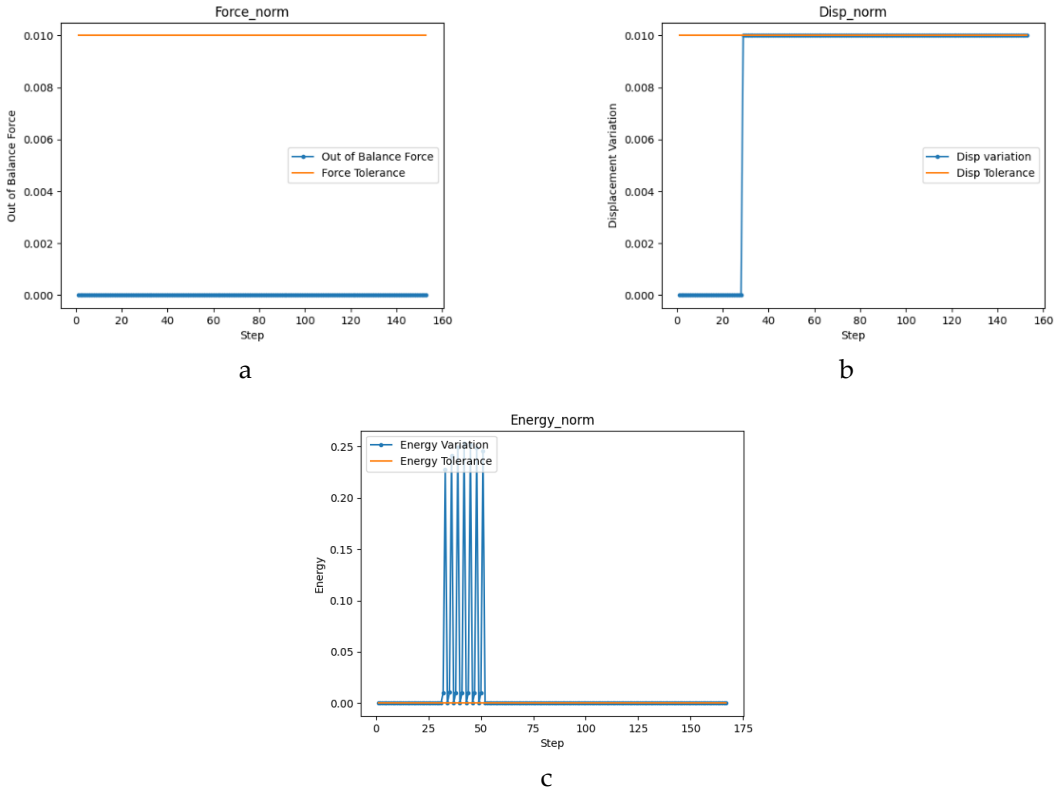

Figure 4.15: Variation in convergence norms : (a) Force, (b) Displacement, (c) Energy

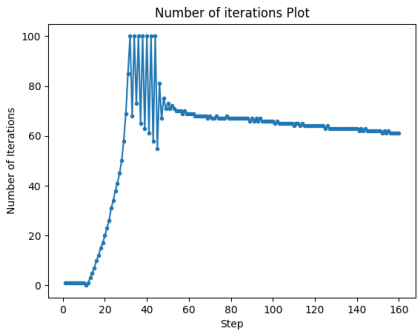

Figure 4.16: Number of iterations for each load-step

Conclusion

In an effort to validate the numerical model, eigenfrequencies from literature were compared against those obtained using the Structural Eigenvalue analysis in DIANA for both unreinforced and timber-reinforced masonry. Figure 4.1 and Figure 4.2 illustrate the correspondence of the obtained natural frequencies to the existing data in literature. Mode I and Mode II frequencies for unreinforced masonry was found to have an error of 11.40% and 16.50%. The same values for timber-reinforced masonry were 7.94%, 23.30% and 21.70%.

Pushover curves, representing the relationship between base shear and displacement, were also plotted for both types of masonry. These curves were further compared with experimental and numerical capacity curves. The maximum lateral resistance achieved in both numerical models (45.77 kN and 45.68 kN) is approximately equal to the experimental value (45.64 kN). For timber-reinforced masonry (62.51 kN and 65.95 kN), the same value is 7-9% less than the experimental value (68.92 kN). The pushover curves for both numerical models correspond closely to each other with a slightly sharper drop in capacity after peak force for the Model T1. The timber-reinforced masonry has a maximum lateral force capacity around 40% higher than that of unreinforced masonry.

Displacement contours, obtained were compared to benchmark studies, reveal that the numerical model provided a reasonable correspondence, although there were differences in the simulation of failure mechanisms between the two iteration methods: Newton-Raphson and Quasi-Newton. The major difference between the two, apart from the localised damage in the former and more distributed damage in the latter, was the failure mechanism developed in the wall. While Model U1 simulated the separation of lateral walls, the Model U2 was able to simulate the failure mechanism observed in the experiment of horizontal flexure (bending) of the frontal wall. For this reason, a choice has been made to conduct the remaining analyses in this thesis with the Quasi-Newton iteration method without any reduction in Poisson's ratio.

Crack widths were analysed to assess damage, where the Models U1 and T1 seemed to simulate experimental crack patterns more precisely. Models U2 and T2, though to a lesser extent, is also able to satisfactorily simulate experimental cracking patterns. The study also monitored convergence based on set criteria.

4.2. Alternative modelling approaches for timber laces and connections

The first set of numerical modelling was done with considerable simplifications and assumptions. In this section, some of those simplifications and assumptions are explored and studies from refinement of those simplifications are presented.

4.2.1. Limit States

To conduct a practical assessment of any analysis, it is pertinent to predefine states of damage (damage limits) and the acceptable damage between the two walls are compared for the corresponding damage limit states. Since Severe Damage and Near Collapse are critical, results corresponding to these limit states are presented in Table 4.2; they are based on the Limit States defined by Eurocode 8 described in detail in Chapter 2.11.2.3.

Table 4.2: Drift levels and lateral resistance at Limit States

Limit State	**Severe Damage**			**Near Collapse**		
	Base Shear	Disp.	Drift	Base Shear	Disp.	Drift
Values from	kN	mm	%	kN	mm	%
Unreinforced Murano et al. (2019)	46.65		0.28	36.52		1.01
Model U1	45.77	1.66	0.12	29.91	3.97	0.29
Model U2	45.68	1.97	0.15	36.55	3.47	0.25
Timber-reinforced Murano et al. (2019)	68.92		0.28	55.13		1.42
Model T1	62.51	3.12	0.23	48.06	6.23	0.46
Model T2	63.95	4.75	0.35	50.98	9.25	0.69

4.2.2. Stresses in timber elements

Murano et al. (2019) do not report damage to the timber elements post the experiment. Therefore, timber elements were modelled as linear elastic elements. However, the stresses generated in the timber elements are verified against the strength of the material.

Figure 4.17 shows the stress contours in the timber elements. Since the model is symmetrical. the left and right timber laces may be assumed to have similar, if not the same stresses. Therefore, only the stresses in one (top right) timber lace are presented. It can be seen in the figure that the inner laces have a higher distribution of respective stresses. Moreover, the inner junction of longitudinal and lateral laces exhibits the highest concentration of stresses.

The stresses plotted in Figure 4.19 are taken at the inner junction of the transverse and longitudinal timber element (Figure 4.18). This node has the highest concentration in the model. The reason for this higher stress concentration could be varied – modelling of the connection as perfectly connected, re-entrant corners or mesh sizes. Mesh sizes were refined

to check the effect of the stresses and it was found that indeed the stresses reduce as they even out across the length and the width of the timber element as the mesh size is refined further. However, for the purpose of a simplified analysis the concentrated stresses at the inner node from the validated model are analysed to verify against the strength of the timber.

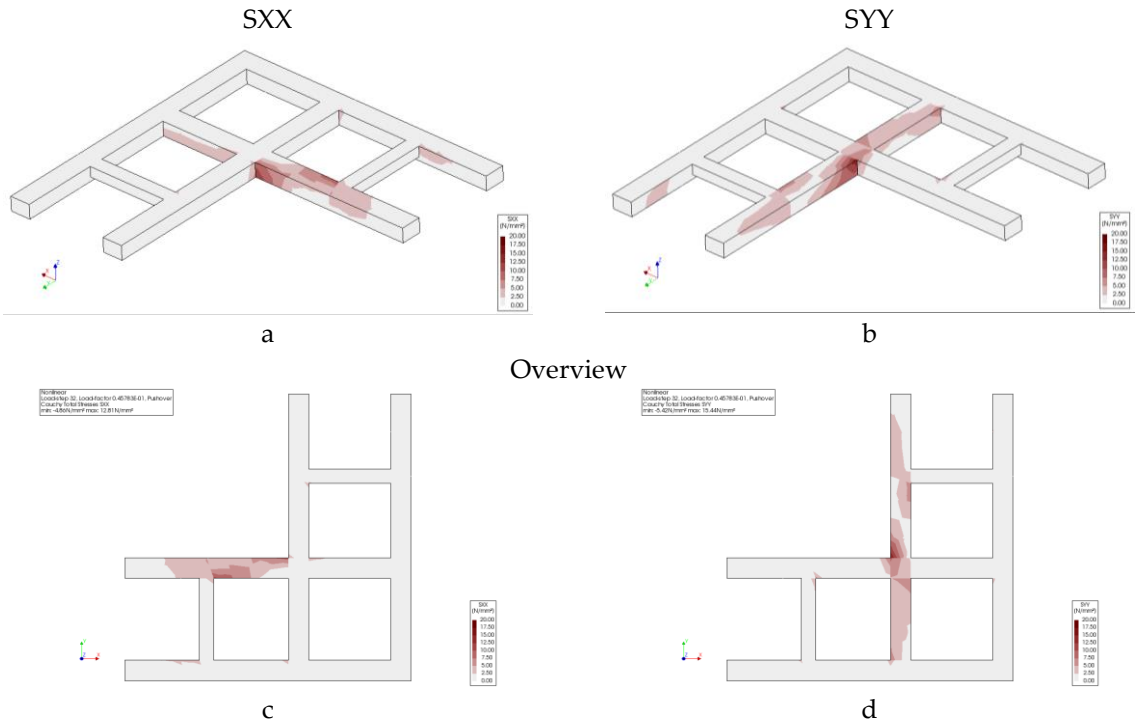

Figure 4.17: Stresses in timber elements : (a) and (c) SXX, (b) and (d) SYY

It can be seen from Figure 4.19 that the stresses remain well below the design bending strength of the D24 class timber section (18.46 N/mm^2). Also note that the SYY stress, in the out-of-plane direction, remains high after undergoing a drop immediately after the peak phase. However, the stresses in the X-direction (SXX), from the timber laces in the frontal wall reduce considerably, though gradually, after the peak has been attained. This can be attributed to the fact that the mid-section of the frontal wall undergoes substantial cracking after the SD limit state. This extensive cracking leads to energy dissipation, resulting in declining stresses in the frontal wall timber band. The laces in the lateral wall, on the other hand, remain activated as the lateral wall does not undergo substantial damage.

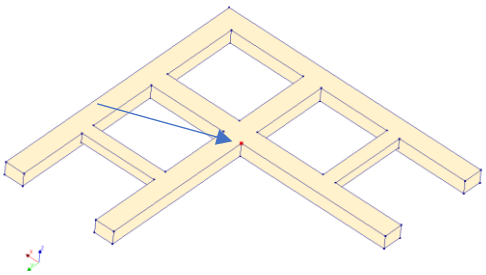

Figure 4.18: Location of node for stresses

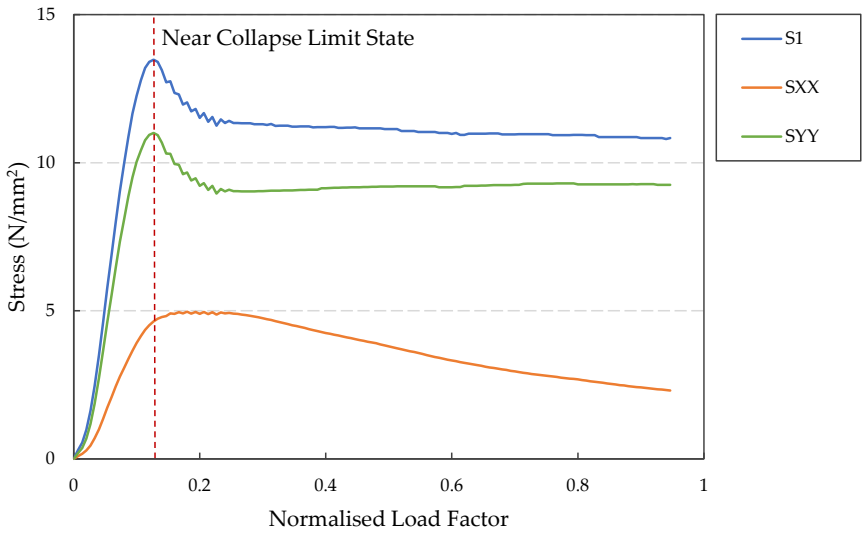

Figure 4.19: Stresses in timber laces

Figure 4.20 provides insight into the activation of the timber laces and the effect of this mechanism to the increase in force capacity of the wall. The normalised base shear and normalised stresses are plotted against normalised displacement, showing that the stresses in timber elements have a direct correlation with the out-of-plane response of the masonry wall. The increasing stress in the timber elements results in an increasing maximum lateral resistance in the timber-reinforced masonry wall while the unreinforced masonry undergoes a considerable loss of capacity. Another point of significance is the relatively lesser degradation of force capacity in the post-peak phase for timber-reinforced masonry compared to the unreinforced one. The persistent stress in the timber lace (SYY) can be one of the influencing factors for this, the lack of which in unreinforced masonry leads to higher degradation of toughness. This phenomenon would lead to a timber-reinforced house to have some residual strength after the earthquake allowing the occupants to leave the house safely while the unreinforced masonry structure might suffer sudden, immediate collapse.

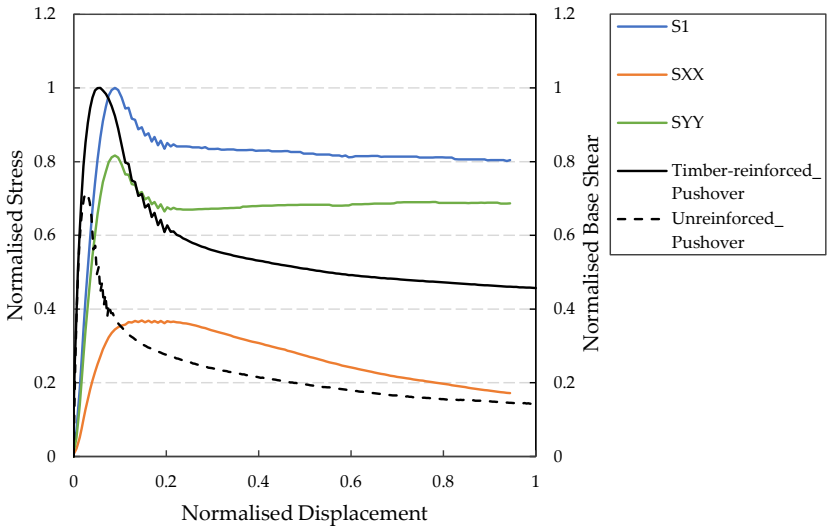

Figure 4.20: Stresses normalised compared with normalised pushover curve

4.2.3. Timber masonry interface

Murano et al. (2019) reported "high level of deformation at the interface between timber elements and mortar joints". The experimental cracking pattern observed also verifies this mechanism. However, in the numerical model, this interaction is assumed to be perfectly connected. Hence, the interaction between timber and masonry is considered as a point of refinement from the numerical point of view. Therefore, an attempt was made in this thesis to simulate the specific cracking that occurs at the interface of mortar and timber by modelling the interface discretely. The literature review for the timber-masonry interface and the numerical model developed can be examined in Chapter 2.9.2 and Chapter 3.1.5.3 respectively. This section presents the results from the study.

From the literature review, material properties for the interface were chosen. All other properties and parameters were kept the same to ascertain the influence of the interaction of timber and masonry. The force-displacement curve is presented in Figure 4.21. From the curve it can be seen that there exists a very minor difference between the behaviour of the model that included a discretely modelled timber-masonry interface to the one that did not.

Figure 4.21: Pushover curve for model with timber-masonry interface

Table 4.3 lists the force capacities and drift limits for both models. There is very minimal difference between the force capacities, displacements (and hence the drift limits) of the two models. Note that the relatively higher difference in the Near Collapse limit state is due to the load-step variation as use of the arc length control means that exactly 20% reduced load cannot be attained and hence the nearest load-step has to be used for representational purpose.

Figure 4.22 shows stresses for the inner corner node of the timber element where the stresses are highest within the length of the timber band. The stresses are plotted against the normalized load factor which also represents the load-steps starting from first till the end of the analysis. The NC limit state, calculated in Chapter 4.2.1 is also indicated. S1_TMI, SXX_TMI, SYY_TMI are the stresses from the numerical model with timber-masonry interface, while S1, SXX, SYY are stresses from the numerical model assuming perfect

connection. As seen from the figure, the stresses at the node with the highest stresses remain within the strength limit of the D24 class timber element.

The stresses between the two models do not vary considerably except much beyond the NC limit state when the stresses in the model assuming perfect connections start decreasing while the stresses in the model with timber-masonry interface continue to either increase or remain constant. Since analysing a structure beyond a highly damaged state is complex, the scope of this thesis remains an assessment of stresses until the NC limit state. Within this limit, the stresses between the models is hardly discernible. However, this study already provides an insight into the potential of an in-depth investigation into the interface of masonry and timber.

Table 4.3: Comparison of Force capacity and drift for Limit States for Timber-Masonry Interface

Limit State	**Severe Damage**			**Near Collapse**		
	Base Shear	Disp.	Drift	Base Shear	Disp.	Drift
Timber-masonry interface	kN	mm	%	kN	mm	%
Perfectly connected	63.95	4.75	0.35	50.98	9.25	0.69
Discretely modelled	63.37	4.81	0.36	51.60	9.28	0.69

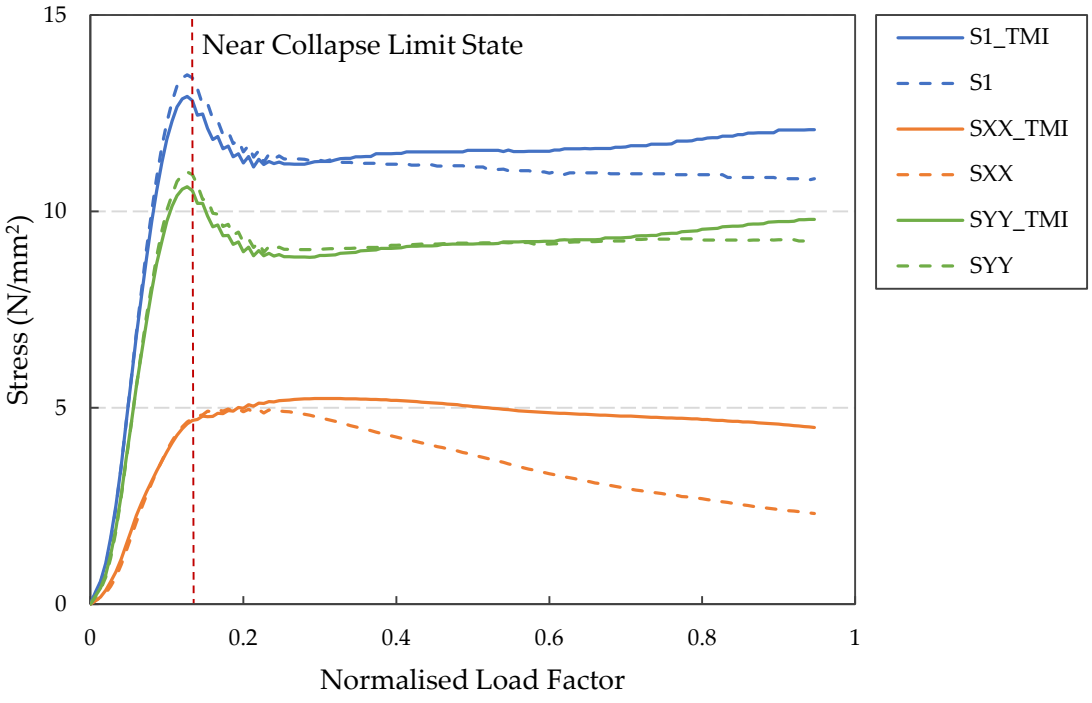

Figure 4.22: Stresses in timber elements at Near Collapse limit state

Figure 4.23 shows the nodes selected for a comparison of stresses at the NC and SD limit state between the masonry model with full connection and the timber-masonry interface. Figure

4.24 displays the stresses at the front nodes of the timber lace shown above. As expected, the highest stress is at the connection of longitudinal and lateral timber brace, while nodes at the ends of the timber bands had the lowest stress. Additionally, the Near Collapse limit state unsurprisingly showed higher stresses than the Severe Damage limit state for all nodes. Interestingly, the Interface model had higher stresses than the model with an assumed perfect connection. This is consistent with the finding in Figure 4.22.

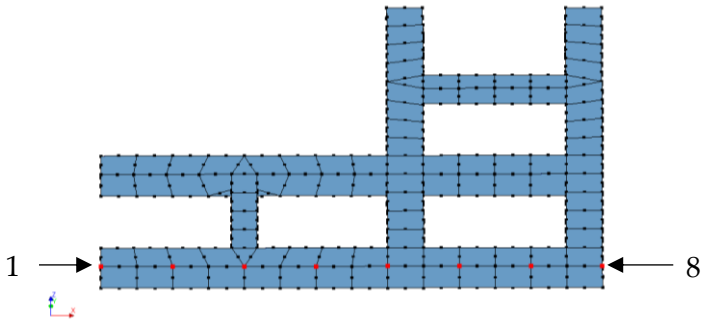

Figure 4.23: Nodes chosen for stress comparison

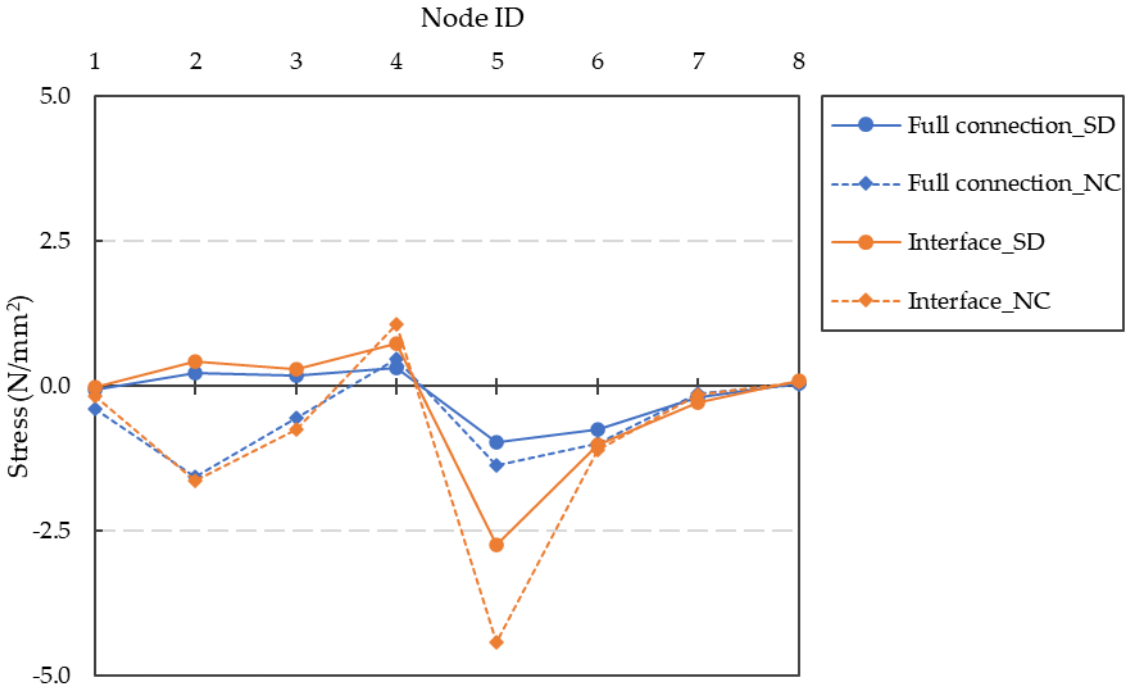

Figure 4.24: 'SXX' Stresses in timber lace in frontal wall

Additionally, more models were analysed with properties from the studies presented in the literature review. The effect of stiffness values, interface and tension cut-off was also studied.

4.2.4. Timber-to-timber connection

The connection between different timber elements (longitudinal beams, transverse beams and crossbeams connecting parallel beams) has been considered as perfectly connected. However, the actual connection is a half-lapped nailed joint that has certain rotational stiffness but is not perfectly connected. This was considered as the second point of refinement in the study. A literature review was conducted to explore discrete modelling of timber-to-timber connections using connectors such as dowels, nails, and screws. However discrete modelling of such a joint was found to be outside the scope of this thesis and this remains a point of future research. The numerical model setup for the hinged connection is described in Chapter 3.1.5.

The effect of the interaction of timber elements at their connections on the behaviour of the structure is studied through a simplified approach. All connections between timber main beams were considered to be hinged, while no other property was changed. The results are presented in Figure 4.25. The presence of hinges does not make a significant difference to either the force capacity or the behaviour of the structure and a 3% reduction of maximum lateral resistance is noticed.

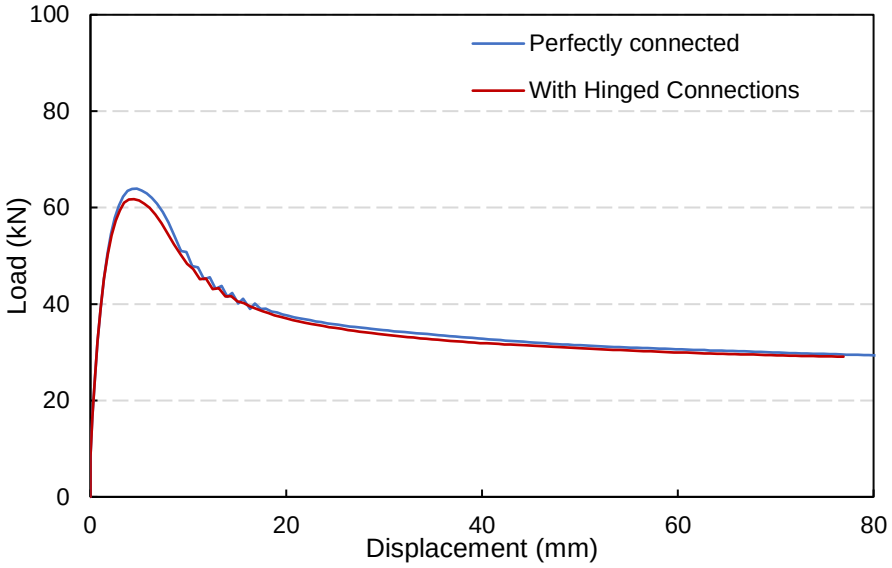

Figure 4.25: Pushover curve for model with hinged connections

4.2.5. Hinged connection and timber-masonry interface

The representation of hinged connections along with the timber-masonry interface did not make a significant difference to either the capacity or the behaviour of the masonry wall. Another model was simulated with both model refinements. Table 4.4 provides a summary of force capacities of the four model variations. The models with timber-interface, hinged connections, and both show a reduction of maximum lateral resistance of 1%, 3% and 7%, respectively. The drift levels at SD and NC limit states remain identical. Note that the very minor discrepancy in the values for NC limit state is due to the inevitable load-step adjustment from arc length control. Figure 4.26 shows the force-displacement curves for the above stated

models. All models show very minimal disparity in terms of force envelope and softening response – key indicators of out-of-plane behaviour.

There is a need for more in-depth investigation and detailed discrete numerical modelling of the interface between timber and masonry as well as the connections between timber elements. However, considering the modelling approach and assumptions made in this study, both show very limited effect on the local and global behaviour of the timber-laced masonry wall, especially until the key examination points – Severe Damage (SD) limit state and Near Collapse (NC) limit state. Therefore, the numerical analyses that follow from hereon, consider the assumptions of perfectly connected timber elements and perfect connection between the timber and masonry elements. This is also done to keep the computational requirements of the numerical analysis manageable.

Table 4.4: Drift levels and lateral resistance at limit states for masonry refinement models with timber-reinforced interface and hinged connections

Limit States	Severe Damage			Near Collapse		
	Base Shear	Disp.	Drift	Base Shear	Disp.	Drift
Numerical model	kN	mm	%	kN	mm	%
Timber-reinforced masonry	63.95	4.75	0.35	50.98	9.25	0.69
With timber-masonry interface	63.37	4.32	0.32	51.60	9.28	0.69
With hinged connections	61.77	4.45	0.33	48.31	9.88	0.73
With timber-masonry interface and hinged connections	59.44	4.18	0.31	47.40	9.63	0.71

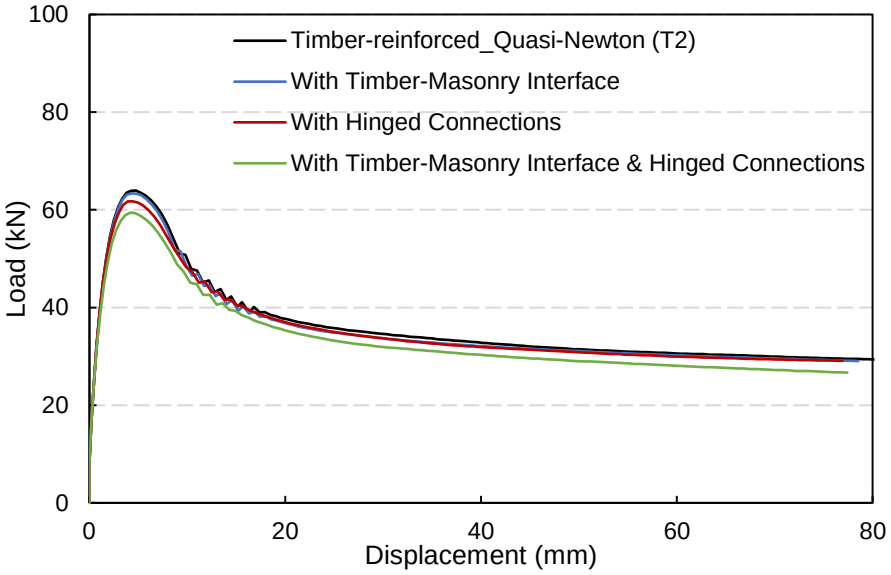

Figure 4.26: Force-displacement curves for refinement models of timber-reinforced masonry

4.2.6. Connected timber braces

A Bhatar building rarely has discontinued timber elements that are only present at the corners. The timber braces are usually connected throughout the length of the wall. Therefore, a numerical analysis was conducted for a model with connected timber braces and all other parameters retained. This section presents the findings of the study. The chapter will refer to the two models as 'Trf_corner' and 'Trf_connected' for the models with timber bands only present at the corners and timber bands connected throughout the wall, respectively.

4.2.6.1. Numerical model

Figure 4.27 shows the numerical model developed. As apparent, the timber members join throughout the frontal wall, but also extend to the end of the lateral walls. The cross beams connecting the parallel timber beams have similar spacing as the previous models.

4.2.6.2. Force capacity

Figure 4.28 shows the pushover curve obtained for the walls with connected bands 'Trf_connected' and corner bands 'Trf_corner'. A remarkable increase can be seen in the base shear force, representing the lateral load the wall is able to resist. There does exist a clear, noticeable softening after the maximum load is attained, however after the initial softening, the force reduction is rather gradual. This depicts higher ductility on the structure's part.

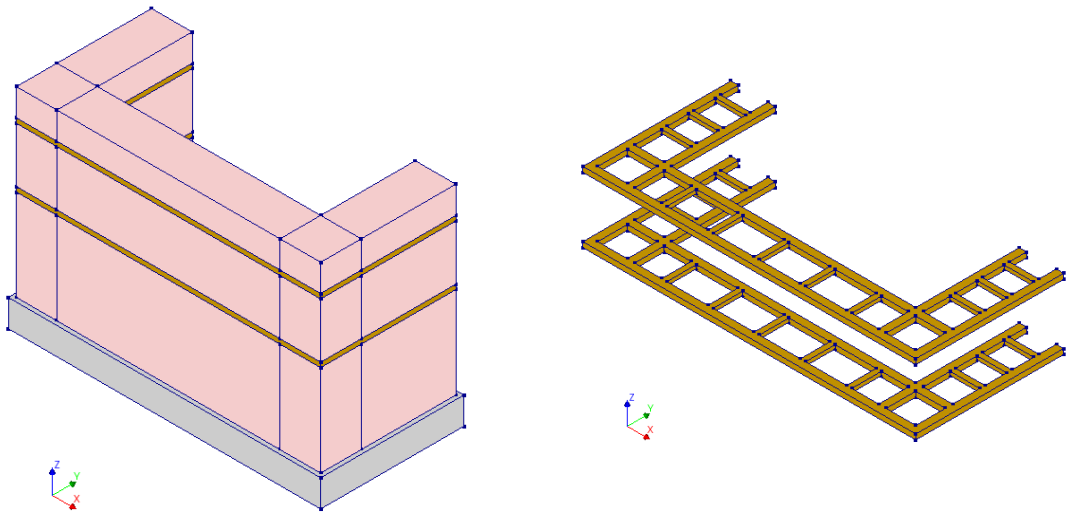

a b

Figure 4.27: (a) Numerical model for connected timber bands, and (b) timber laces

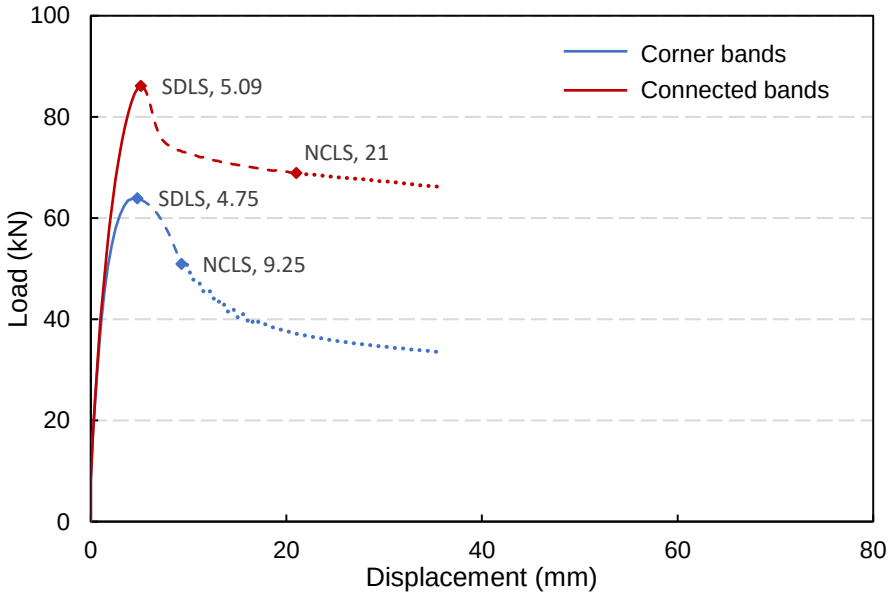

Figure 4.28: Pushover curve for corner and connected bands

4.2.6.3. Drift levels and resistance at limit states

Table 4.5 lists the displacements and base shear force related to the SD and NC limit states. While the base shear for Trf_connected at SD limit state is 35% higher than that of Trf_corner, the drift levels do not show appreciable change. However, the drift level at the NC limit state for the former is significantly higher than for the latter. The higher ductility is evidently the result of the connected timber bands avoiding the localisation of cracks at the centre of the frontal wall, therefore allowing for more gradual damage progression.

Table 4.5: Drift levels and lateral resistance at limit states for masonry wall with bands connected throughout the length

Limit States	**Severe Damage**			**Near Collapse**		
	Base Shear	**Disp.**	**Drift**	**Base Shear**	**Disp.**	**Drift**
Numerical model	kN	mm	%	kN	mm	%
Corner braces	63.95	4.75	0.35	50.98	9.25	0.69
Connected braces	86.14	5.09	0.38	68.91	21.0	1.5

4.2.6.4. Crack patterns

This section compares the cracking patterns between the two masonry walls at the SD and NC limit state. Since the crack widths had high variation – from less than 0.5 mm for Trf_corner at SD limit state, to more than 9 mm for the Trf_connected at the NC limit state; a custom scale was created to ensure appropriate comparison.

Figure 4.29 shows the extent of cracking at the SD limit state – the state when the masonry wall achieves the maximum lateral resistance. Expectedly, the cracking (and hence damage) in Trf_corner was concentrated in the lengthwise mid-section of the wall due to the absence of timber elements in the region (Figure 4.29a). In the event of selective presence of timber bands, the crack seems to prefer the region with a lack of timber elements. On the other hand, the cracks are more distributed throughout the length of the frontal wall for Trf_connected (Figure 4.29b). Figure 4.29d shows a higher extent of damage in the lateral walls in Trf_connected than Trf_corner (Figure 4.29c). Concluding, while the damage is concentrated in the frontal wall for Trf_corner, Trf_connected has a relatively higher presence of cracks in the transversal walls.

Figure 4.30 exhibits the state of cracking at the NC limit state for the walls. It can be seen from comparison of Figure 4.30a and Figure 4.30b that the damage to the frontal wall has reached a significant level in the Trf_corner while it still exhibits a very limited extent of cracking in Trf_connected. Observing the Figure 4.30d, it can be seen that the extent of damage at the base of the lateral wall increases even further in Trf_connected displaying a flexural crack. The large spread of cracking in the Trf_corner (Figure 4.30a) in the façade wall would mean that the collapse of the structure might happen at a lower displacement level.

Additionally, Trf_connected shows a high state of damage at the base of the lateral walls. This cracking should not be perceived as making the structure more vulnerable as Trf_connected has a 35% higher force capacity than Trf_corner. The drift level is also 127% higher for Trf_connected at the SD limit state. In fact, higher in-plane cracking suggests higher energy dissipation in turn suggesting that the structure is able to undergo much larger externally applied loads before failing. A point to note is the occurrence of stepped diagonal cracks at the base of lateral walls representing sliding shear behaviour.

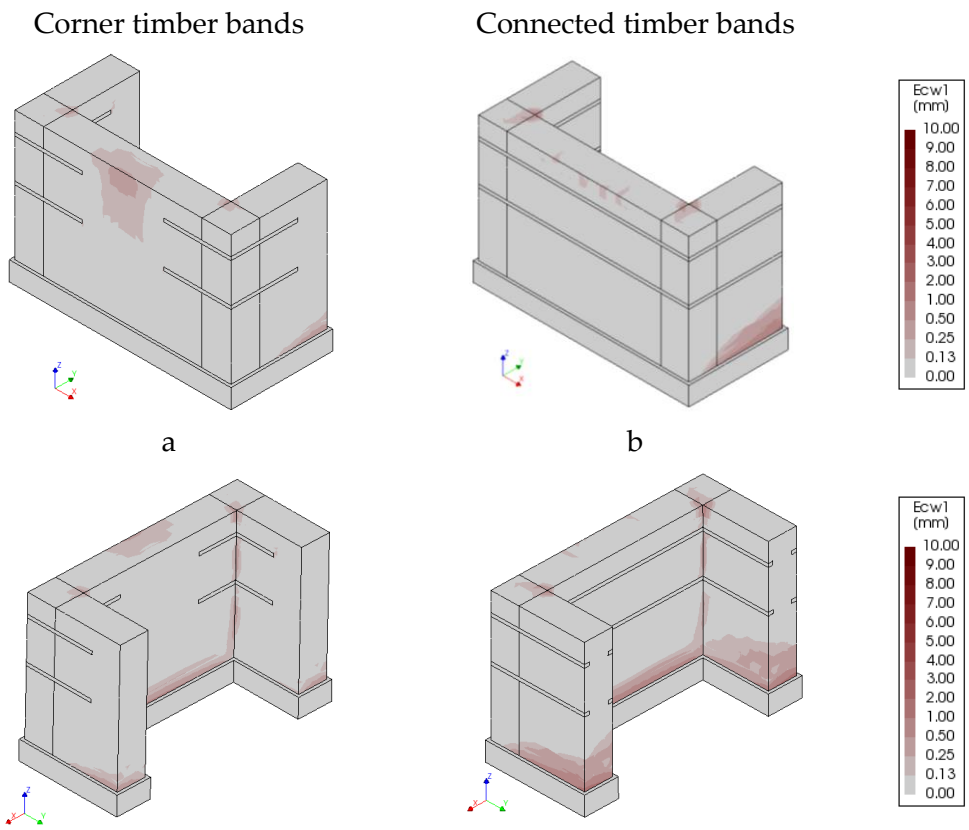

Figure 4.29: Cracking patterns at SDLS: (a) and (b) front view; (c) and (d) rear view

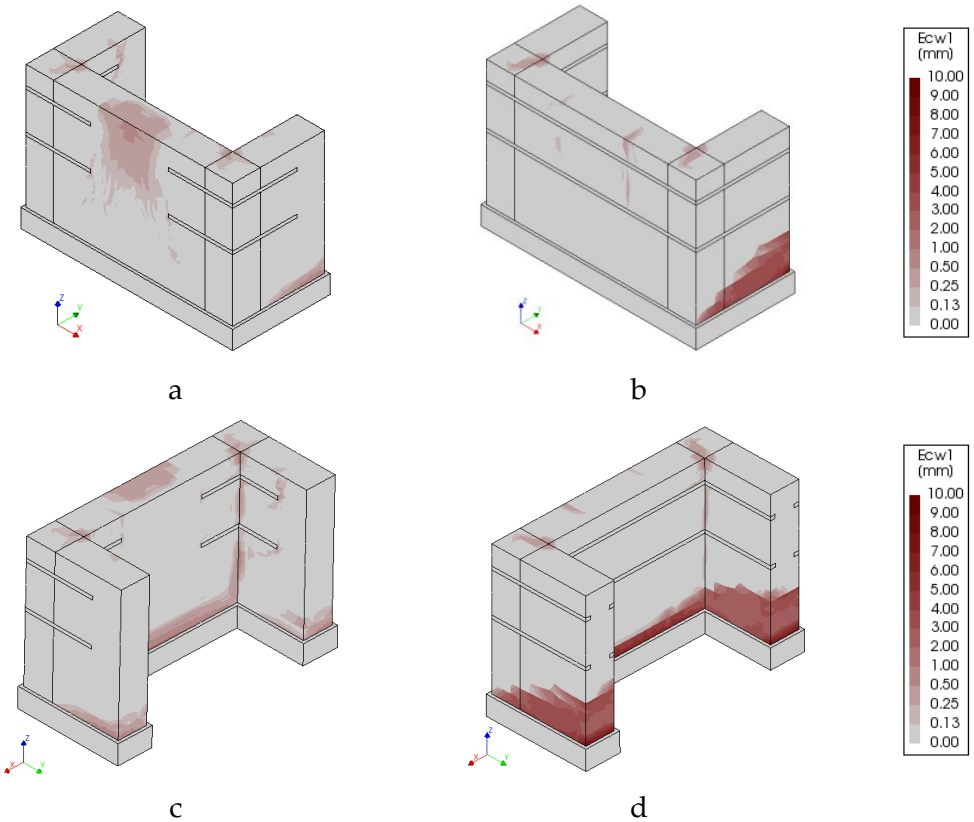

Figure 4.30: Cracking patterns at NCLS: (a) and (b) front view; (c) and (d) rear view

4.2.6.5. Stresses

The difference between the resistance of unreinforced and timber-reinforced masonry can be explained by assessing the stresses generated in the timber laces and comparing them to the stresses in the masonry. To this end, the tensile stresses (SXX) at the bottom row of the top timber lace on the front façade (blue line shown in Figure 4.31) are compared to the stresses in masonry (orange line shown in Figure 4.31) in Figure 4.33. The relative location of the ninety-one nodes chosen for stresses are highlighted in Figure 4.32.

The displacements for timber lace and masonry in Y direction at SD and NC limit state (for same nodes as for stresses in Figure 4.32) are also presented on the same graph for relative comparison. The figure illustrates that the stresses in masonry remain below its tensile strength of 0.074 MPa. However, the stresses in timber at SD limit state are already exceeding 6 N/mm². These stresses are however still lower than the design bending strength of 18.46 N/mm² for D24 strength class timber. On a local level, the stresses in timber laces are low at the location of the cross beams and high at the location between the cross beams. This is attributable to the better connection, and hence, better redistribution of stresses between the inner and the outer longitudinal timber section due to the presence of cross beams. On a global level, the stresses, expectedly, are minimum at the ends near the lateral walls and maximum at the mid-section of the frontal façade wall, mimicking the bending profile of the displacement of the band.

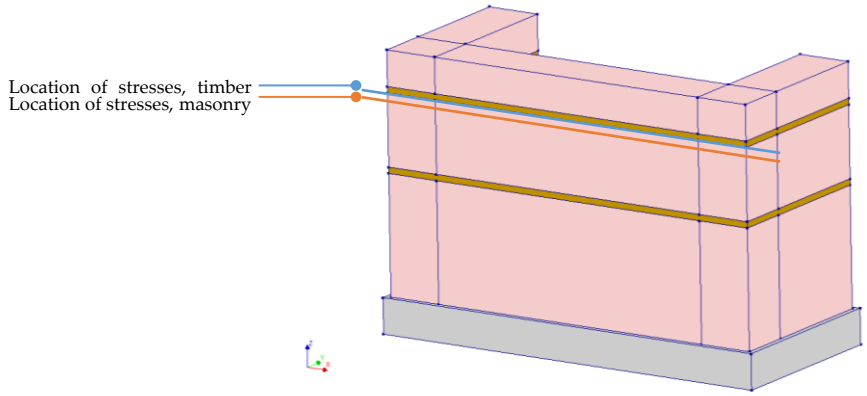

Figure 4.31: Location of stresses for timber and masonry shown in Figure 4.33

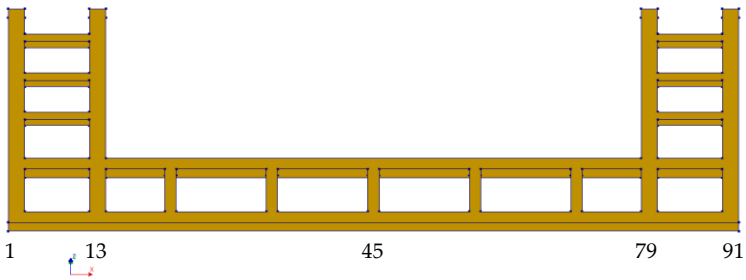

Figure 4.32: Location of nodes for stresses compared in Figure 4.33

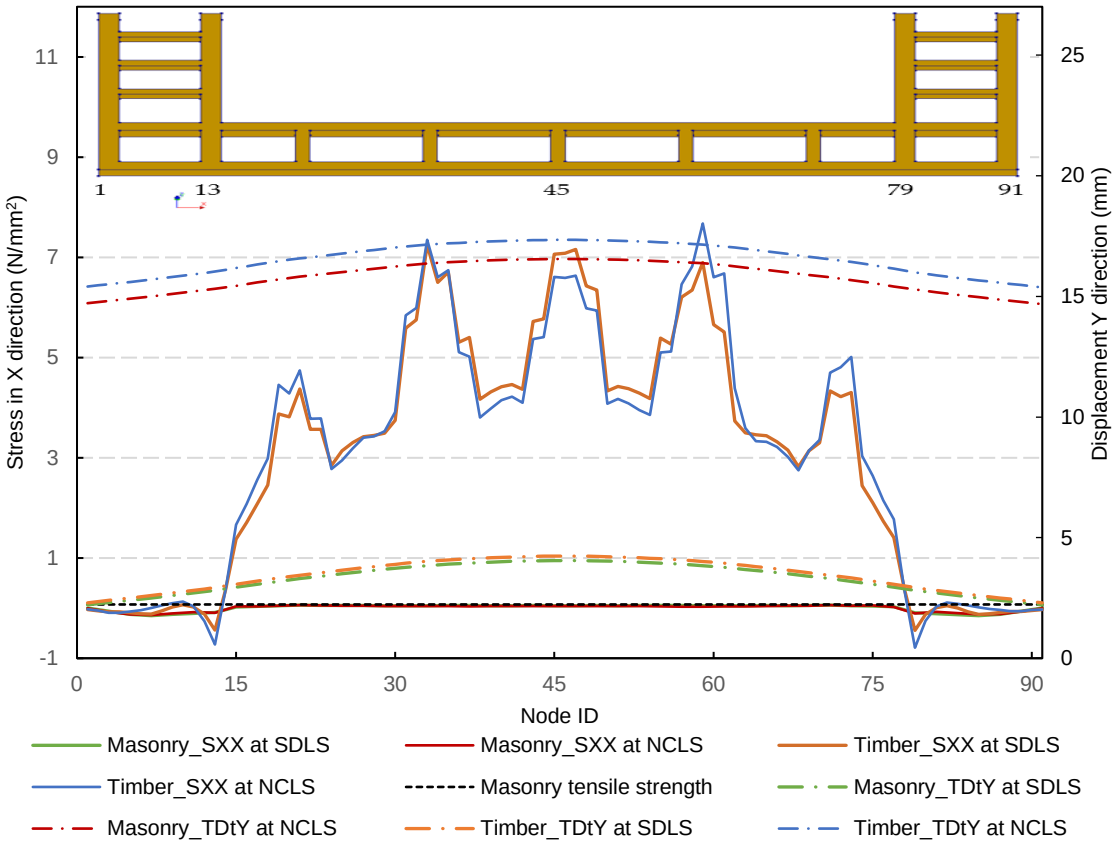

Figure 4.33: Stresses and displacement for timber and masonry on the front façade at SD and NC limit state

Additionally, the stresses in the section of timber close to the lateral walls experience very low tensile stresses due to redistribution of stresses and direct connection with orthogonal timber sections embedded in lateral wall. It can be observed from the figure that the relatively high stresses in timber and very low stresses in masonry depict that the stresses generated by the external lateral load on the structure is drawn towards itself by the timber bands resulting in a higher overall resistance for the structure.

Conclusion

Limit states are predefined states of damage that help assess practical evaluation of analyses. The study presents the drift levels and lateral resistance at Severe Damage (SD) and Near Collapse (NC) limit states for both unreinforced and timber-reinforced masonry based on definitions from the Eurocode. The timber elements in the experiment showed no damage and were modelled as linear elastic. Stresses in these timber elements, especially at inner junctions, displayed higher concentrations. However, the stresses remained well below the strength limit for the D24 class timber section. The reinforcement with timber indicated higher residual strength post-earthquake, potentially providing safety against immediate collapse, unlike unreinforced masonry. The timber-masonry interface was investigated, highlighting the distinction between perfectly connected and discretely modelled interfaces. Although

differences were minimal in the force capacities and drifts between the two models, stresses at specific nodes were more pronounced in the discretely modelled interface, hinting at the potential for more in-depth study into the masonry-timber connection.

In a study examining timber-to-timber connections and timber-masonry interfaces, several key findings emerged. While the different timber elements were initially considered perfectly connected, the reality reflects a half-lapped nailed joint with some rotational stiffness. A literature review revealed potential modelling techniques using connectors such as dowels, nails, and screws, but their discrete modelling was beyond the scope of this study. Simplified numerical modelling assessed the impact of timber element connections on structural behaviour, with results suggesting very minor differences in force capacity and structural behaviour, most notably a 3% reduction in maximum lateral resistance with hinged connections. When integrating hinged connections with timber-masonry interfaces in a single model, only a slight alteration in the structure's behaviour, to the tune of 7% reduction in force capacity, was noted. Regardless of these observations, future research is suggested into a more detailed exploration of the timber-to-masonry interface and their connections.

Finally, connected timber bands in a U-shaped stone masonry wall were assessed, revealing that connected bands exhibited a substantial increased base shear force (35% at both SD and NC limit states) and greater ductility than when the said bands are present only at the corners. This effect was especially pronounced at the Severe Damage limit state. This is largely attributed to the connected timber bands preventing crack localization, leading to a more spread-out damage progression as well as a change in the failure mechanism from a brittle, sudden out-of-plane failure for the setup to a ductile, gradual in-plane damage evolution. The drift level at SD and NC limit state increased by 7% and 127%, respectively, for masonry wall with timber bands connected throughout the frontal wall when compared to the wall with timber bands present only at the corners.

Even so, the high drift level at NC limit state should be regarded with cautiousness as the definition of NC limit state as the displacement level at 20% reduction of the maximum force capacity is somewhat subjective. The limit states greatly depend on specific conditions of a certain structure, and it is possible that for given conditions, large parts of a structure might undergo collapse before the displacement level corresponding to 20% reduction of the maximum force capacity. However, even allowing for conservativeness, the connected timber bands would allow for significantly higher displacement capacity while undergoing lesser damage.

4.3. Sensitivity study

Experimental campaigns reviewed in literature carried out to assess seismic capacity of masonry have shown that primary factors affecting the out-of-plane performance are the masonry tensile strength and the number of horizontal timber bands. Many other factors influence the complex behaviour of masonry. However, the experimental investigation on the influence of all these parameters would be excessively costly and time-consuming. To this end, calibrated and validated numerical models provide a useful avenue to determine these effects. This section presents a sensitivity study of the timber-reinforced masonry building typology, assessing the influence of the following parameters: (i) friction coefficient, (ii) cohesion, (iii) aspect ratio, (iv) pre-compression level (overburden stress), and (v) timber strength class.

4.3.1. Timber-masonry interface

As described in Chapter 4.2.3, the literature revealed a range of frictional coefficient and cohesion values for the interface between timber and masonry. The models were tested for the model with timber bands at corners, with some variations for the frictional angle (in radians) and cohesion (N/mm²). The pushover curves for the models, as seen in Figure 4.34, show that the interface elements discretely modelled for the masonry with timber bands at corners does not have an appreciable change in either the maximum lateral force or post-peak behaviour. This suggests – a) the interaction of timber bands and masonry has marginal effect on the overall behaviour of the masonry, but more importantly, b) the current modelling strategy, of interface elements governed by Coulomb's friction law, is not able to capture the effect of the friction between timber bands and masonry surrounding it, effectively. This points to further refinements to the frictional model between the timber bands and masonry in the future. The continuum modelling strategy implies that the masonry between the timber bands is considered as a part of a single homogenous block of masonry which is perfectly connected to the masonry above and below the timber bands. This however might result in overestimation of strength as it differs slightly from the construction method.

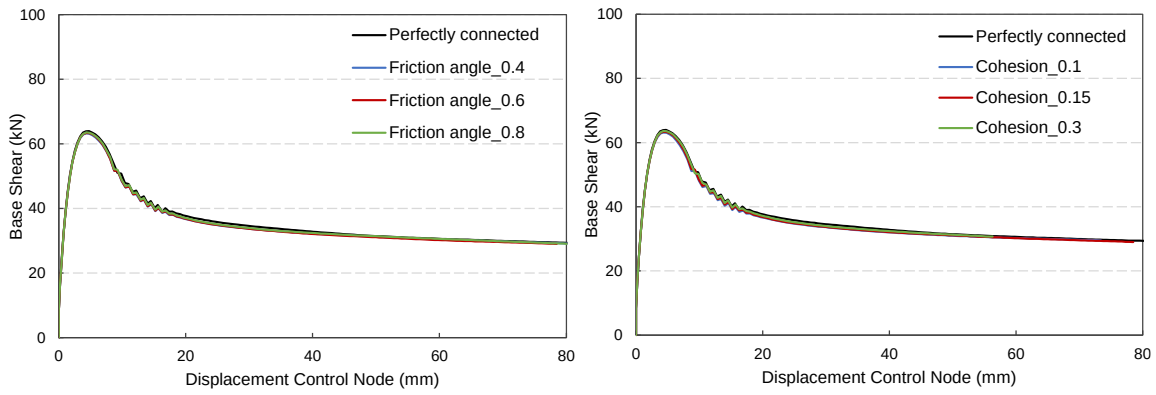

a b

Figure 4.34: Sensitivity study for material properties of interface element : a) Friction angle, and b) Cohesion

This can be resolved by modelling the masonry elements below and above the timber bands. This will result in a strategy that is able to separately include the effects of the weak mortar joints between the masonry above and below the timber bands. However, discrete modelling of the mortar and distinct elements of the masonry has not been conducted for this study.

4.3.2. Aspect ratio

The influence of the aspect ratio on the out-of-plane response of the walls was also explored by varying the ratio of wall height to length between 1.0 and 2.0. Four simulated models with varying aspect ratios are presented in Figure 4.35. The aspect ratio, in this case, is defined as the ratio between wall length and wall height with the latter remaining constant for all models. The load-displacement curves (Figure 4.36) exhibit a trend of increasing stiffness for walls with a lower aspect ratio, while the models with longer frontal walls, predictably, demonstrate larger force capacity than those with shorter walls. All models were allowed to run for 150 load-steps. Plotting normalised displacements against normalised forces also showed that the longer the wall, the higher the overall displacements would be.

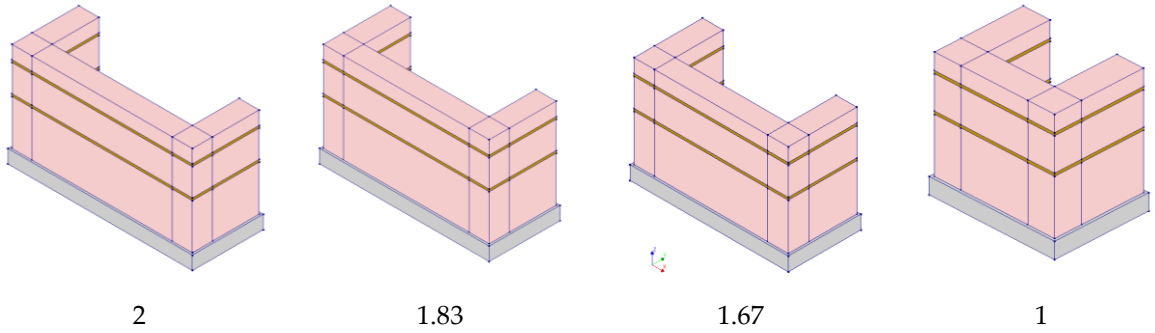

Figure 4.35: Models with varying aspect ratios : a) 2.0, b) 1.83, c) 1.67, and d) 1.0

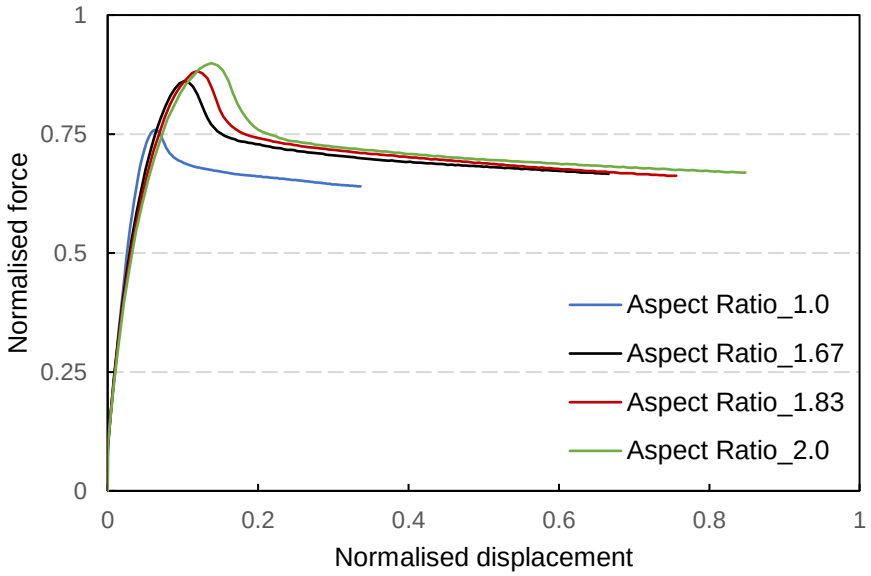

Figure 4.36: Load-displacement curves obtained for varying aspect ratios

4.3.3. Pre-compression

The experimental campaign in benchmark tests applied a normal compressive load on the lateral walls of the specimen to simulate the weight of a traditional heavy timber roof. Therefore, the validated numerical model had a pre-compression of 0.1 N/mm^2. To assess the sensitivity of the validated numerical model to pre-compressive load, two more models were simulated with half (0.05 N/mm^2) and double (0.2 N/mm^2) the original pre-compressive load. The former within this range is representative of an actual timber roof weight calculated in Chapter 5.2.1, while the latter could denote the pre-compressive load resulting from the overburden of more than one floor on masonry walls at lower levels. This analysis was conducted for the model with timber laces connected throughout the frontal wall. The results in Figure 4.37 indicate that the behaviour of the simulated wall is highly sensitive to the vertical compressive load on the lateral walls. The higher pre-compression on lateral walls resulted in a significantly higher force capacity. The maximum base shear force increased by 37% upon doubling the pre-compression and reduced by 18% upon halving it. This suggests a linear relationship between the pre-compression and force capacity. Such a relationship has been found in previous studies on the effect of pre-compression on unreinforced masonry subjected to out-of-plane two-way bending [106]. However, a larger set of analysis results is needed to arrive at a more certain conclusion. The difference between the residual force and force capacity decreases with the increasing pre-compression.

4.3.4. Timber strength

Finally, a preliminary assessment of the effect of the timber material properties on the overall behaviour of the masonry wall was done by changing the linear material properties of the timber used in the numerical model. The validated numerical model had material properties corresponding to timber with strength class D24.

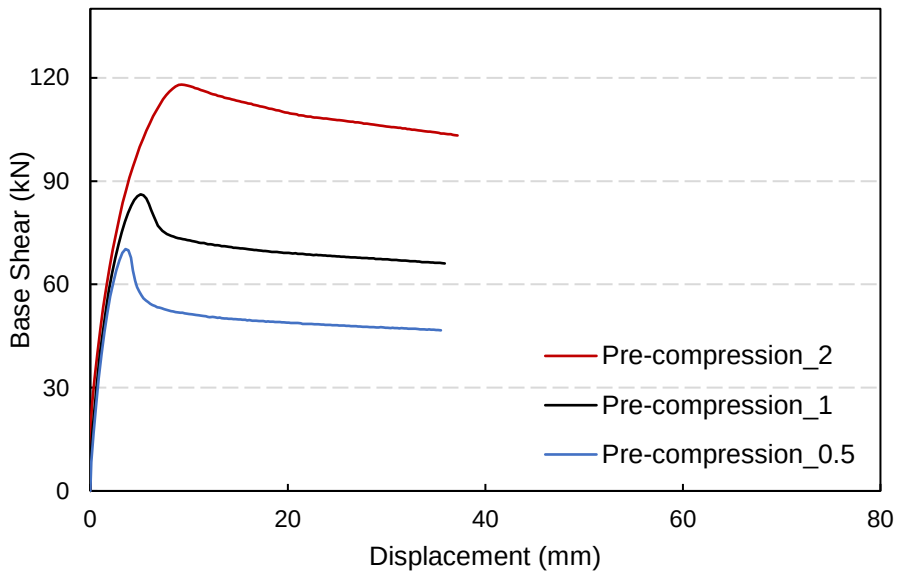

Figure 4.37: Load-displacement curves for varying pre-compression loads

Two more models were simulated for strength classes C24 and D70 with the load-displacement curves shown in Figure 4.38. The values for the three timber strength classes in the numerical model are listed in Table 4.6. The linear material model chosen for timber meant that only variables were mass density and Young's modulus. Changing the density while keeping the modulus of elasticity similar (D24 to C24) did not result in any noticeable difference in the response of the model. However, increasing the modulus of elasticity from 10,000 N/mm^2 to 20,000 N/mm^2 increased the initial stiffness (by 8.53 %) and the maximum force capacity (by 2.53 %) of the model. This indicates that the model is not as sensitive to the density of the timber as it is to the Elastic modulus of the material. This, however, was a preliminary sensitivity study based on a simplified numerical model assuming the behaviour of timber as linear. However, beyond the NC limit state, the timber develops sufficiently high stresses to necessitate employment of non-linear material model for timber. This however was not considered in the present study. In future studies, it would allow the incorporation of orthotropic behaviour of timber with differing mechanical properties in the three perpendicular directions.

Table 4.6: Linear material properties used for sensitivity study for timber strength classes

Strength class	Density (kg/m^3)	Modulus of elasticity (N/mm^2)
D24 (validated model)	600	10,000
D70	900	20,000
C24	350	11,000

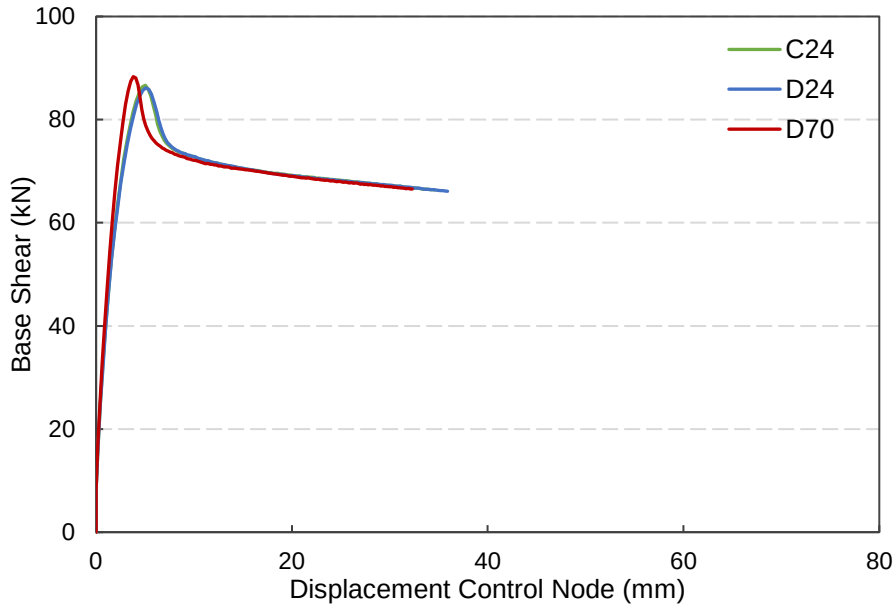

Figure 4.38: Load-displacement curve for timber strength classes

Conclusion

The sensitivity analysis undertaken for timber-reinforced masonry structures under seismic loading offers important insights into the behaviour of these buildings. This analysis emphasized the importance of the interactions between various factors and the contribution to the overall seismic performance.

1. Timber-Masonry Interface: The properties of the interface elements, cohesion and friction angle, were varied within the range found in literature. The findings indicate that the interaction between timber bands and masonry has a limited direct effect on the overall structural behaviour under out-of-plane loads, though having an effect on stresses. The approach, utilising Coulomb's friction law for interface elements along with a complete wall as a single homogenous continuum block, currently falls short in capturing the frictional behaviour between timber and masonry. This points to potential avenues for future work, including refining modelling strategies to consider the effect of weak mortar joints and the distinct behaviour of masonry elements above and below the timber bands.
2. Aspect Ratio: The aspect ratio's influence on the structural behaviour is evident, with structures possessing lower aspect ratios showing increased initial stiffness. Furthermore, walls with longer frontal spans demonstrate higher force capacity. The results reaffirm the inherent trade-offs between structural stiffness and force-bearing capacity concerning wall aspect ratios. The walls with lower aspect ratios were found to be more efficient, faring well for the relationship between wall volume to maximum force capacity achieved.
3. Pre-compression: The influence of pre-compressive loads on the lateral walls of the masonry structures is significant. An apparent linear relationship is observed between pre-compression and force capacity. Specifically, doubling the pre-compression levels enhanced the wall's force capacity by 37%, while halving it reduced the capacity by 18%. This observation aligns with past research on unreinforced masonry subjected to out-of-plane loads.
4. Timber Strength: Preliminary findings on timber strength indicate that the structural behaviour is more sensitive to the modulus of elasticity of the timber than its density. However, the present study's linear assumption for timber behaviour marks a limitation, suggesting that future studies might benefit from integrating a non-linear material model, especially when examining timber beyond the NC limit state.

In conclusion, this sensitivity analysis presents brief results of some of the factors in the seismic response of timber-reinforced masonry structures. While offering valuable insights, it also highlights areas for further research and refinement in modelling techniques.

5. Full-scale Bhatar building

The numerical modelling strategy validated and verified in Chapter 4 and Chapter 4.2 was employed to conduct a numerical analysis on a one-room Bhatar structure. The results from numerical analysis were then used to conduct a seismic assessment described in Chapter 2.11.2

5.1. Geometry

Schacher (2007) illustrated basic rules and guidelines for building a Bhatar house in his manual for artisans. This document forms a good source for the dimensions, geometry, and connection details. A representative sketch from the manual is seen in Figure 5.1a. Building on this, Carabbio (2016) defines a 3.6 m x 3.6 m x 3.0 m house, as seen in Figure 5.1b. With certain minor modifications, this basic structure is used in this thesis to investigate the in-plane and out-of-plane response of Bhatar structures to seismic events.

5.1.1. Openings

Chapter 4 and Chapter 4.2 considered a U-shaped wall without openings. However, a more realistic assessment is possible for a physical building with openings. Therefore, three openings are considered for the Bhatar structure with dimensions in Table 5.1.

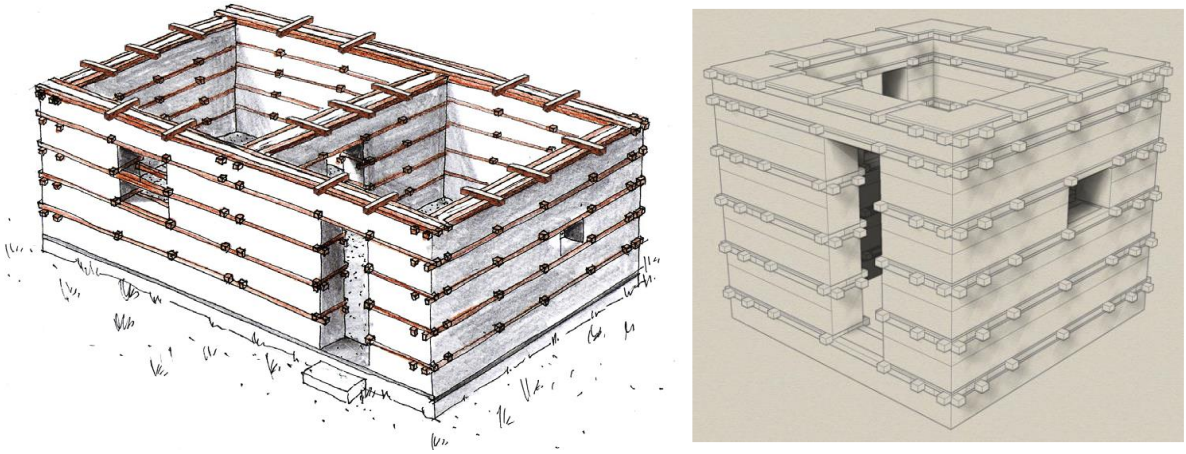

Figure 5.1: A typical Bhatar house : a) Two-room structure [107], and b) One-room structure [63]

Table 5.1: Details of openings for full-scale Bhatar building

Opening	Location	Height (m)	Width (m)
Door	Frontal wall	1.725	0.80
Window	Right lateral wall	1.215	0.80
Window	Light lateral wall	1.215	0.80

5.2. FE modelling

The numerical modelling of the full-scale Bhatar building was conducted according to the methodology established in Chapter 3. This holds true for the finite element model, material model, boundary conditions and material properties. The parameters and procedure for analyses, i.e., iterative techniques, solution control and convergence criteria, are also maintained consistent with those described in Chapter 3.2. The variations to the modelling strategy and analysis are described in this chapter.

5.2.1. Loading conditions

The U-shaped masonry wall was considered to validate the numerical model. Therefore the loading conditions were arranged to mimic the out-of-plane experiment mentioned in [96]. However, to conduct a seismic analysis and assessment, the seismic loads from the actual geographic location have to be considered. The roof load has also been changed to represent the load of a heavy roof typical of this typology.

5.2.1.1. Roof load

A uniformly distributed roof load is applied to the top surface of the lateral walls as the roof beams rest on the transversal walls. The volumes of individual components of the roof shown in Figure 2.21 and their densities are used to calculate the total weight of the roof by Carabbio (2016) in his Master's thesis. These densities were used to calculate the total weight of the roof and are provided in Table 5.2. The uniformly distributed surface value of the roof load on the two lateral walls was determined by calculating the total weight of the roof and then dividing it by the surface area of the top surface of the wall that is in contact with the roof. The weight of the roof provided in the literature is higher than the one calculated by a magnitude of 0.5 kN/m^2. However, it is used for the purpose of this study.

Table 5.2: Total weight of the roof

Weight of individual components of the roof	Volume m^3	Density kg/m^3	Mass kg	Weight kN
Earth/clay	3.04	2300.00	6996.60	68.61
Twigs	0.76	50.97	38.76	0.38
Ring of stones	0.62	2738.02	1700.31	16.67
Planks	0.46	914.75	417.40	4.09
Roof beams	0.70	914.75	642.15	6.30
Total weight of the roof (kN)				96.05
Weight of the roof per m^2 (kN/m^2)				7.41

5.2.1.2. Pushover load

The numerical analysis in Chapter 3.2 prescribes a uniformly distributed horizontal load on the surface of the wall to simulate experimental loading. Modal pushover load is applied to the full-scale Bhatar building instead to simulate the seismic load from an earthquake. A load pattern that approximates the distribution of inertial forces must be defined to conduct the pushover analysis. DIANA offers a generalised form of mode-shape dependent load that can be applied as a modal pushover load, also described in Chapter 2.11.1.2. An eigenvalue analysis has to be performed before conducting a nonlinear static analysis to determine the first vibration mode [98]. An acceleration value of 9.806 m/s^2 as the input along with the first mode shape is specified.

5.2.2. Mesh size

Chapter 3.1.4 specifies a mesh size of 0.10 m and 0.05 m for masonry and timber, respectively. However, the full-scale building chosen for this analysis has a masonry volume 10 times larger than the U-shaped wall chosen for model validation. This rendered the above mesh size to be excessively computationally heavy. Therefore, a sensitivity analysis was done to ascertain the impact of a larger mesh size on the response of the structure. The details of this analysis can be found in Appendix A. It revealed that a mesh size of 0.20 m and 0.10 m for masonry and timber did not have a discernible impact on the overall response compared to the finer mesh sizes. Hence these mesh sizes were applied to the models.

5.2.3. Iteration

The limit of 100 iterations was found to be too computationally heavy to be practical, therefore a sensitivity analysis was done to assess the sensitivity of the results to the iteration number. For unreinforced masonry, it was found to have a significant impact, but the Bhatar structure was not sensitive to the difference between 30 iterations and 100 iterations. The results of the sensitivity to the number of iterations are presented in Chapter 5.3.

5.2.4. Numerical model

To analyse the effect of the timber bands, an unreinforced masonry model is initially developed and subjected to the modal pushover load. Solid elements were used, and the geometry of this DIANA model is presented in Figure 5.2a. Then, a Bhatar structure with identical geometry, dimensions, materials, and properties but with the addition of timber bands is analysed. The geometry of the structure was modelled in DIANA as seen in Figure 5.2b. As a conservative approximation, the roof is assumed to not contribute towards energy dissipation or transfer of lateral forces to orthogonal walls through diaphragm action and hence the roof was not modelled separately.

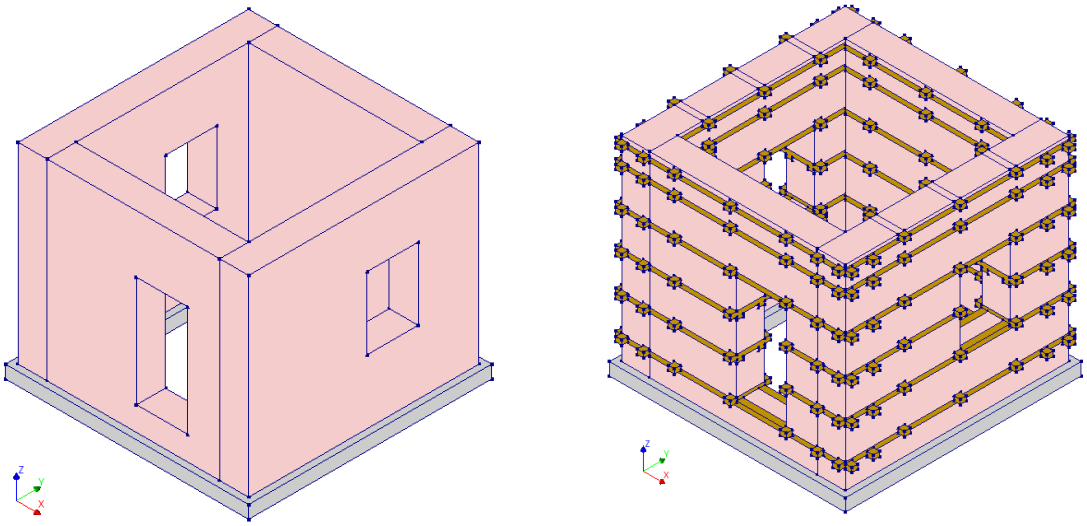

Figure 5.2: Numerical model in DIANA : a) Unreinforced masonry structure, and b) Bhatar structure

Additionally, to find the most effective location of timber bands, various models are developed placing the timber bands at six different levels – bottom, sill, middle, lintel, top and roof. The location of timber bands is outlined in Figure 5.3, with an overview in Figure 5.4. The close view of the connection can be seen in Figure 5.5a and a plan in Figure 5.1b.

These models were identical except for the location of the timber bands. Meshed models of the unreinforced and timber-reinforced masonry structures are shown in Figure 5.6a and Figure 5.6b, respectively.

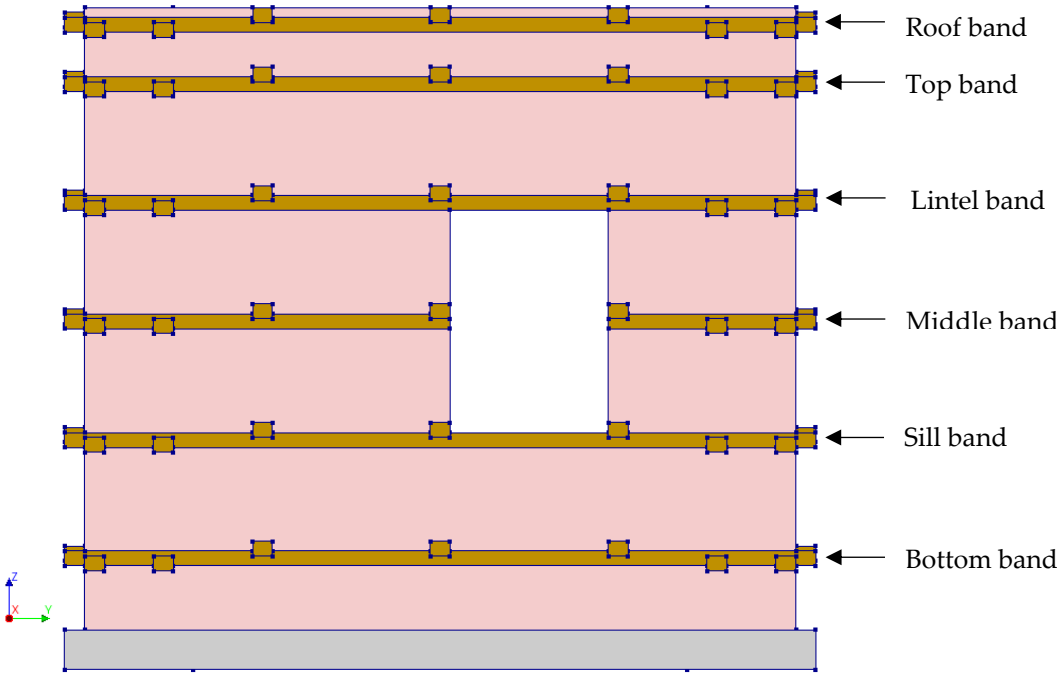

Figure 5.3: Location of timber bands

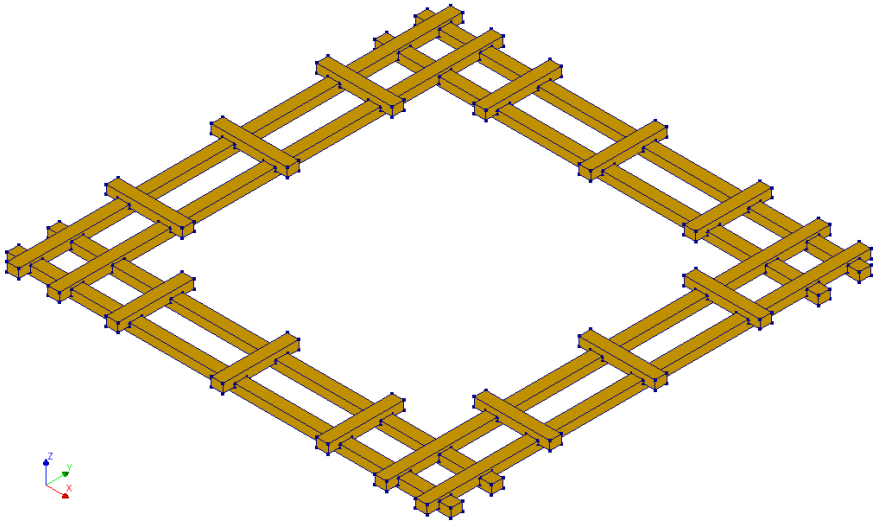

Figure 5.4: Overview of a timber band in the numerical model

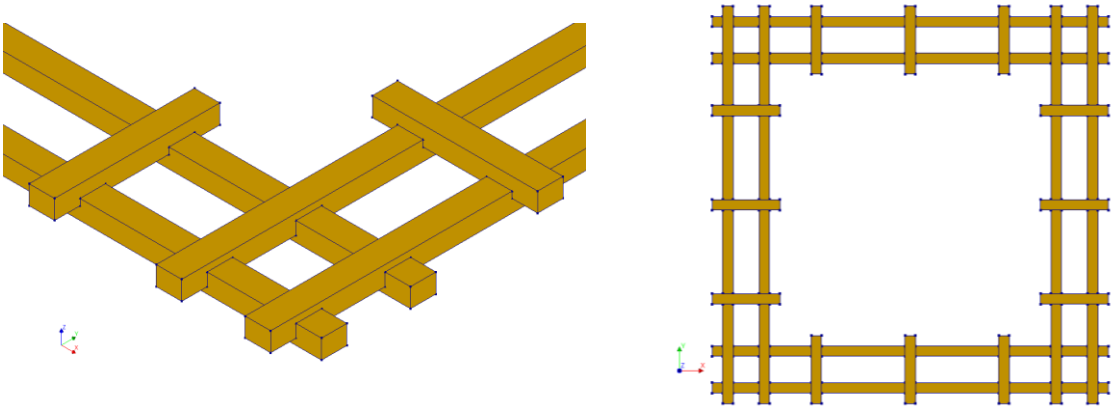

Figure 5.5: Timber band : a) Close view, and b) Plan view

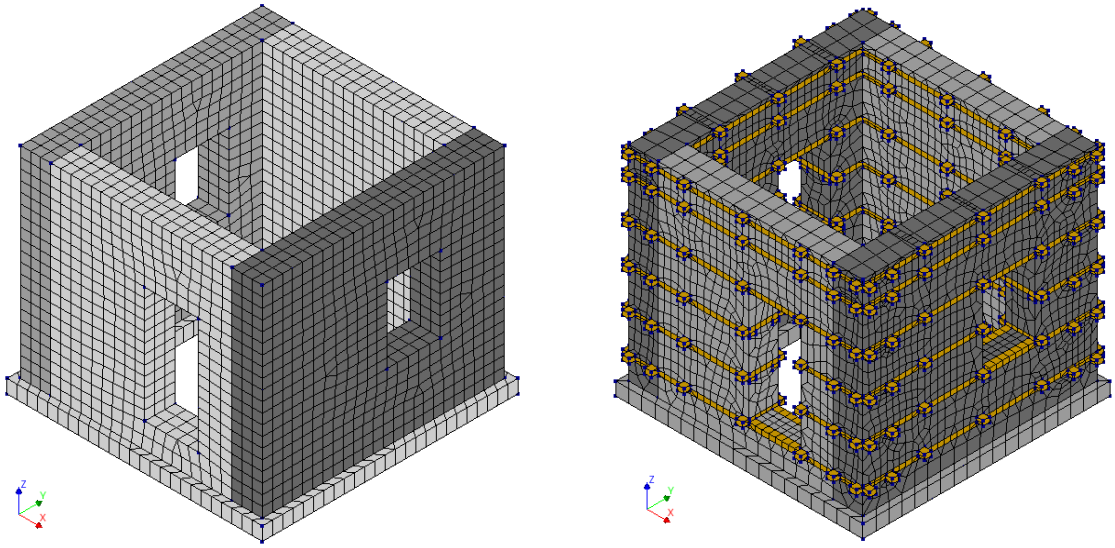

a b

Figure 5.6: Meshed models : a) Unreinforced masonry, and b) Timber-reinforced masonry (Bhatar)

5.3. FE analyses results

This chapter presents the results obtained from FEA numerical analyses:

a) Pushover curves,
b) Displacements, and
c) Crack widths,

All pushover curves relate to the displacement recorded at the mid-node at the top of the rear wall, except in Figure 5.9 in Section 5.3.1.3 that displays the results of the displacements recorded at the top-mid node of the right lateral wall.

5.3.1. Force capacity

5.3.1.1. Iteration sensitivity

Figure 5.7 shows the sensitivity of the unreinforced structure to the number of iterations. The structure presented a more ductile response when the solution was terminated after 30 iterations, than when terminated after 100 iterations. However, the pushover curve for the Bhatar structure showed no difference for termination of solution after 30 iterations or 100 iterations. Since a numerical analysis with 100 iterations is significantly heavier computationally, the Bhatar structure analysis was continued with 30 iterations, while the unreinforced masonry model is allowed 100 iterations to evaluate the force and displacement values with higher accuracy. Due to the high computational time for the Bhatar model, the load-steps were limited to 50 load-steps compared to the unreinforced masonry model that was allowed a run of 200 load-steps. This lower load-step number leads to the lower displacement levels visible in the load-displacement curve in Figure 5.7, rather than stability or convergence issues.

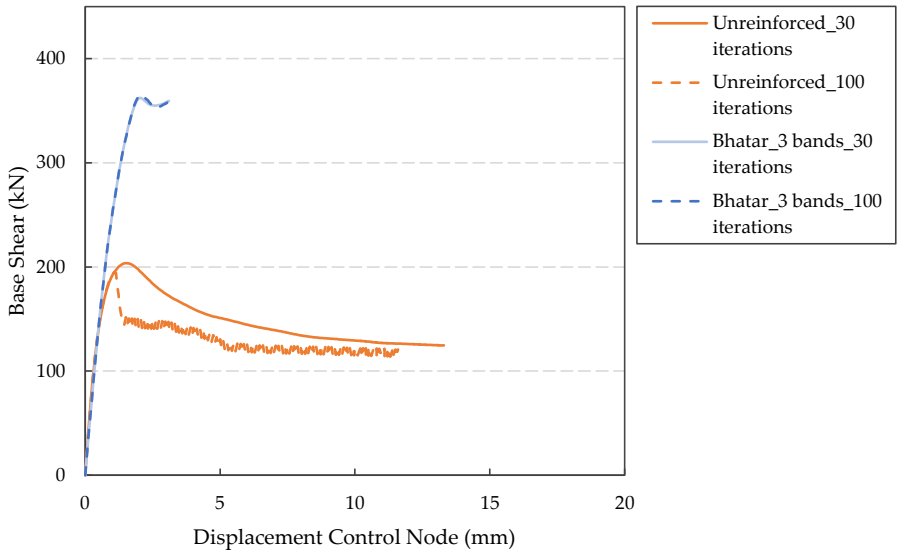

Figure 5.7: Sensitivity to number of iterations

5.3.1.2. Effect of timber laces

Figure 5.8 displays the pushover curves for the three structures described above. The inclusion of timber bands increased the forced capacity of the masonry structure by 109%. The effect was not limited to the force capacity, as a significant improvement in the post-peak behaviour can be seen. The Bhatar structures, after an initial decrease in the resistance, display a further hardening, accountable to the box behaviour imparted by the timber laces. A parametric analysis was done to assess the effect of each location of the timber band on the response of the structure. The findings are presented in Figure B.1. The inference drawn was that the sill, lintel and roof levels were the most effective placements for the timber bands. Therefore, three models were analysed – Unreinforced, Bhatar_3 bands, and Bhatar_6 bands.

Apart from these analyses, multiple analyses were conducted for various parameters to study the effect of absence (or presence) of openings, roof load on two (or four) walls, combination of different timber bands, and mesh sensitivity. These studies can be referred to in Figure A.2, Figure A.3, Figure B.2, Figure B.4 and Figure B.5.

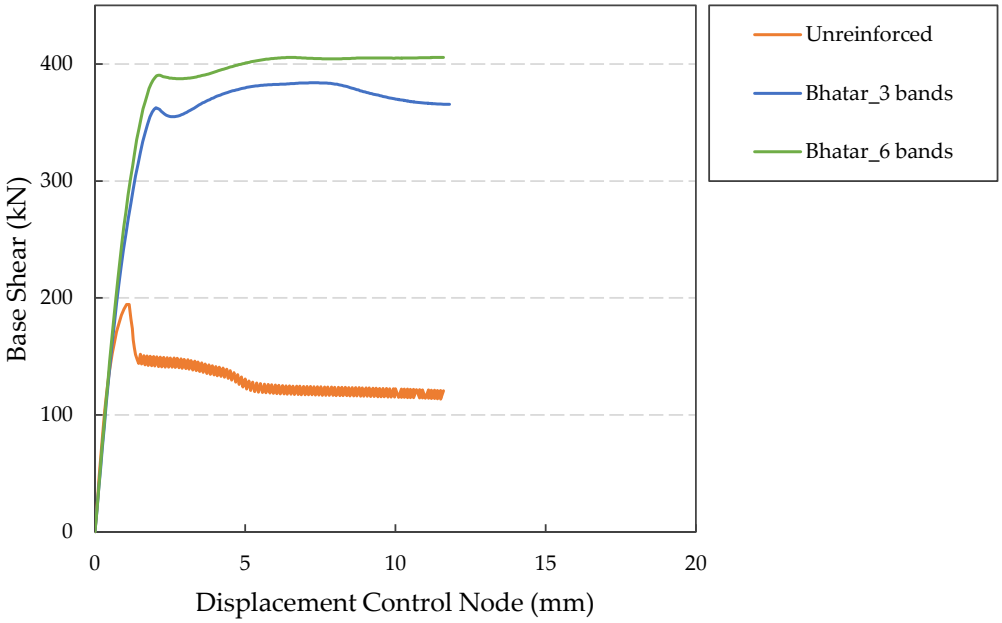

Figure 5.8: Load-displacement curves : Unreinforced and two Bhatar structures

Table 5.3: Maximum force values for unreinforced & Bhatar structures with openings and with timber bands at different heights

Structure	**Maximum force (kN)**	**Increase from unreinforced (kN)**	**%**
Unreinforced	194.34	-	-
Bhatar_3 bands	383.90	189.57	98 %
Bhatar_6 bands	405.69	211.35	109 %

5.3.1.3. Displacement of lateral walls

The displacements for the lateral walls were recorded by choosing the top-mid node of the right lateral wall and plotting it against the resistance of the structure. The curve for unreinforced masonry shows a sudden drop after reaching the peak signifying brittle failure. In contrast, the lateral wall displacement curve of the Bhatar structure shows a behaviour comparable to that of the rear façade wall with out-of-plane force, with marginally lower displacements for similar drift levels. This also proves the *together* or *combined* movement of the frontal and lateral walls in Bhatar structures upon acting of seismic loads in the form of ground acceleration.

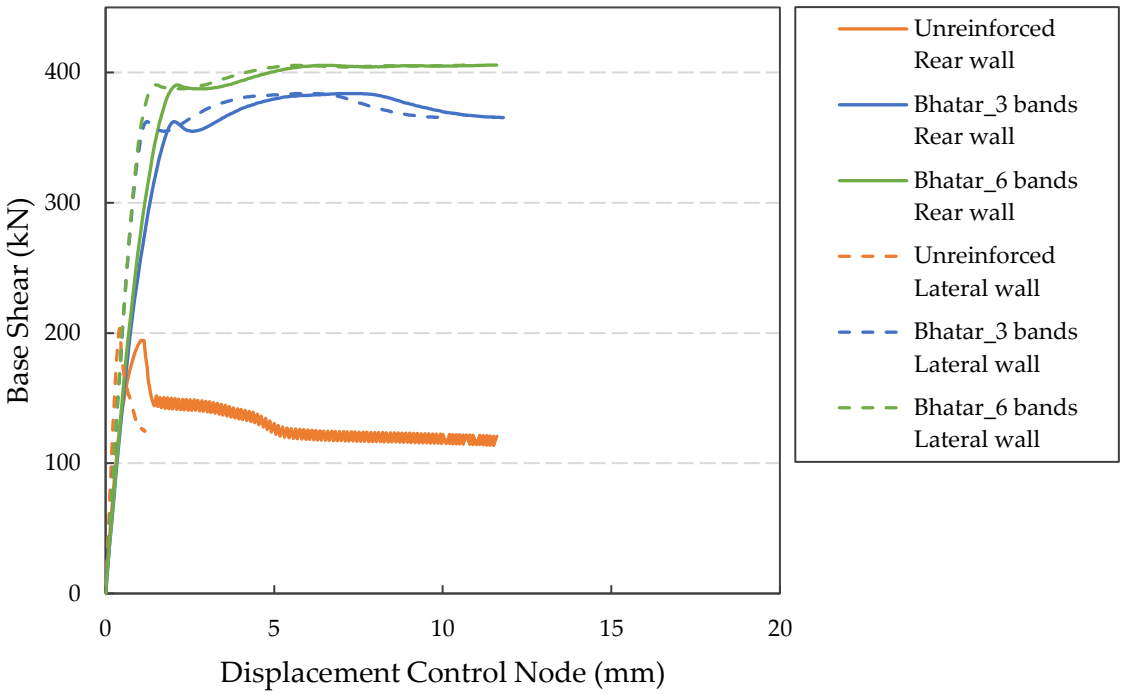

Figure 5.9: Displacement of lateral walls

5.3.2. Displacements

Displacement contours of the following three models are presented in this section:

a) Unreinforced masonry,
b) Bhatar structure with timber bands at sill, lintel, and roof level, and
c) Bhatar structure with timber bands at all levels

Displacements were taken in Y and Z directions, at 4 load steps - 50, 100, 150, 200. The scale for displacement values was kept consistent for the three models.

5.3.2.1. Displacements in Y direction

Since the modal pushover load is in the Y direction, the displacements in Y direction provide information about the deformation of the structure. While only the rear wall undergoes deformation in the unreinforced masonry, even separating from the lateral walls (Figure 5.10a); all four walls undergo deformation in Y direction for the Bhatar structure (Figure 5.10b Figure 5.10c). This indicates the structure's collective movement as a unit without separation. This can be attributed to the box action provided by timber bands as the models are identical apart from the presence (or absence) of the timber bands.

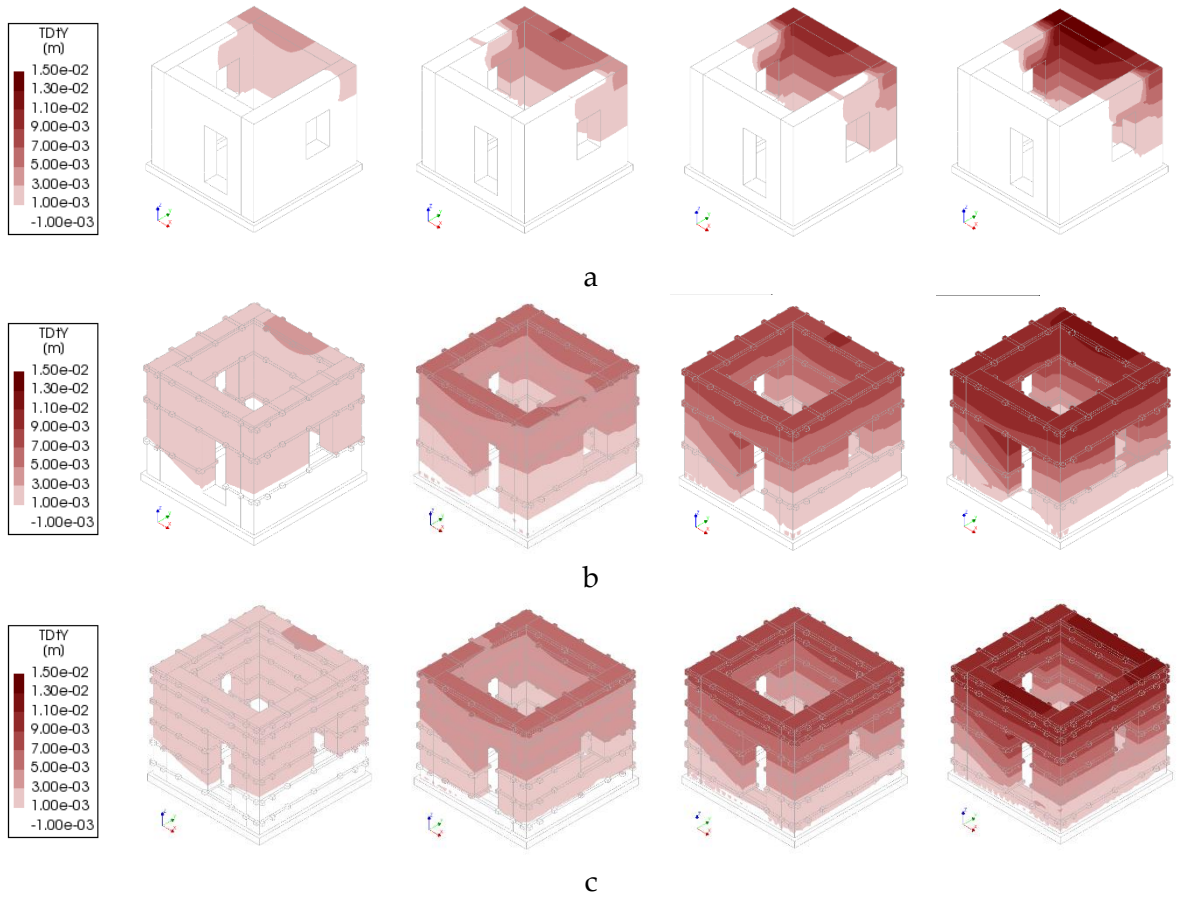

Figure 5.10: Displacement in Y direction : (a) Unreinforced masonry, (b) Bhatar_3 bands, (c) Bhatar_6 bands

Figure 5.11 shows the progression of displacement throughout the analysis.

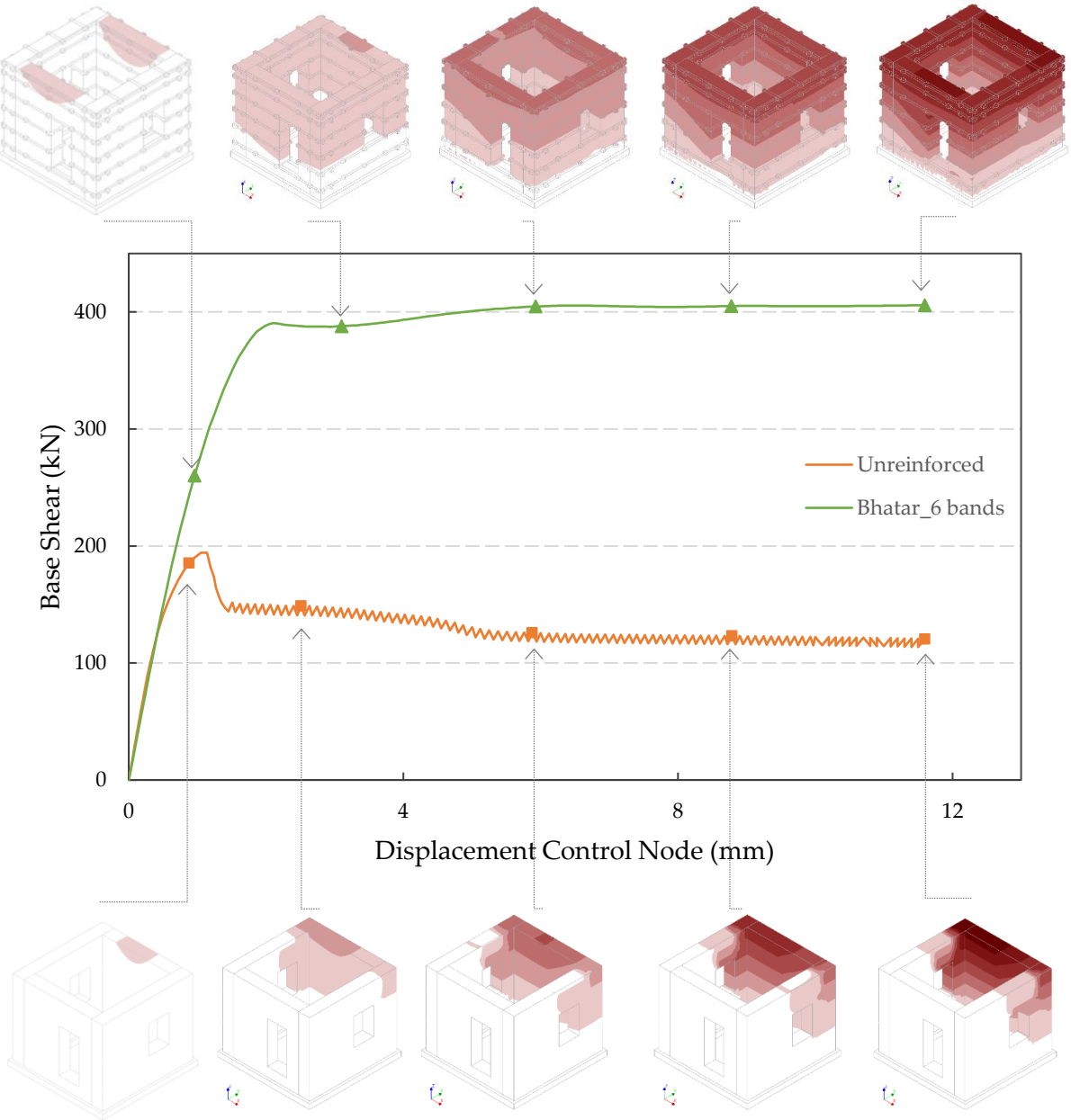

Figure 5.11: Progression of displacement (Y direction)

5.3.2.2. Displacements in Z direction

Displacement in Z direction is an indication of uplift and provide insight into the deformation of the structure. Similar to Y direction, the displacements in Z direction are displayed for four load-steps - 50, 100, 150, 200. For the unreinforced masonry structure in Figure 5.12a, only the rear wall experiences uplift and all other walls remain unaffected. On the other hand, the frontal wall, rear wall and both lateral walls of the Bhatar structures experience uplift sequentially indicating to the entire structure entering the rocking motion (Figure 5.12b and Figure 5.12c). The load-steps for the analysis were limited to 200 due to computational limitations as the time required for more load-steps for the Bhatar structure was not feasible. However, if the analysis were to be continued, further activation of the rear wall and increase in uplift suggesting rocking motion with the axis at the base of the rear wall can be seen.

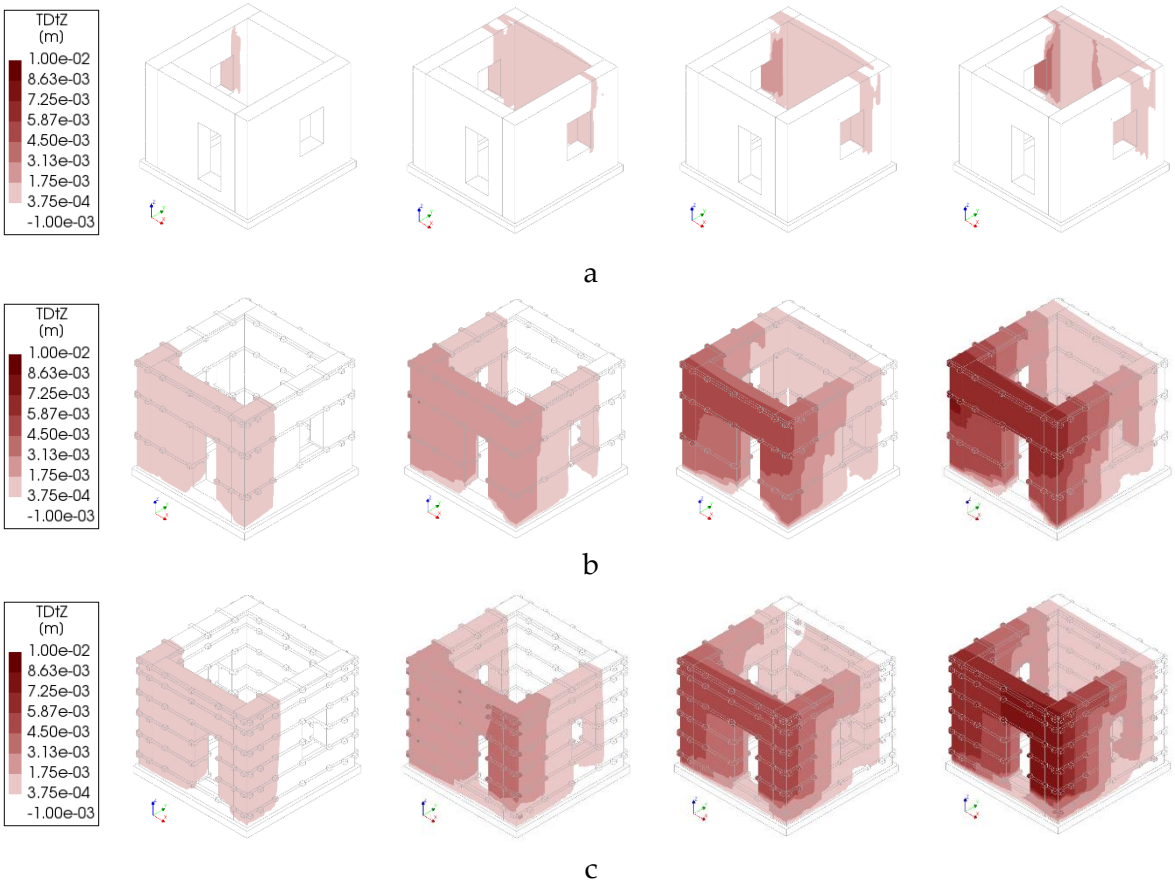

Figure 5.12: Displacement in Z direction : (a) Unreinforced masonry, (b) Bhatar_3 bands, (c) Bhatar_6 bands

5.3.3. Crack widths

This section presents the principal crack widths from the results of numerical analysis in DIANA FEA. The magnitude of the crack widths is maintained in order to compare the three masonry models. From the observation of Figure 5.13a, it is apparent that the unreinforced masonry suffers failure through separation of the rear wall. It occurs in the form of diagonal cracks emerging from the rear wall into the lateral wall. Additional cracks can be seen propagating in diagonally opposite directions towards the corners of the windows. Additionally, the rear wall fails in bending, visible as an additional crack propagating downwards from the mid-top of the rear wall.

Bhatar structure, on the other hand, develops a different mechanism. The entire structure tries to rotate around the base of the rear wall as an axis, simulating rocking of the structure as a whole. This generates considerable stresses, and hence large cracks, at the base of separation of the frontal wall from the concrete base (Figure 5.13b-c). Timber bands can be seen arresting cracks from propagating throughout the height of the masonry wall. A horizontal crack can be seen under the lintel band, due to debonding of the mortar-timber interface plane that faces a combination of tensile and shear stresses as the structure tries to overturn in a rocking manner. Another set of horizontal cracks is visible at the mid-height of the junction of the left lateral wall and frontal wall. Both these cracks are either non-existent (latter) or reduced considerably (former) in the Bhatar structure with all bands (Figure 5.13).

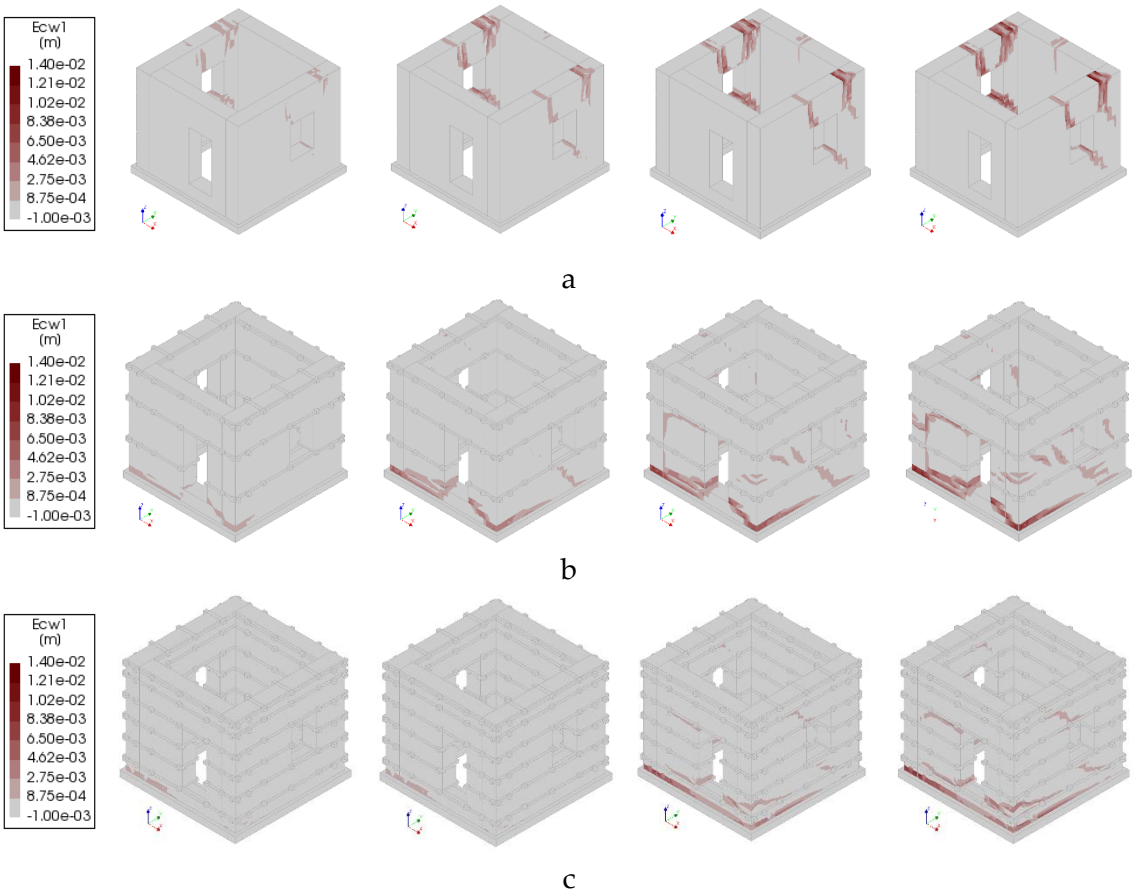

Figure 5.13: Principal crack width, Ecw1 : (a) Unreinforced, (b) Bhatar_3 bands, (c) Bhatar_6 bands

It is noteworthy that there is asymmetry in the cracking patterns between the left and right lateral walls (for both unreinforced and Bhatar structures), explainable by the non-centred door on the frontal wall, which results in non-uniform mass and stiffness across the centreline, hence torsional irregularity. While keeping in mind some differences, the crack and damage patterns observed in the numerical model are similar to those found in the shake table test on a two-storey drystone unreinforced and timber-reinforced masonry structure conducted by Wang et al. (2019). These include the diagonal cracks from the corner of the wall to the sill of the window and separation of the rear wall from the lateral walls in unreinforced masonry leading to collapse of the upper part of the wall. Moreover, the experiment displayed more damage for the timber-reinforced structure just below the lintel band on the frontal wall, which was also seen in the numerical model representing Bhatar structure in the form of significant horizontal crack. Figure 5.14 shows the evolution of crack widths for unreinforced and Bhatar structure relating it to the load-step on the pushover curve.

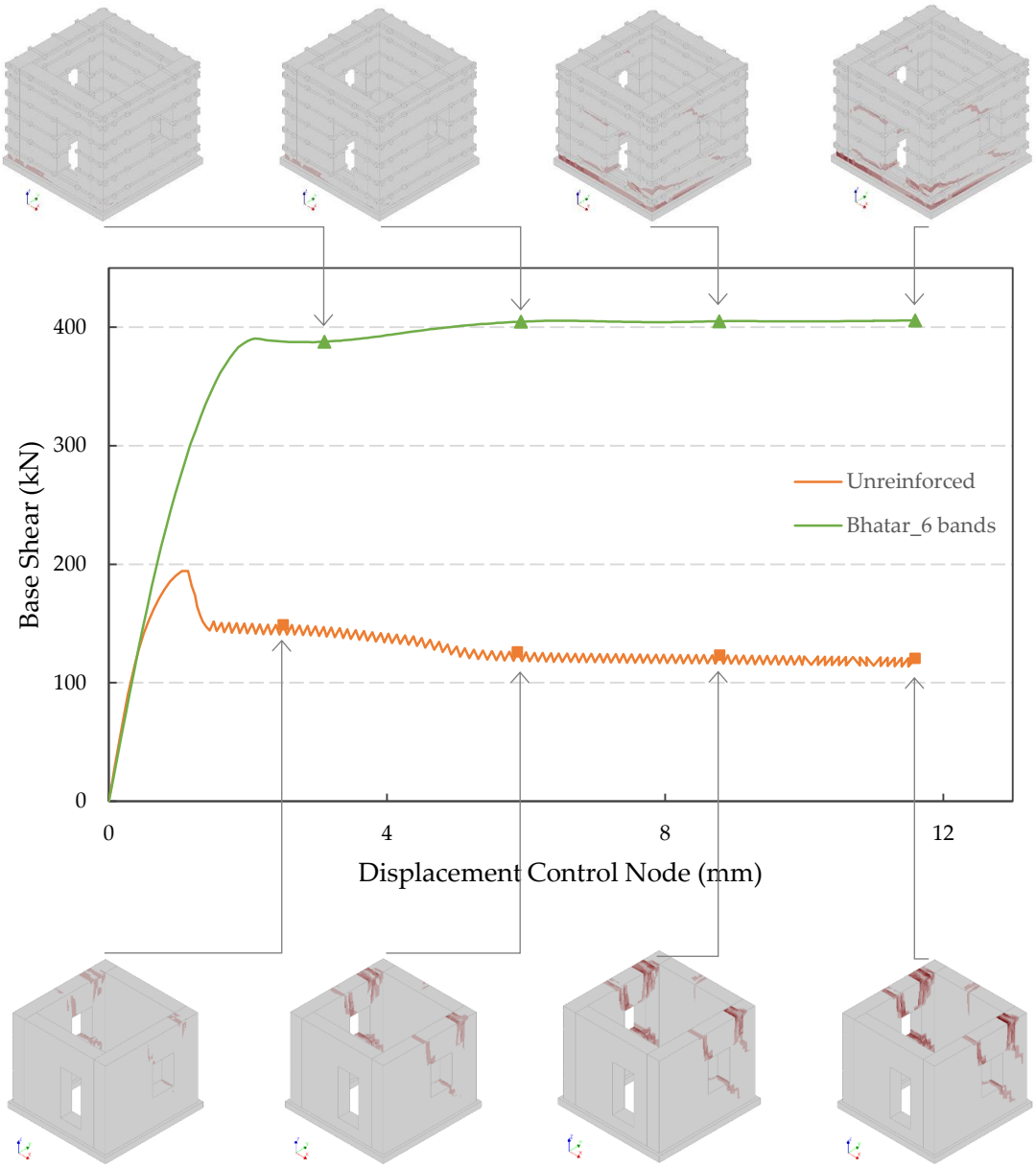

Figure 5.14: Evolution of crack patterns

5.4. Seismic assessment

A brief overview of the seismic assessment is provided in Chapter 2.11.2. For seismic assessment of the masonry structure through CSM in absence of the spectral reduction factor, a slightly modified approach is taken, described in this chapter. Non-linear Pushover analysis (NLPO) is performed on DIANA to generate the capacity curve for the structure. The capacity curve is plotted for base shear vs. displacement of the top node. This has been described and presented in previous chapters.

The capacity curve obtained from NLPO is transformed into ADRS format to compare with the demand spectrum directly. This requires converting base shear and displacement into spectral acceleration and spectral displacement. Since the Bhatar structure is a single degree of freedom (SDOF) structure, this requires dividing the force obtained at each load-step by the effective seismic weight of the building. The capacity curve and transformed version of it in ADRS format are presented in Figure 5.15.

Ground motion records or code-specified spectra are utilised to generate the acceleration-displacement response spectrum. In this case, the IS code provides response spectra for the design acceleration coefficient for different soil types, normalised with peak ground acceleration, corresponding to the natural period T of the structure, as shown in Figure 5.16. Using Figure 5.16, Acceleration Response spectrum from IS Code is generated. However, this is not scaled for site-specific conditions, seismic zone factor, damping, importance factor of the building and response reduction factor.

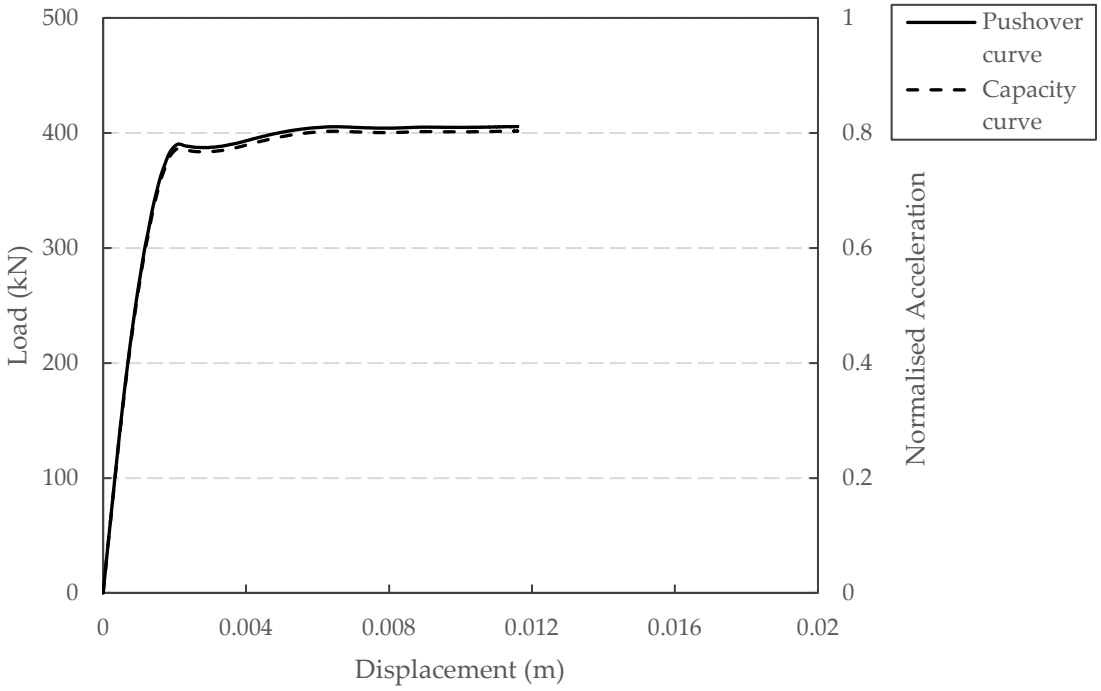

Figure 5.15: Pushover curve conversion to Capacity curve

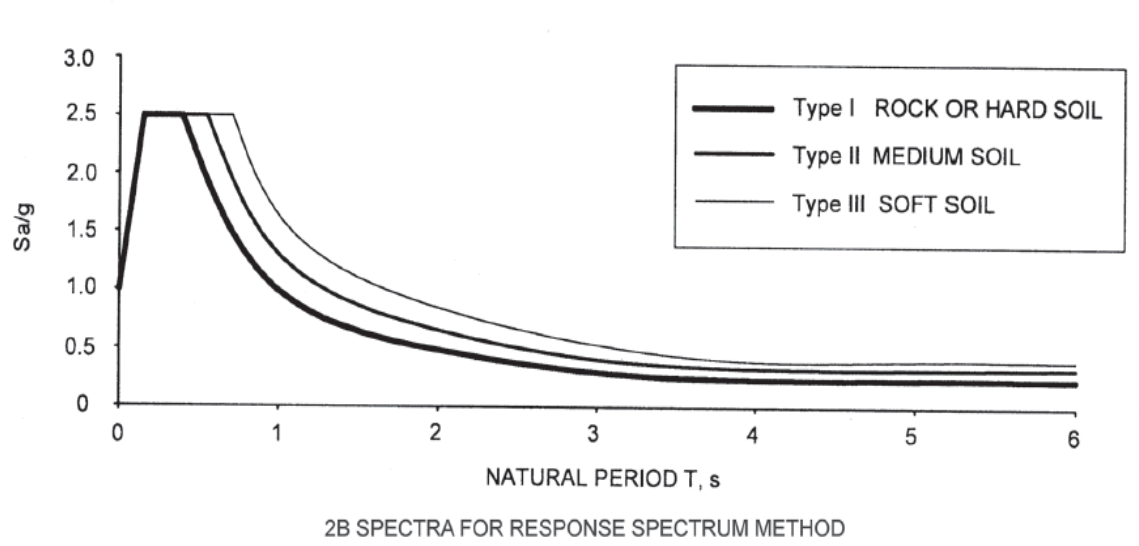

Figure 5.16: Design Acceleration Coefficient (S_a/g) (Corresponding to 5 per cent damping)

To use this as a demand spectrum, the following formula has to be applied:

$$A_h = \frac{(Z)\left(\frac{S_a}{g}\right)}{\left(\frac{R}{I}\right)}$$

Where, according to IS 1893 (Part 1):

Z: Zone factor, which is for the Maximum Considered Earthquake (MCE) and service life of structures in a zone.

I: Importance factor, which takes into account the consequences of failure and is dependent on the function and type of building.

R: Response reduction factor, which takes into account the ductility of the building.

T: Natural time period of the structure.

$\frac{S_a}{g}$: Design acceleration coefficient for different soil types, normalised with peak ground acceleration, corresponding to natural period T of the structure.

The values used for these factors are listed below in Table 5.4. Figure 5.16 and Section 6.4.2 of the IS Code 1893 (Part 1) are used in conjugation with the above formula and the values in Table 4.10 to obtain the Reduced Acceleration Demand Spectrum. The design acceleration response spectrum is the smoothened envelope of all acceleration response spectra of the ground motions for which the building should be designed. The following formula is used to generate the Displacement response spectrum and subsequently, a reduced displacement response spectrum is generated.

$$S_d = S_a \frac{4\pi^2}{T^2}$$

Table 5.4: Values used for calculation of horizontal design acceleration coefficient

Notation	Parameter	Value	IS Code reference
Z	Seismic Zone factor	0.36	Table 3
I	Importance factor	1.0	Table 8
R	Response reduction factor	1.0	Table 9
$\frac{S_a}{g}$	Design acceleration coefficient	Dependent on T, taken for rocky soil	Section 6.4.2 (b)

The Acceleration and Displacement Spectrum plotted for time period are shown in Figure 5.17. The Reduced Acceleration Response Spectrum and Reduced Displacement Response Spectrum shown in Figure 5.18 is transformed to the Demand Spectrum in Figure 5.19 by plotting Acceleration spectra (S_a) on the Y axis and Displacement spectra (S_d) on the X axis.

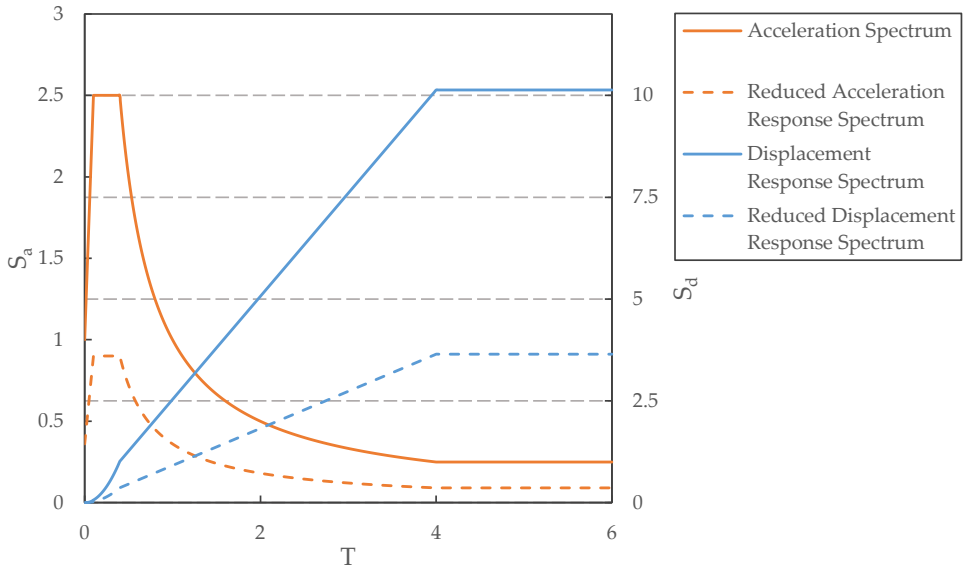

Figure 5.17: Reduced Acceleration Response Spectrum

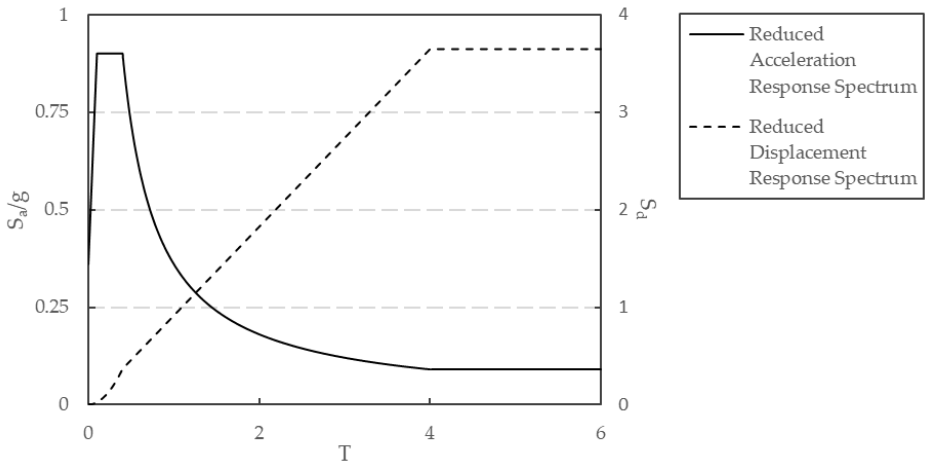

Figure 5.18: Acceleration and Displacement Response Spectrum against Time Period

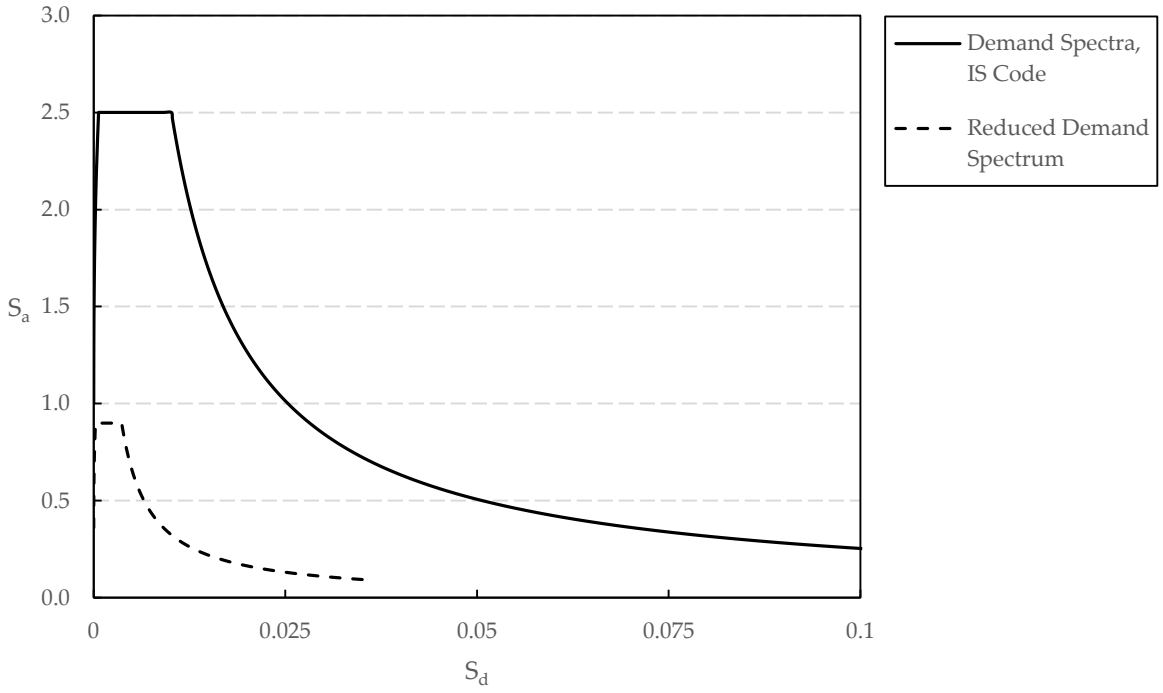

Figure 5.19: Acceleration Demand Spectra for Response Spectrum Method

Finally, the generalised pushover curve derived earlier is bi-linearised. The capacity of the system in terms of the spectral yield acceleration of the equivalent SDOF system $S_{a;y}$ is computed assuming an elastoplastic force-displacement relationship and the equal energy criterion, and expressed as the following equation:

$$S_{a;y} = \frac{u_{cap;sys}K_{init} - \sqrt{\left(u_{cap;sys}K_{init}\right)^2 - 2E_mK_{init}}}{m^*}$$

Where,

E_m is the deformation energy up to the spectral displacement $u_{cap;bilin}$.

m_{eff} is the effective mass of the masonry building.

K_{init} is the initial lateral stiffness of the SDOF system. It is calculated as the secant stiffness at a base shear force equal to 60 % of the maximum base shear.

$u_{cap;sys}$ is the maximum spectral displacement of the masonry building, equal to

$u_{cap;bilin}$ as the lateral NC (near collapse) displacement capacity of the SDOF system for the Bhatar structure.

An example of a typical bilinear pushover curve can be seen in Figure 5.20 from NPR 9998:2020. For simplification, and since the exact values of $u_{cap;sys}$ are not available, the $0.9S_{a;max}$ is considered for the bilinearisation. This is a conservative approximation as the $S_{a;max}$ value for timber-reinforced masonry is underestimated.

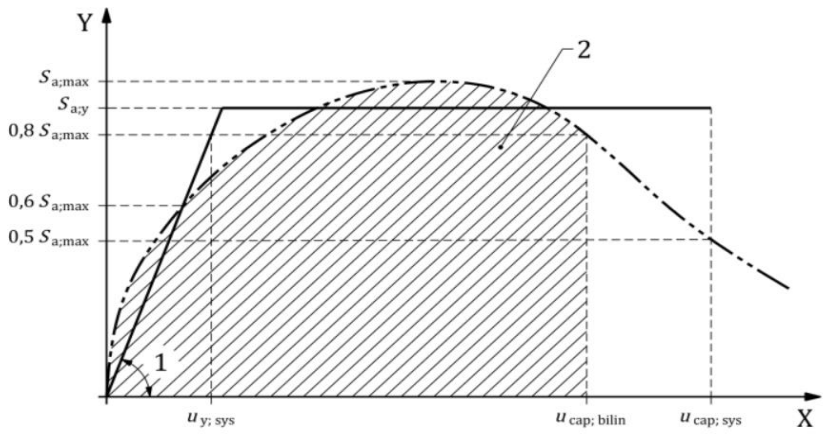

Figure 5.20: Example of bilinearization of a non-linear pushover capacity curve for the equivalent single-degree-of-freedom system

Figure 5.21 shows the bilinearised pushover curves. By studying the intersection point and other aspects of the capacity and demand spectra, it can be assessed whether the structure meets predetermined performance objectives, such as life safety, damage limitation, or near-collapse states. The Capacity and Demand curves are plotted together to assess the seismic capacity of the Bhatar structure. Figure 5.21 depicts that the Unreinforced structure does not have the deformation capacity required by the demand curve based on the Seismic code. On the other hand, it can be seen that the capacity of the timber-reinforced Bhatar structure exceeds the deformation demands placed by the Indian Seismic code for Zone V Earthquake.

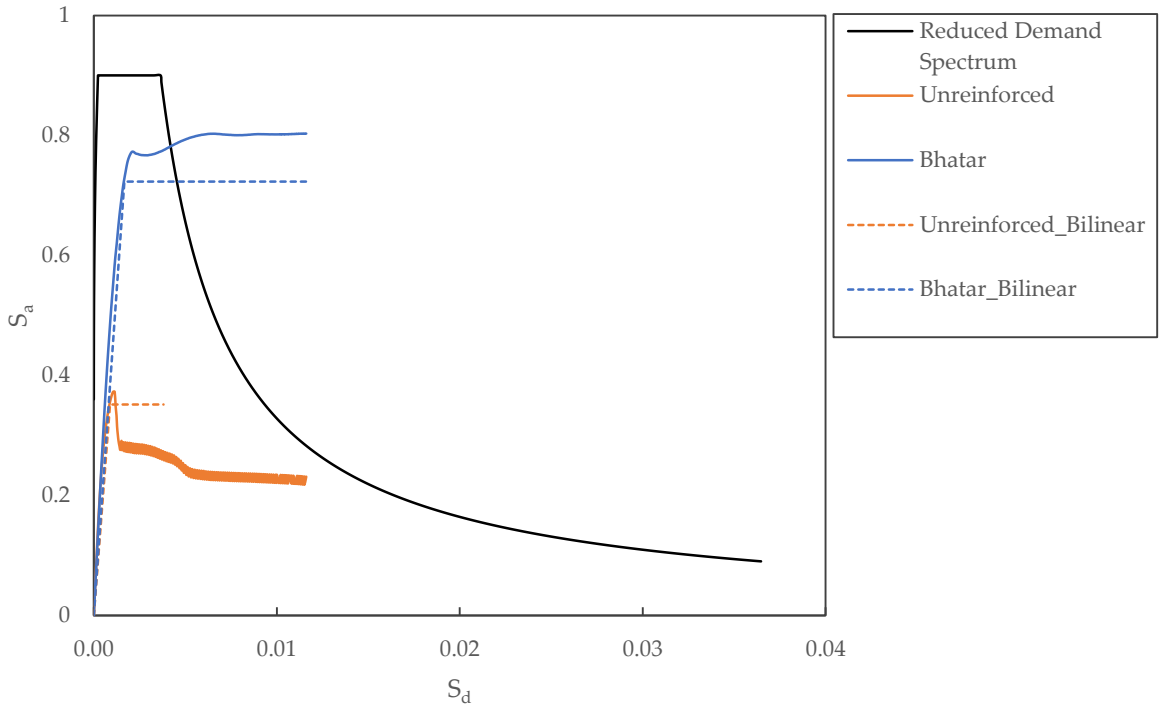

Figure 5.21: Bilinearised Capacity curve v/s ADRS Demand curve

The allowable acceleration for the unreinforced masonry and timber-reinforced Bhatar structure was found to be 0.35g and 0.72g, respectively. This proves that the unreinforced masonry is not able to undergo a typical earthquake in the Zone V according to IS Code without collapse. Contrarily, the timber-reinforced masonry is able to have sufficient ductility and capacity to survive the earthquake with minor local damage and cracks.

The numerical analysis shows that the collapse of the unreinforced masonry structure is a local out-of-plane collapse. However, the pushover analysis is not accurate for local out-of-plane collapses of the structure. The current assessment assumes that the rest of the structure still contributes to the overall resistance of the structure even after the failure at the local level. Therefore, it can be concluded that the capacity of unreinforced masonry is overestimated in the current assessment strategy and the value of 0.35g is the upper limit of allowable acceleration. The seismic assessment of the analysis of the unreinforced masonry at the local level would take a more detailed approach outside the scope of this study. When the local collapse is taken into account, the actual capacity, and hence the allowable acceleration of the unreinforced masonry would be lower than the current calculated value.

Similar values have been observed from shake table tests conducted by Wang et al. (2019) on unreinforced and timber-reinforced masonry structure. While keeping in mind the differences (described in Chapter 2.7.3) between the experimental prototype model and the Bhatar structure for this numerical study; it is of note to compare the results. The unreinforced models had a PGA of 0.31g for 0.35g in experimental campaign and this numerical study, respectively. The timber-reinforced models had PGA of 0.51g and 0.72g for the former and latter, respectively. The larger difference in the timber-reinforced models can be largely attributed to one additional storey and dry-stone masonry in the experimental model and more locations of timber bands and lime-mortar masonry in this numerical model for Bhatar structure.

The area under the pushover curve represents the energy absorption capacity of a structure up to a certain deformation level or performance point. Specifically, it quantifies the amount of work done or energy absorbed by the structure as it deforms under lateral loading before reaching a predefined collapse or failure limit in terms of displacement, drift limit or drop in maximum force or strength. The greater the area under the pushover curve, the more energy the structure can absorb without experiencing catastrophic failure and transitioning from elastic to inelastic behaviour. The energy absorption capacity is a critical parameter in performance-based seismic design. Advanced non-linear time-history analyses or incremental dynamic analyses (IDA) are required to capture more complex energy dissipation mechanisms not fully represented in a pushover analysis. However, it can be used to gauge a structure's resilience and robustness during seismic events. A smaller area under the curve (Unreinforced_Bilinear) would generally indicate a more brittle structure that may not perform well during an earthquake. In contrast, a higher area under the pushover curve (Bhatar_Bilinear) generally indicates a more ductile and energy-absorbing structure, which is desirable in seismic-prone areas. It also indirectly indicates higher ductility in the structure, enabling the structure to undergo larger deformations without experiencing significant loss of strength.

Conclusion

In an exploration of Bhatar house construction, this research focuses on assessing the response of Bhatar structures to seismic events. A realistic, though simple model for the Bhatar house includes three defined openings: a door and two windows. For the Finite Element (FE) modelling, established methodologies from earlier chapters are utilized, with considerations made for the seismic loads associated with the geographic location, weight of a heavy roof, and loading conditions such as the modal pushover load. The study looks at mesh sizes and iterations in analysis, noting that refining the mesh in sensitivity analyses revealed only a small increase in the structure's capacity. However, the added computational demands outweigh the benefits. Hence, a 0.20 m mesh size for masonry was deemed sufficient. Additionally, a smaller number of iterations suffice for the Bhatar structure. A crucial part of this study is evaluating the effects of timber bands in reinforcing the masonry structure. FE analyses results, which include pushover curves, displacements, and crack widths, are presented. These results highlight the significant enhancement in force capacity when timber bands are used, with certain positions of these bands (sill, lintel, and roof levels) being more effective than others. The inclusion of these bands notably improves the structure's response by an increase of 109% in the maximum resistance to lateral forces (from 194.34 kN for Unreinforced to 405.69 kN for a Bhatar structure). The presence of timber bands substantially increased the structure's resistance, with the models with just top and roof bands exhibiting high maximum resistance (339.71 kN and 335.15 kN respectively). However, in absence of sill band, this was followed by a capacity drop due to cracking in the masonry section below the bands located at the top of the wall. The continuity of timber bands is crucial as structures with middle bands, disrupted by openings, had the lowest resistance. Different timber band combinations were explored. Combinations with top, roof, and lintel bands offered high resistance. Notably, the combination of a sill band with either a lintel, top, or roof band was found to be most effective with better maximum resistance values as well as reduced softening in post-cracking stage. A model with timber bands at three most effective locations - sill, lintel, roof, was found to have a maximum lateral resistance of 383.90 kN; 98% higher than Unreinforced masonry.

The box behaviour of a structure is indicated by the involvement of lateral walls in the failure mechanism. The timber-reinforced Bhatar structure showed such behaviour, which lent it more resistance and ductility compared to an unreinforced structure. Lastly, seismic assessment through modified Capacity Spectrum method demonstrated that a Bhatar structure had a significantly better ability to withstand earthquakes with larger accelerations (0.72 g), showcasing their enhanced earthquake resistance compared to unreinforced masonry structures (0.35 g). The Bhatar structure's resilience and response to seismic events are evident in the results, underscoring the effectiveness of the timber reinforcements.

6. Concluding remarks

Unreinforced Masonry (URM) structures in the seismically active Himalayan region have historically suffered extensive damage, leading to significant loss of life. However, timber-reinforced masonry structures have consistently shown superior seismic resilience. Historically, local seismic culture has developed using reinforcing materials like timber in masonry, exemplified by techniques such as Bhatar, which have demonstrated strong earthquake resistance. While past studies have explored masonry's response to lateral loads, few studies have explored the integration of timber reinforcements and their ability to enhance structural integrity, arrest cracks and distribute loads, preventing collapses.

A benchmark study highlighted that timber-reinforced walls exhibited greater lateral force capacity than their unreinforced counterparts. The present study uses macromodelling and the rotating crack formulation in DIANA FEA software to investigate the out-of-plane response of masonry structures reinforced with horizontal timber bands. The numerical model employed in the study demonstrated satisfactory correspondence with literature eigenfrequencies. The error percentages remained within acceptable ranges, with timber-reinforced masonry showing varied values based on mode frequencies. While numerical models were effective at approximating experimental maximum load values and pre-peak behaviour, they indicated increased softening post-peak compared to experimental observations.

Results reveal that timber integration in masonry notably improves out-of-plane performance. Specifically, placing timber bands at corners increased the lateral load-bearing capacity of unreinforced masonry by 35% and the displacement capacity by 49%, preventing, or at least, delaying collapse. While numerical models were effective at approximating experimental maximum load values, they indicated increased softening post-peak compared to experimental observations. There was a clear difference in the simulation of failure mechanisms when comparing the two iteration methods. Crack width analysis showed that the Newton-Raphson model provided a more accurate representation of experimental crack patterns. However, based on a more accurate representation of experimental failure mode, the Quasi-Newton iteration method was chosen for subsequent analyses. Limit states were defined and used to analyse damage levels for both masonry types. Timber reinforcement proved beneficial, providing substantially higher residual strength (35.5 kN compared to 14.13 kN for unreinforced) post seismic events and a potential for safety against sudden collapse.

The interactions between various components, including timber and masonry, were modelled discretely, to explore the effect of these local mechanisms on global behaviour of the wall. The differences in force capacities between different models remained minimal with only 1-3% reduction in force capacity, and no discernible difference in the load-displacement curves. This indicates the limitation of the current modelling strategy of the hinged timber-to-timber connections and masonry-timber interface governed by Coulomb friction law in combination with the entire masonry wall as a continuum.

Connected timber bands in U-shaped masonry walls, on the other hand, had a 35% higher base shear force than the wall with timber bands only at the corners. Moreover the uninterrupted timber lace through the front wall (subjected to out-of-plane load) substantially increased the ductility of the wall. While the drift level increased by 7% by the SD limit state, it increased by 127% by the NC limit state. Although considering the uncertainty regarding the actual behaviour of the wall at the NC limit state, and assuming the 127% increase in drift level as an overestimation, it nevertheless indicates significantly higher displacement capacity of the Trf_connected.

Though NLTHA provides insight into the behaviour of a structure to a higher degree of complexity and accuracy; given the computational constraints of the present study, the current research employed pushover analysis to evaluate the seismic response of the Bhatar structure due to its detailed modelling capabilities, considering both linear and non-linear material properties. The integration of timber bands notably enhanced the structure's seismic resistance by 109%. The continuity and positioning of these timber bands were essential for achieving maximum resistance against lateral forces as confirmed by the model with the middle band obtaining the least force capacity amongst all models. The most efficient locations for the bands were found to be sill, lintel and roof level. It was found that the higher a band is placed across the height of the wall, the higher would be the positive effect on the force capacity. Therefore, top and roof band were found to have the highest contribution to the lateral resistance. However, sill and lintel band were found to be important for ductility of the structure. In the absence of a sill band, the structure would achieve a high maximum load but would then suffer a sharp drop in its capacity.

Observations of the displacements in Y direction (the direction of load application) and Z direction (normal direction) reveal that timber-reinforced Bhatar structures displayed a *box behaviour*, which contributed to their enhanced resistance and ductility when compared to unreinforced structures. Seismic assessment using the Capacity Spectrum Method further attested to the resilience of Bhatar structures (0.72 PGA), showing a significantly improved ability to withstand ground accelerations from code-specified earthquakes when reinforced with timber bands contrary to unreinforced masonry (0.35 PGA) that does not meet displacement demands. The cracking pattern also emphasizes the collapse of the URM structure at the local level through the separation of the rear wall from the lateral walls whereas the Bhatar structure did not suffer collapse and the lateral walls remained activated. The location of damage and cracks in the numerical model was found to be similar to that in literature on similar building typology.

Overall, this research underscores the vital role of horizontal timber bands in enhancing the seismic response of masonry structures, especially in the earthquake-prone Himalayan region. The integration of timber not only augments the resistance and ductility of the structures but also significantly changes the failure mechanisms, leading to safer outcomes during seismic events. Further research is suggested in understanding the behaviour of timber-masonry interface and timber-to-timber connections in detail, which could potentially explain even more robust construction methodologies for seismic regions.

The seismic vulnerability of masonry structures in the Himalayan region is undeniable, with many tragic events underscoring the importance of reinforced construction. Through numerical modelling and subsequent seismic assessment, this thesis underscores the seismic advantages of integrating horizontal timber bands into masonry structures. Techniques like Bhatar stand out as resilient, cost-effective, and environmentally friendly solutions. The pushover analysis, benchmark study comparisons, and numerical modelling of the Bhatar structure provide valuable insights, paving the way for safer construction practices in seismically active regions. While the current research has made some significant strides, further exploration into the behaviour of such structures through NLTHA and discretisation of some interfaces could lead to analytical formulations that, in the future, could further enhance our understanding and application of timber reinforcements in masonry structures.

6.1. Practical recommendations

Some practical recommendations for the design and construction of masonry structures reinforced with timber, based on the results of this thesis are presented:

- Horizontal timber bands should be integrated in masonry across the height of the masonry at key locations – with sill, lintel and roof level to be considered as a priority.
- As far as possible, the bands should be continuous, and the inner and outer surface should be joined by crossbeams.
- Both upper and lower edges of the openings should be connected to the timber bands.
- The outer wall should have uninterrupted timber bands to avoid premature collapse under out-of-plane loading.
- The timber bands should be anchored into the masonry at certain locations to avoid additional slip which would result in lesser resistance.

6.2. Further research

Refining the details of the numerical model will be instrumental in enhancing the understanding and ensuring the resilience and longevity of timber-reinforced masonry buildings in seismic zones.

- A more advanced discrete modelling approach to simulate the interaction between timber elements and masonry would provide realistic indication of the stresses generated and would inform accurately the impact of such frictional behaviour on the global behaviour of the wall.
- A discrete modelling approach for the timber-to-timber connections with nail or dowel modelled discretely along with the material properties would inform appropriate strength verification of timber connections and the fasteners.
- Given the availability of computational resources, a nonlinear time history analysis is more suited for seismic assessment as it simulates the accelerations from an actual earthquake while also having the option of observing the impact of vertical acceleration along with horizontal accelerations.

- Modelling of roof (or floor) for the numerical analysis will allow to account for the contribution of the diaphragm action.
- A more extensive sensitivity analysis will inform about relative criticality of different geometrical or material parameters for the masonry.

In conclusion, the seismic vulnerabilities of masonry in the Himalayas emphasize the need for reinforced masonry. This research emphasises the seismic benefits of using timber as reinforcement in masonry and advances building techniques like Bhatar as having larger seismic capacity than unreinforced masonry, sufficient to resist a code-specified earthquake without collapsing. While this study offers crucial insights, further exploration of diverse analytical methods and numerical modelling approaches could augment comprehension and implementation of timber reinforcements in masonry.

References

1. Singh, Y., D.H. Lang, and D. Narasimha. *Seismic risk assessment in hilly areas: case study of two cities in Indian Himalayas*. in *Proc. SECED 2015 Conference: Earthquake Risk and Engineering towards a Resilient World*. 2015.
2. Khattri, K.N., *Great earthquakes, seismicity gaps and potential for earthquake disaster along the Himalaya plate boundary.* Tectonophysics, 1987. **138**(1): p. 79-92.
3. Wyss, M., S. Gupta, and P. Rosset, *Casualty Estimates in Repeat Himalayan Earthquakes in India.* Bulletin of the Seismological Society of America, 2018. **108**(5A): p. 2877-2893.
4. Kulkarni, A., et al., *Policy Brief: State of Himalayan glaciers and future projections*. 2018.
5. Bilham, R., *Himalayan earthquakes: a review of historical seismicity and early 21st century slip potential.* Geological Society, London, Special Publications, 2019. **483**(1): p. 423-482.
6. Brett, W.B., *A Report on the Bihar Earthquake: And on the Measures Taken in Consequence Thereof Up to the 31st December 1934*. 1935: Superintendent, Government Print.
7. Pandey, M. and P. Molnar, *The distribution of intensity of the Bihar-Nepal earthquake of 15 January 1934 and bounds on the extent of the rupture zone.* Journal of Nepal Geological Society, 1988. **5**(1): p. 22.
8. Singh, S., et al. *Damage during Kinnaur earthquake of January 19, 1975 in Himachal Pradesh, India*. in *Proc. Sixth World Conf. Earthquake Engineering, New Delhi*. 1977.
9. Wyss, M., *Human losses expected in Himalayan earthquakes.* Natural hazards, 2005. **34**: p. 305-314.
10. Parajuli, R.R. and J. Kiyono, *Ground Motion Characteristics of the 2015 Gorkha Earthquake, Survey of Damage to Stone Masonry Structures and Structural Field Tests.* Frontiers in Built Environment, 2015. **1**.
11. Gautam, D., et al., *Vernacular masonry construction in Nepal: History, dynamics, vulnerability and sustainability.* Masonry: design, materials and techniques. Nova Science Publishers Inc., New York, 2018.
12. Gautam, D. and H. Chaulagain, *Structural performance and associated lessons to be learned from world earthquakes in Nepal after 25 April 2015 (MW 7.8) Gorkha earthquake.* Engineering Failure Analysis, 2016. **68**: p. 222-243.
13. Sharma, A.K., A. Kumar, and V. Sarhosis. *Evaluating the Seismic Performance of Domestic and Historical Masonry Structures in Himachal Pradesh Region of India*. in *Recent Advances in Earthquake Engineering*. 2022. Singapore: Springer Singapore.
14. Karababa, F. and P. Guthrie, *Vulnerability reduction through local seismic culture.* Technology and Society Magazine, IEEE, 2007. **26**: p. 30-41.
15. Bostenaru Dan, M., *Timber Frame Historic Structures and the Local Seismic Culture—An Argumentation*, in *Earthquake hazard impact and urban planning*. 2014, Springer. p. 213-230.
16. Langenbach, R., *Bricks, mortar and earthquakes.* Apt Bulletin, 1989. **31**(3-4): p. 31-43.
17. Vasconcelos, G., P.B. Lourenço, and E. Poletti, *An Overview on the Seismic Behaviour of Timber Frame Structures*, in *Historical Earthquake-Resistant Timber Frames in the Mediterranean Area*, N. Ruggieri, G. Tampone, and R. Zinno, Editors. 2015, Springer International Publishing: Cham. p. 119-132.
18. Carabbio, R., et al., *How Can Vernacular Construction Techniques Sustain Earthquakes: The Case of the Bhatar Buildings.* Frontiers in Built Environment, 2018. **4**.

19. Hicyilmaz, K.B., Jitendra K and M. Stephenson, *Housing Report Dhajji Dewari.* World Housing Encyclopedia, 2011.
20. Gani, A., D.C. Rai, and J. Banday, *Seismic behavior of Timber framed masonry: A comprehensive review.* 2021.
21. Rahul, A., et al., *Thathara houses in Himachal Pradesh.* 2013.
22. van der Zanden, M., *Assessment of the seismic performance and sustainability of the Kath-Kuni building style in the Indian Himalaya.* 2018.
23. D'Ayala, D. and S.S. Bajracharya, *Housing report: traditional Nawari house in Kathmandu valley.* World Housing Encyclopedia, 2003.
24. Chand, B., H. Kaushik, and S. Das, *Experimental Study on Traditional Assam-type Wooden House for Seismic Assessment*. 2017. Paper-No.
25. Chand, B., H. Kaushik, and S. Das, *Material Characterization of Traditional Assam-Type Wooden Houses in Northeastern India.* Journal of Materials in Civil Engineering, 2020. **32**: p. 04020384.
26. Kaushik, H. and K.S.R. Babu, *"Assam-type House", World Housing Encyclopedia Report No. 154, Published by Earthquake Engineering Research Institute (EERI), USA and International Association for Earthquake Engineering (IAEE), Japan*. 2012.
27. Schacher, T., *"Bhatar" in Battagram*. 2008.
28. Schildkamp, M.
29. Sharma, H., *DHAJJI DEWARI - Traditional Earthquake Resistant Construction of Kashmir*, in *The Himalayan Architect*. 2022.
30. Jain, S.K., *Earthquake safety in India: achievements, challenges and opportunities.* Bulletin of Earthquake Engineering, 2016. **14**(5): p. 1337-1436.
31. Rautela, P. and G.C. Joshi, *Earthquake-safe Koti Banal architecture of Uttarakhand, India.* CURRENT SCIENCE, 2008. **95**(4): p. 475.
32. Shah, M. and J. Thakkar, *The Himalayan Vernacular: Kath-Khuni Architecture.* 2018.
33. Gautam, S., *300 year old Newari house*. 2018, myRepublica.
34. Sheth, A., *Typical Ikra House*.
35. Celano, T., et al., *Literature Review of the In-Plane Behavior of Masonry Walls: Theoretical vs. Experimental Results.* Materials, 2021. **14**(11): p. 3063.
36. Proença, J., A. Gago, and A. Vilas Boas, *Structural window frame for in-plane seismic strengthening of masonry wall buildings.* International Journal of Architectural Heritage, 2018. **13**: p. 1-16.
37. Moon, F.L., et al., *Recommendations for Seismic Evaluation and Retrofit of Low-Rise URM Structures.* Journal of Structural Engineering, 2006. **132**(5): p. 663-672.
38. Bruneau, M., *Seismic evaluation of unreinforced masonry buildings — a state-of-the-art report.* Canadian Journal of Civil Engineering, 1994. **21**(3): p. 512-539.
39. Galvez, F., *Discrete Elements Method to predict failure mechanisms of unreinforced masonry walls*. 2016.
40. Naseer, A., et al., *Observed seismic behavior of buildings in northern Pakistan during the 2005 Kashmir earthquake.* Earthquake Spectra, 2010. **26**(2): p. 425-449.
41. Vlachakis, G., E. Vlachaki, and P.B. Lourenço, *Learning from failure: Damage and failure of masonry structures, after the 2017 Lesvos earthquake (Greece).* Engineering Failure Analysis, 2020. **117**.
42. Vaculik, J., *Unreinforced masonry walls subjected to out-of-plane seismic actions*. 2012.
43. Lawrence, S. and A. Page, *Manual 4: Design of clay masonry for wind and earthquake*, in *ThinkBrick Technical Manuals*. 2013, Artarmon, NSW 1570 Australia.

44. Ismail, N. and N. Khattak, *Building Typologies Prevalent in Northern Pakistan and Their Performance during the 2015 Hindu Kush Earthquake.* Earthquake Spectra, 2016. **32**(4): p. 2473-2493.
45. Ali, Q., et al., *Seismic Performance of Stone Masonry Buildings Used in the Himalayan Belt.* Earthquake Spectra, 2013. **29**.
46. Javed, M., et al. *Behavior of masonry structures during the Kashmir 2005 earthquake*. in *Proc. Of the First European Conference on Earthquake Engineering and Seismology, Geneva, Switzerland, Paper*. 2006.
47. Langenbach, R., *From "Opus Craticium" to the "Chicago Frame": Earthquake-Resistant Traditional Construction∗.* International Journal of Architectural Heritage, 2007. **1**(1): p. 29-59.
48. Gosain, N. and A. Arya, *A report on Anantnag earthquake of February 20, 1967.* Bulletin of the Indian Society of Earthquake Technology, 1967. **4**(3).
49. Kaushik, H. and K. Dasgupta, *Assessment of Seismic Vulnerability of Structures in Sikkim, India, Based on Damage Observation during Two Recent Earthquakes.* Journal of Performance of Constructed Facilities, 2013. **27**: p. 697-720.
50. Rai, D.C. and C. Murty, *Preliminary report on the 2005 north Kashmir earthquake of October 8, 2005.* India: Department of Civil Engineering, IIT Kanpur, 2005.
51. Rautela, P. and G.C. Joshi, *Earthquake safety elements in traditional Koti Banal architecture of Uttarakhand, India.* Disaster Prevention and Management: An International Journal, 2009. **18**(3): p. 299-316.
52. Varum, H., et al., *Chapter 3 - Seismic Performance of Buildings in Nepal After the Gorkha Earthquake*, in *Impacts and Insights of the Gorkha Earthquake*, D. Gautam and H. Rodrigues, Editors. 2018, Elsevier. p. 47-63.
53. Dizhur, D., et al., *Building typologies and failure modes observed in the 2015 Gorkha (Nepal) earthquake.* Bulletin of the New Zealand Society for Earthquake Engineering, 2016. **49**(2): p. 211-232.
54. Adhikari, R.K. and D. D'Ayala, *2015 Nepal earthquake: seismic performance and post-earthquake reconstruction of stone in mud mortar masonry buildings.* Bulletin of Earthquake Engineering, 2020. **18**(8): p. 3863-3896.
55. Shakya, M. and C.K. Kawan, *Reconnaissance based damage survey of buildings in Kathmandu valley: An aftermath of 7.8Mw, 25 April 2015 Gorkha (Nepal) earthquake.* Engineering Failure Analysis, 2016. **59**: p. 161-184.
56. Gautam, D., et al., *Common structural and construction deficiencies of Nepalese buildings.* Innovative Infrastructure Solutions, 2016. **1**(1).
57. Rai, D., et al., *Performance of Residential Buildings during the M 7.8 Gorkha (Nepal) Earthquake of 25 April 2015.* Current Science, 2015. **109**: p. 2126.
58. Hughes, R., *Cator and Cribbage Construction of Northern Pakistan.* 2000.
59. Erarslan, A., *Timber Construction Systems in Anatolian Vernacular Architecture.* 2020. **12(61)**: p. 37-52.
60. Kavas, K., *Patterns of Environmental Coherence in the Rural Architectural Tradition of Ürünlü (Akseki-İbradi Basin).* METU JOURNAL OF THE FACULTY OF ARCHITECTURE, 2011. **28**: p. 23-40.
61. Vintzileou, E., *Effect of Timber Ties on the Behavior of Historic Masonry.* Journal of Structural Engineering, 2008. **134**(6): p. 961-972.
62. Khadka, B., *A Detailed Study on the Mud-Bonded Masonry Houses in Nepal Both Before and After 2015 Gorkha Earthquake*, in *Accessible Housing for South Asia: Needs, Implementation*

and Impacts, A. Kundu, et al., Editors. 2022, Springer International Publishing: Cham. p. 167-188.
63. Carabbio, R., *Semi-Engineered Earthquake-Resistant Structures: One Story Buildings Made With Bhatar Construction Technique*, in *Department of Civil, Chemical, Environmental, and Materials Engineering*. 2016, University of Bologna: Bologna.
64. Yadav, S., et al., *Effects of horizontal seismic band on seismic response in masonry structure: Application of DIC technique.* Progress in Disaster Science, 2021. **10**.
65. Aranguren, J., et al., *Experimental analysis of timber inclusions effect on paraseismic behavior of earth masonry walls.* Engineering Structures, 2020. **212**: p. 110429.
66. Wang, M., et al., *Increasing the lateral capacity of dry joint flat-stone masonry structures using inexpensive retrofitting techniques.* Bulletin of Earthquake Engineering, 2019. **17**(1): p. 391-411.
67. Yadav, S., et al., *Effects of horizontal seismic band on seismic response in masonry structure: Application of DIC technique.* Progress in Disaster Science, 2021. **10**: p. 100149.
68. Shrestha, K.C., et al., *Strengthening of rammed earth structures with simple interventions.* Journal of Building Engineering, 2020. **29**: p. 101179.
69. Misir, I.S., et al., *Experimental out-of-plane damage limits of historical stone masonry walls.* Construction and Building Materials, 2022. **333**: p. 127098.
70. Candeias, P.X., et al., *Experimental Assessment of the Out-of-Plane Performance of Masonry Buildings Through Shaking Table Tests.* International Journal of Architectural Heritage, 2017. **11**(1): p. 31-58.
71. Mouzakis, C., et al., *Seismic behaviour of timber-laced stone masonry buildings before and after interventions: shaking table tests on a two-storey masonry model.* Bulletin of Earthquake Engineering, 2018. **16**(2): p. 803-829.
72. Wang, M., et al., *Shake table tests on the two-storey dry-joint stone masonry structures reinforced with timber laces and steel wires.* Bulletin of Earthquake Engineering, 2019. **17**(4): p. 2199-2218.
73. Yadav, S., et al., *Shake table tests on 1:2 reduced scale masonry house with the application of horizontal seismic bands.* Engineering Structures, 2023. **283**: p. 115897.
74. Lourenco, P., *Recent advances in Masonry modelling: micromodelling and homogenisation.* Multiscale Modeling in Solid Mechanics: Computational Approaches, 2009.
75. Endo, Y., et al., *Comparison of seismic analysis methods applied to a historical church struck by 2009 L'Aquila earthquake.* Bulletin of earthquake engineering, 2015. **13**(12): p. 3749-3778.
76. Pelà, L., A. Aprile, and A. Benedetti, *Comparison of seismic assessment procedures for masonry arch bridges.* Construction and Building Materials, 2013. **38**: p. 381-394.
77. Wangmo, P., et al., *Assessment of out-of-plane behavior of rammed earth walls by pull-down tests.* International Journal of Architectural Heritage, 2019. **13**(2): p. 273-287.
78. Chácara, C., N. Mendes, and P.B. Lourenço, *Simulation of shake table tests on out-of-plane masonry buildings. Part (IV): macro and micro FEM based approaches.* International Journal of Architectural Heritage, 2017. **11**(1): p. 103-116.
79. Angulo-Ibáñez, Q., et al., *Traditional braces of earth constructions.* Construction and Building Materials, 2012. **30**: p. 389-399.
80. Khadka, S.S., et al., *Enhancement of Himalayan irregular stone masonry buildings for resilient seismic design.* Frontiers in Built Environment, 2023. **9**.

81. Lourenço, P.B., et al., *Traditional techniques for the rehabilitation and protection of historic earthen structures: The seismic retrofitting project.* International Journal of Architectural Heritage, 2019. **13**(1): p. 15-32.
82. Parajuli, H.R., *Dynamic analyses of low strength masonry houses based on site specific earthquake ground motions.* 2009.
83. Misir, I.S. and G. Yucel, *Numerical Model Calibration and a Parametric Study Based on the Out-Of-Plane Drift Capacity of Stone Masonry Walls.* Buildings, 2023. **13**(2): p. 437.
84. Ortega, J., et al., *Assessment of the efficiency of traditional earthquake resistant techniques for vernacular architecture.* Engineering Structures, 2018. **173**: p. 1-27.
85. Murano, A., et al., *Comparison of different numerical modelling approaches for the assessment of the out-of-plane behaviour of two-leaf stone masonry walls.* Engineering Structures, 2023. **291**: p. 116466.
86. Al Qablan, H., et al., *On the use of wooden beams as an anti-seismic device in stone masonry in Qasr el-Bint, Petra, Jordan.* Journal of Building Engineering, 2019. **21**: p. 82-96.
87. Mirra, M. and G. Ravenshorst, *Seismic characterization of timber-masonry connections based on experimental results.* Delft University of Technology, 2019.
88. Almeida, J.P., et al., *Characterization of mortar–timber and timber–timber cyclic friction in timber floor connections of masonry buildings.* Materials and Structures, 2020. **53**(3): p. 51.
89. Endo, Y. and T. Goda, *Pull-out test and numerical simulation of beam-to-wall connection: Masonry in earthen mortar and hardwood timber.* Engineering Structures, 2023. **275**: p. 115206.
90. Dimovska, S., et al., *Modelling of in-plane seismic behaviour of one-way steel or timber jack arch floors in existing buildings. Application to the Eixample district of Barcelona.* Engineering Structures, 2022. **262**: p. 114343.
91. Costa, A.A., et al., *Simulation of masonry out-of-plane failure modes by multi-body dynamics.* Earthquake Engineering & Structural Dynamics, 2015. **44**(14): p. 2529-2549.
92. Mohammadi Nikoo, M., اخویسی .ا, and A. Permanoon, *An Investigation of Performance of Masonry Wall Reinforced with Timber lumbers.* 2021. **9**: p. 114-138.
93. Endo, Y. and T. Hanazato, *Seismic Behaviour of a 20th Century Heritage Structure Built of Welded Tuff Masonry and Timber Frames.* International Journal of Architectural Heritage, 2022: p. 1-23.
94. AlShawa, O., D. Liberatore, and L. Sorrentino, *Pre- and post-simulations of shake-table tests on a stone masonry building aggregate using finite-discrete elements.* Bulletin of Earthquake Engineering, 2022.
95. Illampas, R., D.C. Charmpis, and I. Ioannou, *Laboratory testing and finite element simulation of the structural response of an adobe masonry building under horizontal loading.* Engineering Structures, 2014. **80**: p. 362-376.
96. Murano, A., et al., *Influence of traditional earthquake-resistant techniques on the out-of-plane behaviour of stone masonry walls: Experimental and numerical assessment.* Engineering Structures, 2019. **201**.
97. Karim, M., *Explorative nonlinear pushover analyses for historical unreinforced masonry churches: A case study in Zandeweer, Groningen.* 2019.
98. DIANA - Finite Element Analysis, D.m.A., *User's Manual - Release 10.5*, D. Ferreira, Editor. 2021, DIANA FEA BV: Delft, The Netherlands.
99. Lourenço, P.B., et al., *Analysis of Masonry Structures Without Box Behavior.* International Journal of Architectural Heritage, 2011. **5**(4-5): p. 369-382.

100. Endo, Y., L. Pelà, and P. Roca, *Review of Different Pushover Analysis Methods Applied to Masonry Buildings and Comparison with Nonlinear Dynamic Analysis.* Journal of Earthquake Engineering, 2017. **21**(8): p. 1234-1255.
101. Standards, B.o.I., *IS 1893 (Part 1) : 2016*, B.o.I. Standards, Editor. 2016, Bureau of Indian Standards: New Delhi.
102. Doudoumis, I.N., *Analytical Modelling of Traditional Composite Timber-Masonry Walls.* Advanced Materials Research, 2010. **133-134**: p. 441-446.
103. Kouris, L., et al., *Simple and complex modelling of timber-framed masonry walls in Pombalino buildings.* Bulletin of Earthquake Engineering, 2014. **12**: p. 1777-1803.
104. Endo, Y., *Modelling and Structural Analysis of historical masonry systems including vaulted structure.* 2015.
105. Maccarini, H., et al., *Out-of-plane behavior of stone masonry walls: Experimental and numerical analysis.* Construction and Building Materials, 2018. **179**: p. 430-452.
106. Chang, L.-Z., J.G. Rots, and R. Esposito, *Influence of aspect ratio and pre-compression on force capacity of unreinforced masonry walls in out-of-plane two-way bending.* Engineering Structures, 2021. **249**: p. 113350.
107. Schacher, T., *Bhatar construction, Timber reinforced masonry: An illustrated guide for craftsmen*. 2007, Swiss Agency for Development and Cooperation (SDC), French Red Cross (FRC): Manshera, NWFP. p. 12.

Appendix A Sensitivity to iterations

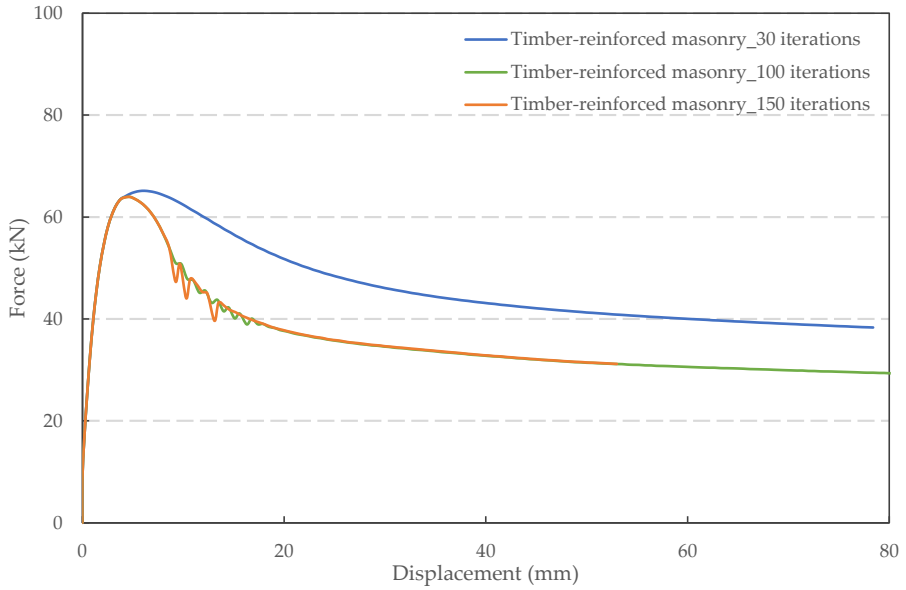

Figure A.1: Timber-reinforced model with increasing number of iterations

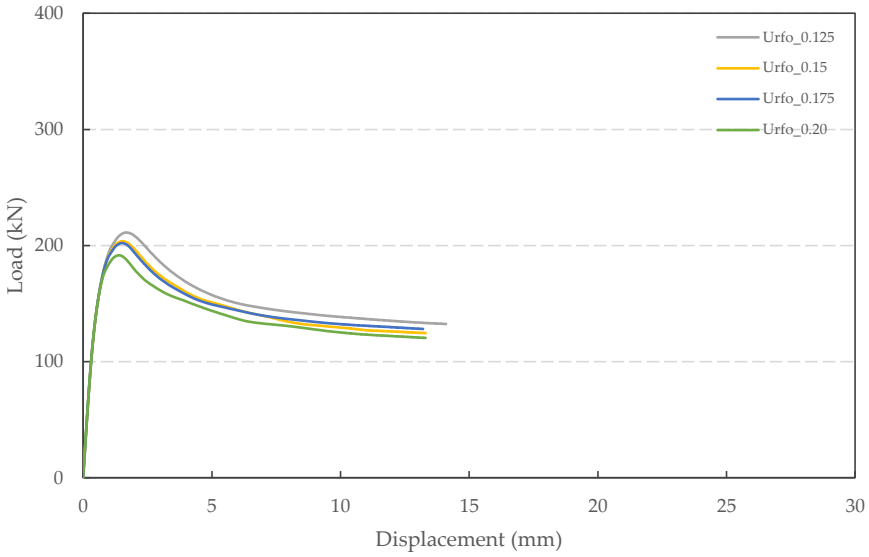

Figure A.2: Mesh sensitivity for full-scale Unreinforced masonry one-room structure

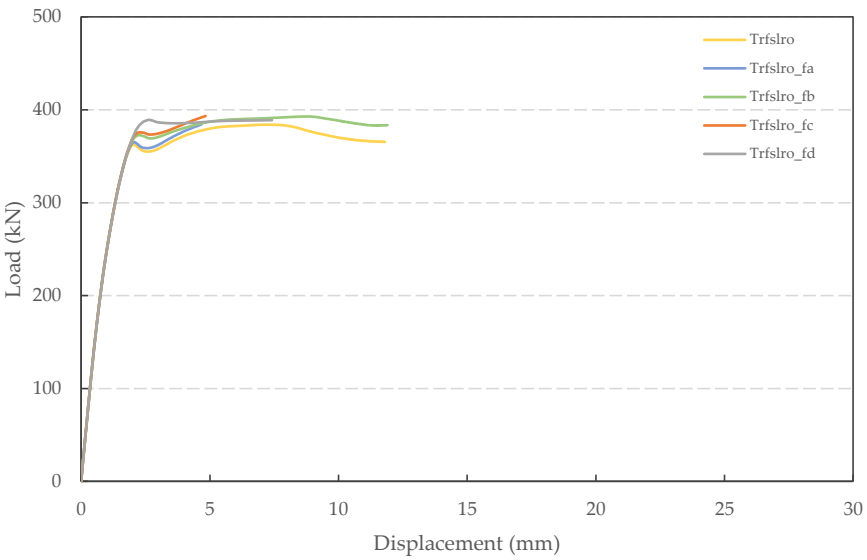

Figure A.3: Mesh sensitivity for full-scale Unreinforced masonry one-room structure

Appendix B Effect of timber bands and openings

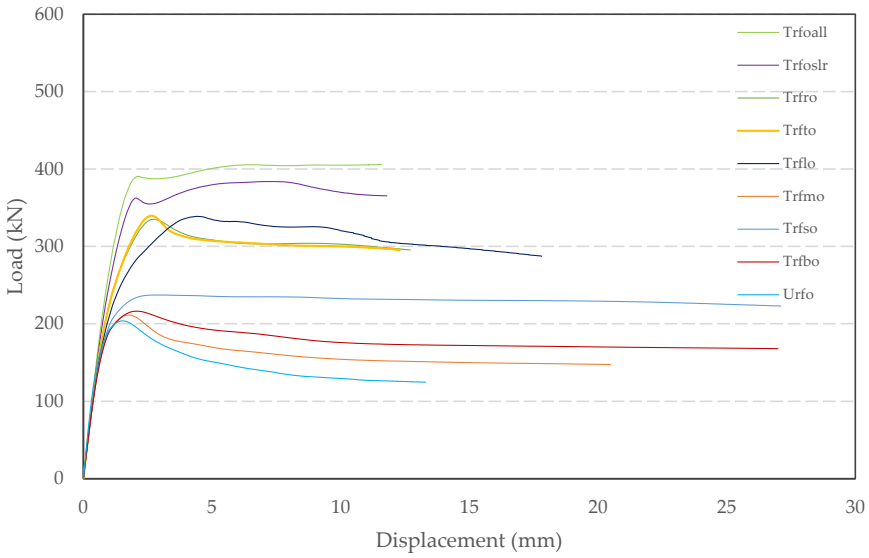

Figure B.1: Effect of single timber bands on unreinforced masonry

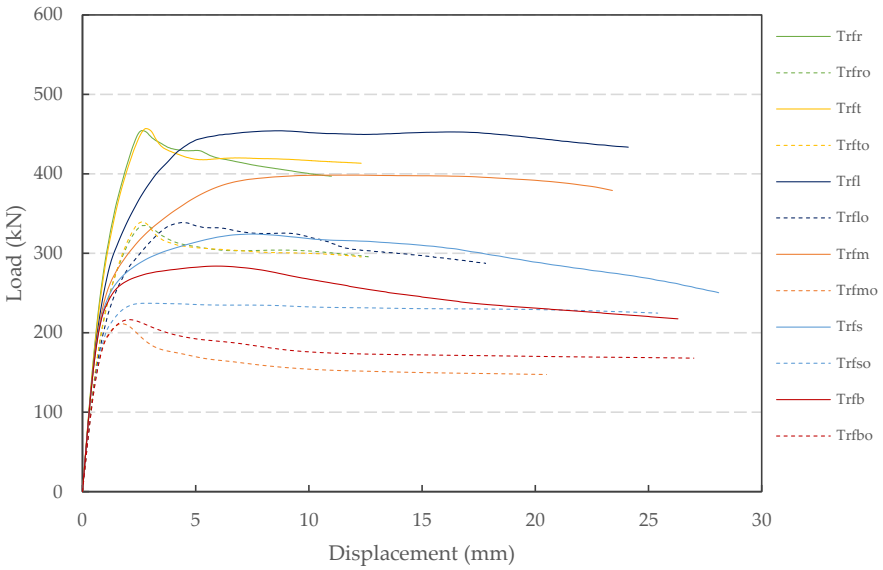

Figure B.2: Effect of openings on force capacity

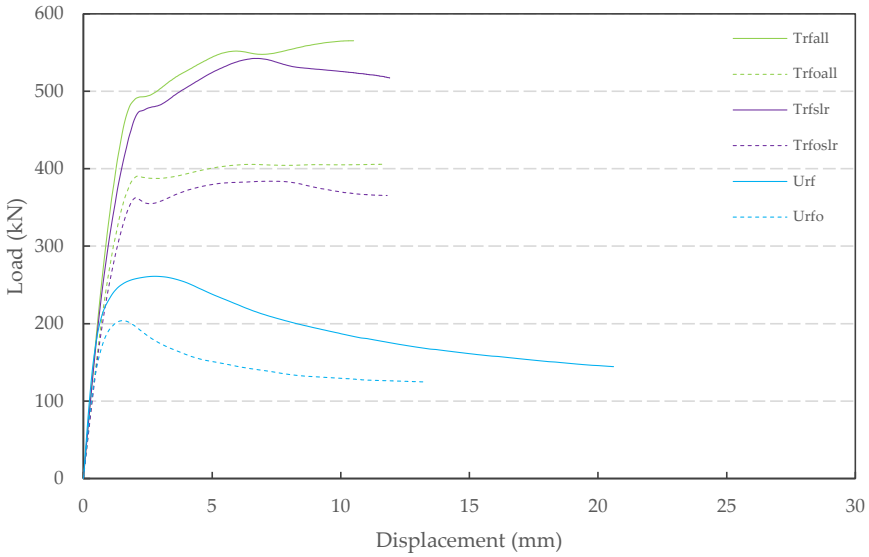

Figure B.3: Effect of openings on force capacity

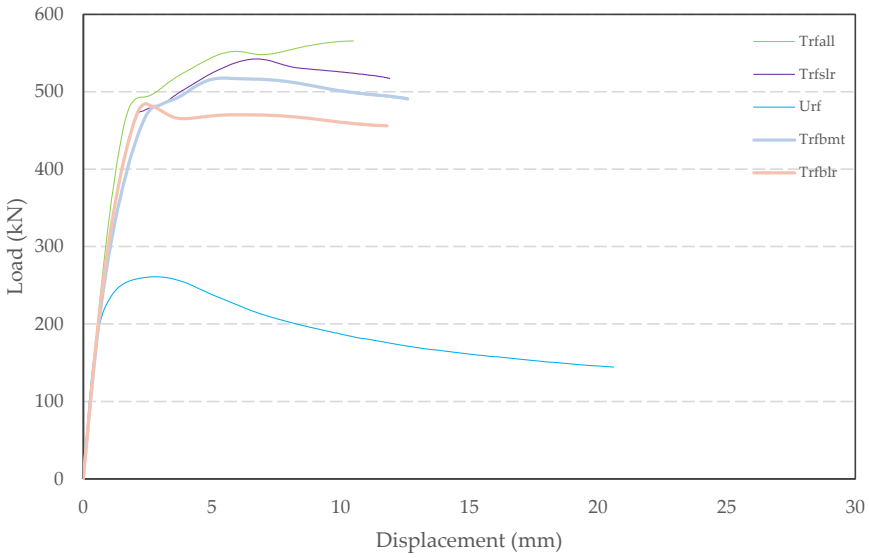

Figure B.4: Combination of three timber bands on force capacity

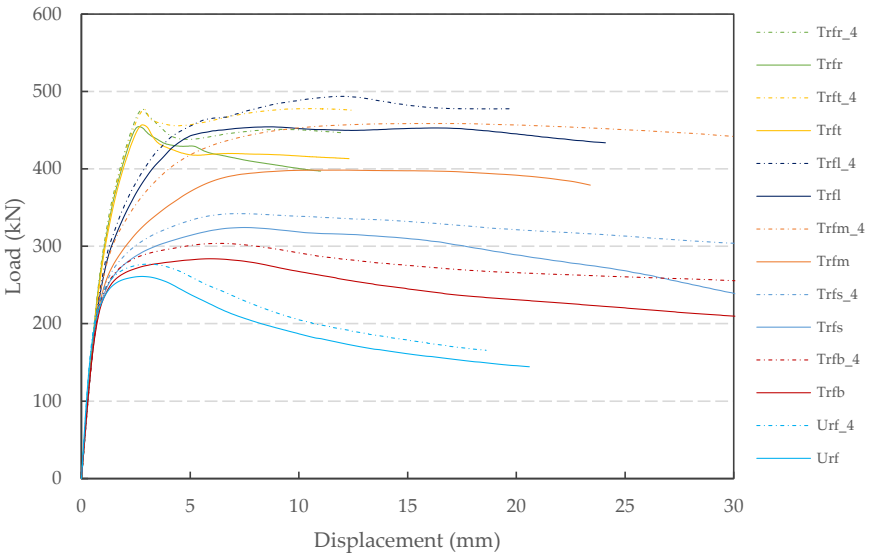

Figure B.5: Effect of roof load transfer on load-displacement curve

Appendix C Contour Plots

Figure C.1 compares the displacement contour plots of Model T1 against displacements obtained from literature [105], during experimental investigation on a similar stone masonry wall.

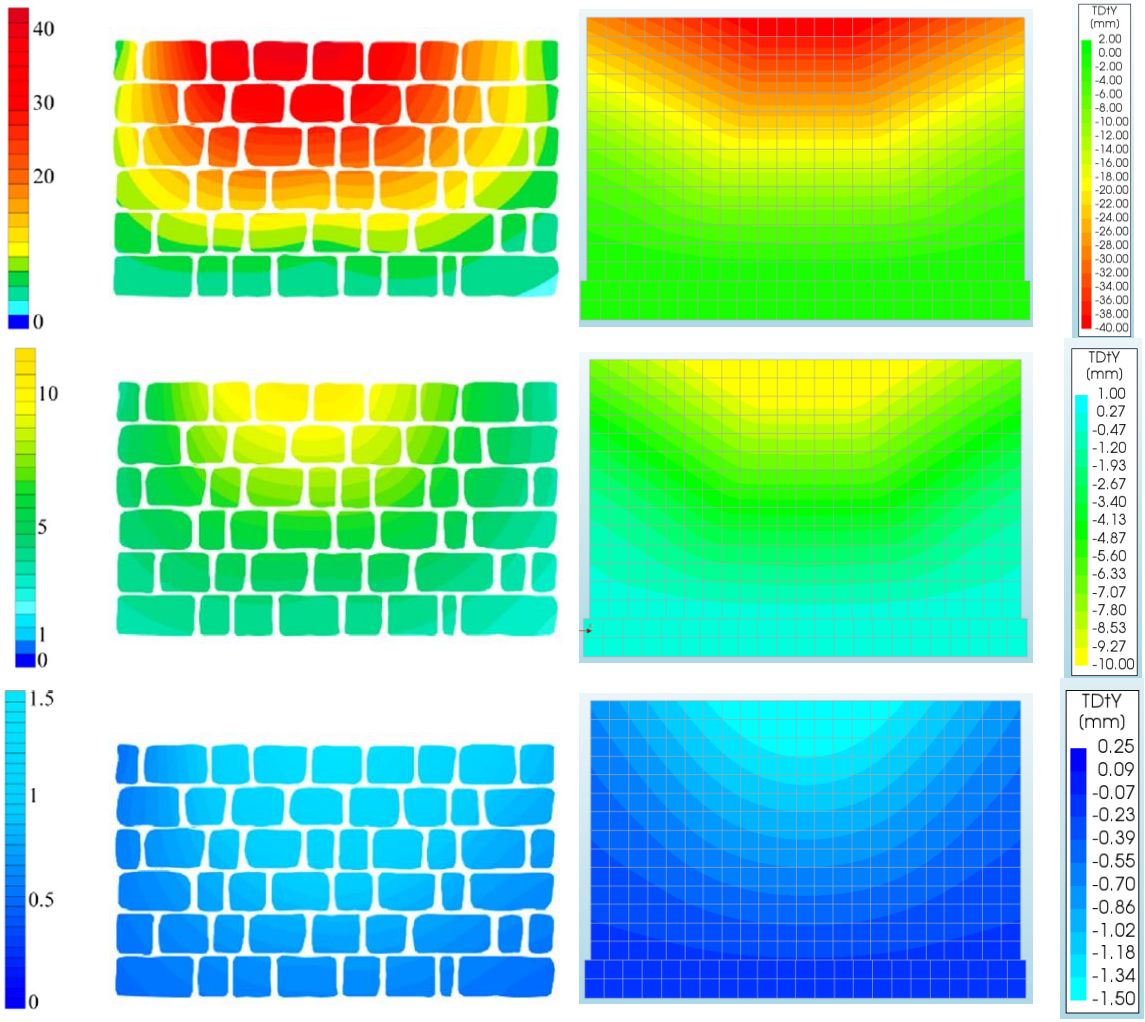

Figure C.1: Comparison of displacement contour with benchmark studies

Figure C.2 shows the separation of the rear wall from the lateral walls. The displacement contours are shown for the load steps 5, 15, 25, 35, 45, 60, 80, 100, 125, 150, 175, 200. The above load-steps and the given scale is chosen as they are more suited to display the displacements for the unreinforced masonry structure. This figure shows that for the initial load-steps, the lateral and front walls are active in displacement. However, as the pushover load increases, especially after reaching the maximum capacity of the structure, it exceeds the tensile strength and the interlocking effect at the corners (junctions between out-of-plane and in-plane walls); the rear wall starts separating from the lateral walls through diagonal cracks rendering the rest of the three walls uninvolved in failure mechanism and energy dissipation.

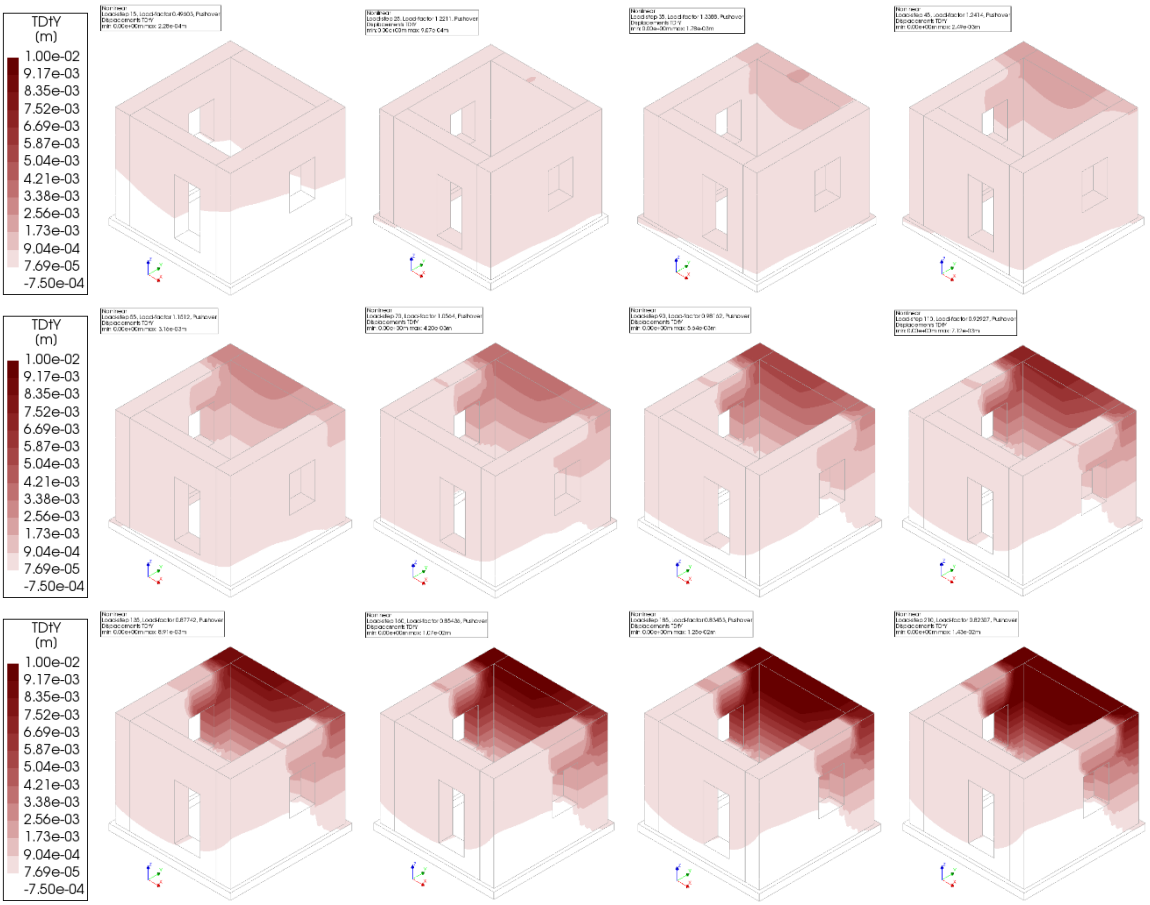

Figure C.2: Displacement in Y direction, Unreinforced masonry (Ufro)